Downloaded from orbit.dtu.dk on: Dec 19, 2017

Technical University of Denmark

# Characterization, Modeling, and Optimization of Light-Emitting Diode Systems

**Thorseth, Anders; Thomsen, Jan W.; Dam-Hansen, Carsten**

*Publication date:*
2011

*Document Version*
Publisher's PDF, also known as Version of record

Link back to DTU Orbit

*Citation (APA):*
Thorseth, A., Thomsen, J. W., & Dam-Hansen, C. (2011). Characterization, Modeling, and Optimization of Light-Emitting Diode Systems. Kgs. Lyngby: Technical University of Denmark (DTU).

DTU Library
Technical Information Center of Denmark

**General rights**
Copyright and moral rights for the publications made accessible in the public portal are retained by the authors and/or other copyright owners and it is a condition of accessing publications that users recognise and abide by the legal requirements associated with these rights.

- Users may download and print one copy of any publication from the public portal for the purpose of private study or research.
- You may not further distribute the material or use it for any profit-making activity or commercial gain
- You may freely distribute the URL identifying the publication in the public portal

If you believe that this document breaches copyright please contact us providing details, and we will remove access to the work immediately and investigate your claim.

FACULTY OF SCIENCE
UNIVERSITY OF COPENHAGEN

# Ph.D. thesis

Anders Thorseth

## Characterization, Modeling, and Optimization of Light-Emitting Diode Systems

Principal supervisor: Jan W. Thomsen
Co-supervisor: Carsten Dam-Hansen
Submitted: 31/03/2011

DTU Fotonik
Department of Photonics Engineering

DTU

*"Here forms, here colours, here the character of every part of the universe are concentrated to a point."*
Leonardo da Vinci, on the eye [156, p. 20]

# Abstract

This thesis explores, characterization, modeling, and optimization of light-emitting diodes (LED) for general illumination.

An automated setup has been developed for spectral radiometric characterization of LED components with precise control of the settings of forward current and operating temperature. The automated setup has been used to characterize commercial LED components with respect to multiple settings. It is shown that the droop in quantum efficiency can be approximated by a simple parabolic function. The investigated models of the spectral power distributions (SPD) from LEDs are the strictly empirical single and double Gaussian functions, and a semi empirical model using quasi Fermi levels and other basic solid state principles. The models are fitted to measured SPDs, using the free parameters. The result show a high correlation between the measured LED SPD and the fitted models. When comparing the chromaticity of the measured SPD with fitted models, the deviation is found to be larger than the lower limit of human color perception. A method has been developed to optimize multicolored cluster LED systems with respect to light quality, using multi objective optimization. The results are simulated SPDs similar to traditional light sources, and with high light quality. As part of this work the techniques have been applied in practical illumination applications. The presented examples are historical artifacts and illumination of plants to increase photosynthesis.

# Resumé

Denne afhandling udforsker karakterisering, modellering og optimering af lysemitterende dioder (LED) til generel belysning.

En automatiseret forsøgsopstilling er blevet udviklet til spektro-radiometrisk karakterisering af LED komponenter, for forskellige indstillinger af strøm og driftstemperatur. Den automatiserede forsøgsopstilling har været brugt til at karakterisere kommercielle LED komponenter. Det er vist, at kvante effektivitet kan tilnærmes ved en simpel parabolsk funktion. De undersøgte modeller af spektralfordelinger fra lysdioder enkelt og dobbelt Gauss-funktioner som er strengt empiriske, og en semi empirisk model baseret på kvasi Fermi niveauer og andre basale faststof principper. De frie parametre in modellerne er fittet til de målte spektralfordelinger. Resultatet viser en høj korrelation mellem den målte LED spektralfordelinger og modellerne. Når man sammenligner kromaticiteten af de målte spektralfordelinger med de modellerede spektralfordelinger viser afvigelsen sig at være større end den nedre grænse for menneskets opfattelse af farver. En metode er udviklet til at optimere flerfarvede klynge LED systemer med hensyn til lyskvalitet, ved hjælp af flermålet optimering. Resultaterne er simulerede spektralfordelinger med egenskaber lig traditionelle lyskilder, og med høj lyskvalitet. Som en del af dette projekt er disse teknikker blevet anvendt i praktiske belysningsprojekter. De beskrevne eksempler er belysning af historiske genstande og belysning af planter for at øge fotosyntesen.

# Preface

This PhD project was carried out in the period from April 2007 to June 2010 at *Department of Optics & Plasma* (OPL) at *Risø National Laboratory*, Roskilde and in the *Diode Lasers & LED Systems group* at *DTU Fotonik* at *Technical University of Denmark*. Academic supervision was provided by the *Niels Bohr Institute* (NBI), *University of Copenhagen*. Principle advisor was Jan W. Thomsen from NBI and project advisor was Carsten Dam-Hansen from DTU Fotonik. A period of four months was spent working with Nadarajah Narendran at the *Lighting Research Center* at *Rensselaer Polytechnic Institute*, Troy, New York. The project was funded by OPL and was subsequently transferred to DTU Fotonik, following Risø National Laboratory's merger with DTU in 2007.

## Acknowledgments

This work is dedicated to my wonderful wife Katja, and delightful children Balder and Iben.

I would like to express my gratitude towards my advisor at DTU Fotonik; Carsten Dam-Hansen, for invaluable suggestions, support, and encouragement during the work. I would also like to thank Jan W. Thomsen and Birgitte Thestrup for their help and assistance. I am thankful for having being able to work with the members of the Diode Lasers & LED Systems group, and would like to thank group leader Paul Michael Petersen for this opportunity. From the group I would especially like to thank Peter Behrensdorff Poulsen, Søren Stentoft Hansen, Dennis Dan Corell, Peter Jensen, and Bjarne Sass, for their effort, work, and many inspirational conversations in the laboratory. I would also like to thank Dr. Narendran of the LRC for providing me with the privilege of working at the center, and Patric Lockhart and Lalith Jayasinghe for the good ideas and collaboration I received during my stay. I would also like to thank Tracy Meyer, Rosa Irizarry, Danny Miller, and Aaron Smith at the LRC for the their generosity towards my family and I during our stay in Troy. I would also like to express my appreciation for the help and patience from my friends, family the residents of Borchs Kollegium. Furthermore, I would like thank Louise Munk for helpful proofreading and Toke Lund Hansen for discussions and constructive criticism.

Anders Thorseth, Copenhagen, March 2011

# Outline

First an introduction to the LED lighting opportunities and challenges is given in Chapter 1, with an overview of the historical development of the light-emitting diode and an overview of the developments within the field of multichannel LED lighting. Chapter 2 is a presentation of the theory related to the properties of LED with emphasis on the spectral characteristics and modeling of LED spectra. Chapter 3 covers the used methods of characterization of light sources with respect to light quality as perceived by human beings. Chapter 4 presents the methods used for spectral radiometric measurements of the light output from LEDs. Chapter 5 presents the results of the current and temperature characterization of LED light sources. In Chapter 6, a method for optimization of clustered LED light sources is presented. Chapter 7 covers two cases where different aspects of the previously covered work are used. Finally, a conclusion and outlook is given.

# Contents

# List of Figures

# Chapter 1

# Introduction

Lighting has been an integral part of human civilization since before recorded history. Today artificial lighting is a critical part of modern life. However, traditional methods of lighting, such as fuel-based and incandescent lighting are highly inefficient. This has led to a situation, where lighting takes up 6.5 % of the total energy usage world wide [96]. Energy savings are becoming increasingly important, given that easily accessible energy resources are becoming scarce. As a consequence, use of inefficient lighting products is being phased out across the industrialized world as for instance in the the European Union [38, 147] and Australia [146]. The introductions of fluorescent tubes and compact fluorescent tubes have decreased the energy demand for lighting, in applications these technologies can be used. However, the narrow optical atomic transition lines emitted by this type of light sources results in a reduced light quality with regards to color rendering. Furthermore, the relatively large and fragile glass tubes containing mercury, pose limitations to applicability as well as environmental problems.

The notion of the *light-emitting diode* (LED) was introduced in 1907, when the effect of *electroluminescence* was discovered by Round [130]. This led to the development of the LED throughout the second part of the twentieth century. The first commercial LED was produced in the 1960s, eventually leading to the high power white LED, developed in the late 1990s. With increasing efficiency, color rendering, and reduction in component size and prize, the LED is currently gaining usage in a wide field of lighting applications. Section 1.1 gives a short overview of the development of the LED and section 1.2 is a discussion of the general impact of solid state lighting. An introduction to white light generation with multicolor LED systems is given in section 1.3. In section 1.4 a summary of the introduction is given.

As a light source, the LED has several advantages over traditional light sources, based on incandescence and fluorescence. The luminous efficacy of LEDs has increased throughout the development history. The efficacy of incandescent light sources was exceeded around the year 2000 and it is projected that also most fluorescent light sources will be surpassed in the coming years [78]. The energy saving obtained by

using LED devices to replace incandescent light sources can today approach 90 %. The LED components are comparably small and shock resistant due to the absence of pressurized glass parts and fragile filaments. The light output can be varied freely or *dimmed* by adjusting the forward current up to the rated maximum. Dimming can also be achieved relatively easy by modulating a constant current with a square wave signal of high frequency. The ratio between on and off time then determines the reduction in light level. This method is called pulse width modulation (PWM) and it is used widely for dimming. Incandescent lighting and to a lesser degree fluorescence tubes radiate the excess heat produced by the light source as infrared radiation along with the useful light. In an LED system heat is conducted away from the LED via the mounting opposite to the direction of light emission. This is an advantage in situations where heating of illuminated objects is unwanted. Section 7.1 shows the successful application of LED lighting for fragile historical artifacts.

An advantage of LED lighting that is often highlighted is the long lifetime of the devices. A typical high power LED will have a useful service life of 50,000 hours. Compared to incandescent and fluorescent light sources, this is an increase of a factor of 50 and 4-5 respectively. Considering that an LED lamp, that has been used moderately, will not need a "bulb change" for approximately 25 years, this could have positive environmental and economical consequences. However, in order to maintain the long service life, the implementation of the LED system has to be meticulous, avoiding excess heating and excess current flow that can shorten the lifetime of the device significantly [62, 87].

The introduction of a new technology in the field of general lighting presents a number of opportunities and challenges. The challenges associated with the implementation of LED lighting are both of a technical and cultural nature. The technical aspects are mostly related to the sensitivity of the solid state device to the working conditions, mainly the applied voltage and the temperature of the active region. Small variations in conditions may have large adverse effects on light output, energy efficiency, and service lifetime. Heat management, for instance, has not previously been a critical consideration in the general lighting industry. Another aspect is that light source, fixture, and power supply can no longer be regarded as separate unrelated parts. An LED based lighting solution should be considered a system of integral parts. Figure 1.1 shows the various parts for a LED system: A controller is needed for dimming and control of color, incorporating signals from temperature sensors and perhaps light detectors. A power supply is needed for the constant current which is generally needed to drive LEDs. A circuit board is needed for circuit lines to the LED and thermal transport. A heat sink is needed to transfer the heat produced by the LED away from the device such that the temperature does not rise above a certain level. The light from the LEDs can be directed and/or mixed by mounted optics. Some components will not be strictly necessary such as light sensors and advanced control-

ling, but may be used to enhance the utility of the LED system. The system aspect is exemplified in the following: Different LEDs can have vastly different characteristics with regard to for instance color rendering and efficiency. High color rendering will typically decrease efficiency. With lower efficiency, more current is needed and more excess heat is generated to produce the same amount of light. The heat produced by the LEDs determines the size of the needed heat sink. If the temperature of the LED rises above a specific threshold, the power supply should initiate dimming or turn off to avoid damaging the LED. Therefore, the temperature at a position near the LED must be measured, and the temperature at this position must be related to the junction temperature of the LED component. The result is that replacing an LED component in a lamp will have implications on the color rendering, energy efficiency, the design of the heat sink, the value of threshold temperature, and the amount of current needed from the power supply. All these aspects must be considered when designing an LED fixture. In this work several of the important aspects of LED systems will be discussed. These aspects are modeling of spectral emission from LEDs, thermal management and optimizing light quality for multicolor light sources. This system approach is new in the lighting industry where, many components, such as light sources and reflectors, have been interchangeable and operating on standardized household power or low constant voltage. Another issue, is the one regarding measurement of useful lifetime, where long time spans are needed for reliable results. Lifetime measurement and characterization are not discussed in this work, but techniques [62] and metrics [65] has been proposed and are officially recommended by, for instance, the *US Department of Energy* [108].

The cultural challenges to LED implementation within lighting has both to do with the normal problems with introducing a new "disruptive" technology to an established industry [12], and with the fact that LED illumination has certain perceptible properties that differ from traditional light sources. The traditional characterization of light quality (discussed in Chapter 3) has been put into question when trying to characterize these new light sources [34]. Traditionally, light has been produced by black body radiation or *incandescence* from different sources. The sun has been the primary source of energy, and illumination since life started evolving on earth. Artificial lighting from combustion of organic material, gas lighting and early electrical lighting are all based on incandescence at various temperatures. Human vision is closely optimized to advice us on our immediate environment by responding to sunlight reflected off objects in our surroundings. Therefore, temperature radiator light sources are used as quality references. Lighting that deviates too much from incandescent light sources is considered to be of lower light quality due to the higher degree of unfamiliarity for human observers. Because of the inherent subjectivity in human perception of light and color, there is an ongoing debate over the definitions of the metrics for color and

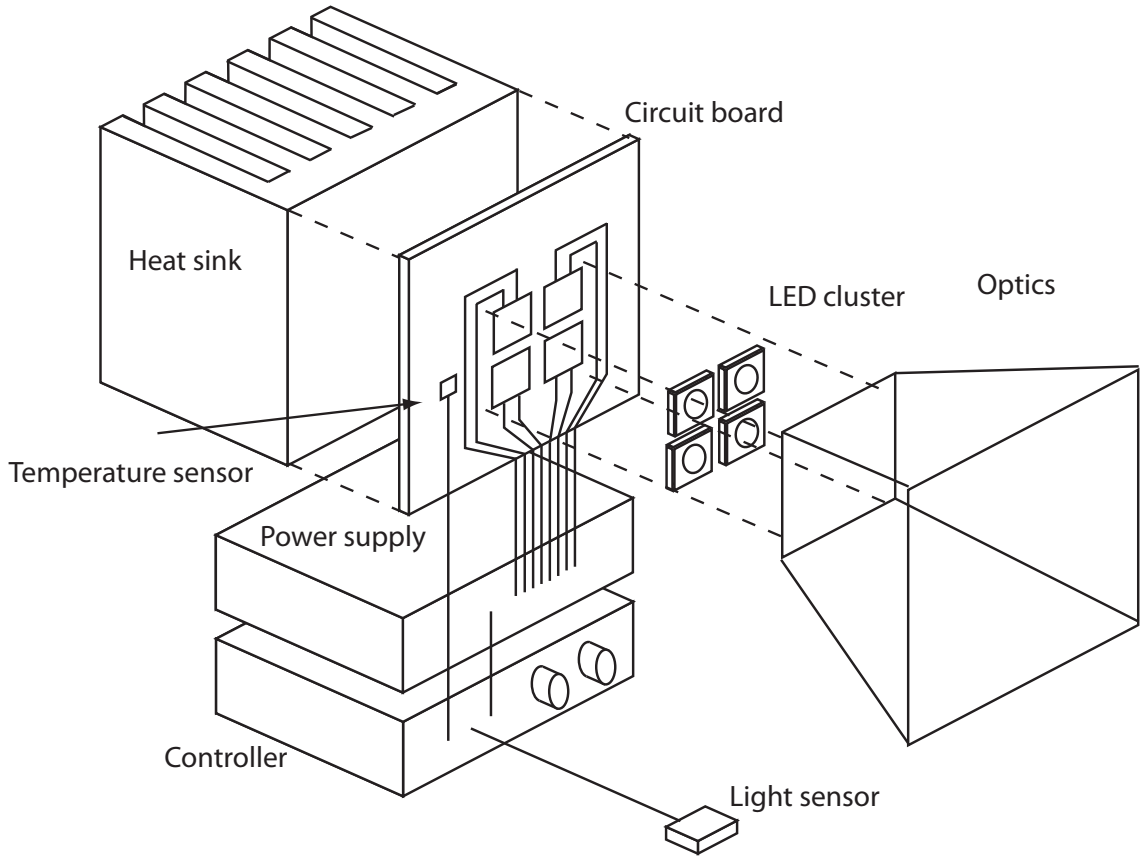


*Figure 1.1: An LED system, consisting of a LED light sources, mounted on a printed circuit board with an attached heat sink. Current is supplied from a dedicate power supply. The controller can use user input, temperature measurements, and light measurements to adjust the current for individual LEDs. In this work, focus is on the effect of heat and current, and control with respect to light quality.*

light quality. In this work, the widely used working standards recommended by the *International Commission on Illumination* (CIE) are used.

LED technology provides new possibilities within lighting in the form of dynamic light sources, where not only the luminous output but also other characteristics of the light, can be controlled dynamically. In traditional light sources, the perceptible properties of the illumination are highly constricted by the light source, for example the low pressure sodium tubes have the characteristically fixed spectrum yielding yellow light with poor color rendering, which means that it is primarily used for street lighting and greenhouse lighting. Low wattage incandescent bulbs have the characteristically reddish light with high color rendering. LED systems with multiple channels controlling light sources of distinct colors can be used to dynamically alter the lighting characteristics of the light from the lighting system. These systems are often referred to as LED clusters. Chapter 6 presents a method, developed during this work, for optimization of such systems, with respect to light quality. It has been used on var-

ious configurations of LEDs and the results are presented. Although such dynamic control has been possible for some times in LED systems for stage and architectural lighting as well as other niches involving colored illumination, these possibilities are now within reach for the field of general lighting. As the applications of LED get more advanced, color stability and color rendering stability will be increasingly important, examples of critical applications include medical applications, machine vision, and the graphical industry. The main challenge here is that the total light output and the spectral power distribution (SPD) of LEDs depend on both the forward current $I$ and the temperature of the n-p junction $T_J$. Changes in these can cause visible changes in the perceived color of the light and color rendering may also be affected. To correct for these effects, control mechanisms have been suggested using temperature and optical sensors for feedback control algorithms (See Muthu et al. [99], Žukauskas et al. [159], Perduijn et al. [122]). The use of optical sensors can be expensive and impractical. It will therefore be beneficial if a useful model can be found that can used to calculate the SPD from easily measurable quantities ($I$,$T_J$). A model would simplify the control mechanisms, for precise color and luminance stabilization. A consistent model might also be used to infer various important internal characteristics, such as the quasi Fermi levels, doping density etc. of a given LED using the spectral output alone. In Chapter 2 some of the possible components of such a model are presented. To validate the models presented the LEDs has been experimentally examined with radiometric spectroscopy, as part of this work. The experimental setup is described in Chapter 4. The next sections will give some background on the development of LED technology, the introduction of LEDs in lighting, and the possibilities for clustered LED light sources.

## 1.1 Development History of the LED

Working on diode technology for radios in 1907, H. J. Round found the effect now known as *electroluminecence*. Applying 10-110 V to a SiC crystal a faint yellow glow could be seen [130]. Later O. Lossev reported that the light was not a product of incandescence and that the light could be switched on and off with high speed [169, 86]. However, SiC has a indirect band gap. This meant that the efficiency was very low, (0.003%) [42] and the technology gained little interest. With the discovery of III-V materials in the 1950s, a range of optically interesting possibilities where laid open. In 1962, the first realization of GaAs LEDs, with p-n junctions made with epitaxial growth, were reported by multiple groups [118, 58, 107]. The first LED with visible red light was realized with GaAsP by Holonyak in 1962 [61]. These LEDs where made commercially available in the early 1960s. Development of fabrications techniques continued through the 1970s and 1980s. The first blue LED was introduced by Akasaki et al. [2] in 1992. It was based on GaN and had a, for the time, surprisingly high

efficiency of 1 %. Green LEDs could be made using GaInN with efficiencies up to 10 % [104].

With bright red, blue, and green LEDs available, the possibility of color displays was realized. Combinations of red, green, and blue light are required to additively mix most perceptible colors. Moreover, the development of the blue InGaN LED also lead to the possibility that the *white LED* could be made, using wavelength converting materials to convert short wavelength radiation to longer wavelength radiation via the Stokes shift [102]. With the introduction of white light sources, the concept of *solid state lighting* was introduced to describe lighting application using solid state materials and to distinguish the method from other forms of lighting.

An important aspect of the development of LED lighting is the way in which light output has increased at an accelerating rate since the development began. The efficiency and light output has seen a doubling approximately every 36 months. This effect is know as Haitz's Law [53]. It is clear that this development cannot continue indefinitely, however as long as the trend continues, it creates a strong incentive to further develop fabrication techniques and work on new lighting applications. It is expected that when the development enters the mature stage characterized by a decreasing improvement rate and diminishing returns with respect to energy efficiency, the LED systems will have surpassed most other lighting methods with regards to luminous efficacy [150].

## 1.2 Solid State Lighting

A large percentage of the world's energy consumption is used for lighting. The use of 2.7 PWh/yr for electrical lighting accounted for 16 % of generated electricity and 6.5 % of overall energy consumption in 2005 [151] with an increase of 35 % since 1997 [96]. In the developed parts of the world where electrical lighting is used primarily, the increasing energy consumption, growing concern for energy availability, and the emission of green house gasses and other pollutants, have caused an increased focus on efficiency within lighting. In the developing parts of the world, approximately 2 billion people live without access to electrical lighting, relying on fuel based lighting such as kerosene [121]. This form of lighting causes fire hazard and health problems for example from inhaling nitrogen dioxide [98]. LED technology or *solid state lighting* presents an effective and robust solution to decrease the energy demand for general lighting. Combined with solar cells and efficient batteries, LED technology can for instance be utilized for off-grid lighting in underdeveloped rural areas [135].

One of the key motivations for the recent development in LED lighting is the possibility for increasing efficiency and light output. The discovery of electroluminescence and the invention of the LED in the early 20th century was merely a starting point for a development that continues today. The development of LED technology has since

the 1960s run parallel to the general development in semiconductor materials used in electronics and computers. This has enabled the accelerating increase in light output and decrease in price [77] described by Haitz's Law. The first LED light sources where dim and barely visible. However, with the increasing lumen output from LEDs, the applications crossed from pure signaling to uses within lighting. An important threshold was reached around the year 2000, when LED devices surpassed the incandescent light bulb in terms of efficiency (10 lm/W - 15 lm/W). This initiated an emerging market for niche applications within lighting [53]. With the introduction of 1 watt class of LEDs with 30-50 lm/W, general lighting applications was within reach. As of the fall of 2010, a white LED with an efficiency of 160 lm/W LED should be commercially available [30]. Using this technology, it should be possible to achieve significant energy savings compared both to incandescent and compact fluorescent lighting. From 1995 to 2005, the market for high power LEDs grew with an average annual rate of 42 % [140] and was in 2008 $ 5.1 billion. It is expected to grow to $ 14.9 billion in 2013 [141], half of which is expected to be for lighting applications [142].

General lighting requires white light, which can be generated by many methods, corresponding to many different spectral power distributions. However, the spectral power distribution of the illumination is important with respect to light quality perceived by humans using the lighting. This has been evident in the slow adaptation of compact fluorescent light sources by consumers, partly due to a general perception of the low light quality of these light bulbs [152]. Therefore, characterization of light sources with respect to light quality and standardization of relevant quality characteristics is of importance for consumer adaptation of LED lighting.

White light can be generated by converting short wavelength LED light to longer wavelengths, by the Stokes shift. This is done by placing the wavelength converting materials such as yttrium aluminum garnet (YAG) phosphor on top of a blue or UV LED. The materials, normally coated directly on the diode, convert a portion of short wavelength light to a range of longer wavelengths, producing broad-spectrum white light [102]. The process of Stokes shift conversion decreases efficiency dramatically, due to inherent losses in the wavelength conversion process. This means that phosphor based white light sources must be made with a tradeoff between high efficiency and high color rendering, since high color rendering requires costly conversion from short to long wavelengths. Another method for white light generation is to use differently colored LED devices in a cluster formation and use additive color mixing to create white light. Since the simplest version of this method involves only red, green, and blue light sources, this method is often referred to as RGB mixing [37, 99]. Other methods for generating white light are Organic LED [41], and wavelength conversion by quantum-dots [168], and silicon carbide [109]. For lighting purposes, these methods are still in early development. The focus of LED development in recent years has been to create efficient, and inexpensive lighting using phosphor based white LEDs for general lighting

and RGB systems for dynamic effect lighting for stage and architectural purposes. In Chapter 6 it is argued that the two techniques can be used in conjunction, to create illumination with both dynamic possibilities and high light quality.

## 1.3 Clustered LED Systems

Clustering of multiple LEDs is used widely for illumination applications, where large quantities of light are required, due to the small size and relatively low light output of individual LED components. In this work it is shown how, by using LEDs of different color and apply color mixing, it is possible to achieve several effects. By adding individual color LEDs to broad spectrum white LEDs, the color rendering can be increased. Furthermore, the correlated color temperature can be adjusted by balancing the spectral components to fit different needs.

LED systems of this kind are more complex with regards to both driver electronics, color mixing optics, and user interaction. Therefore the concept has only seen little use in general lighting application, but has been used in niche applications such as stage lighting, architectural lighting and surgical lighting. Examples of niche applications where LED can used are given below: By utilizing the narrow peaks of individual colored LEDs custom spectra can be designed where light emission at unwanted wavelengths is near zero, while maintaining an acceptable white chromaticity and high efficiency. This can be useful if spectrally photosensitive materials are present, as for instance in workspaces for photolithography [27], or in relation to medical conditions causing increased vulnerability to light, such as xeroderma pigmentosum [66, p. 574]. LED cluster technology has been used for surgical lighting, either mounted on goggles [137], or as overview lightning [76]. A highly publicized example is the illumination of the painting of *Mona Lisa* by Leonardo da Vinci. In this instance a system consisting of seven color channels is used to compensate for discoloration from the bulletproof glass of the display case, as well as compensate for the age depreciation of paint pigments [97, 48].

The following is an overview of some of the results within the field of clustered multicolor LED light source: As seen in section 2.1.6 and 2.2.2, wavelength shifts and changes in light output can occur for both junction temperature and forward current or pulse width (PWM) duty cycle. To address these issues, Robinson and Ashdown [129] have used an RGB sensor with a feedback loop. Using a control algorithm, they obtain chromaticity stability of an RGBA (red, green, blue and amber) system of $\Delta_{u'v'} = 0.003$ for dimming from 10 %-100 %. With poor results for lower intensities. Perduijn et al. [122] realized a similar RGB system with $\Delta_{u'v'} = 0.002$ for environment temperatures from 25 - 70°C. A comprehensive review of the problems and methods of feedback control is given by Muthu et al. [100]. Another issue in implementation of LED solutions is the variations in color characteristics of LED components that

necessitate color binning. With refinement of production techniques this problems is decreasing. However, Ashdown et al. proposes a six-color source with feedback control that does not need color binning of the LEDs [5].

When using several different types of LEDs the effects of operational parameters, such as temperature and current, becomes increasingly important. The characteristics of LEDs with spectral output at different wavelength also have different responses to changes in the operational parameters. Changes in the balance between the individual parts of the spectral power distribution will be perceptible by human users of the illumination. Since monitoring of individual light output can be cumbersome, it could be beneficial to model the spectral power distribution of LED illumination given only the operational parameters. Models for this purpose are presented in Chapter 2.

Dynamically adjustable light sources, will have varying properties according to the balance between the power outputs in the different parts of the visible spectrum. The multitudes of possible configurations of the driving current of LEDs in a lighting system present an optimization problem, where different aspects of light quality need to be considered. The light quality characteristics used in this work is reviewed in Chapter 3. For assessment and utilization of these lighting systems the configurations, with the highest possible light quality, should be found. Chapter 6 presents a method to optimize the spectral light quality from various LED systems. This is done using computer aided simulation, and the results for the lighting systems are compared.

## 1.4 Summary

LED lighting system presents many opportunities within lighting from an increase in device lifetime to a decrease in power consumption for general lighting. However, the technology also presents challenges in terms of both the technical implementation of LED systems and with regards to the qualitative aspects of the illumination. Therefore, work is needed on characterization of LED systems with respect to operational parameters and light quality, and further on how these properties are interrelated. If LED lighting is to replace incandescent lighting, as seems unavoidable, light quality must be characterized in a meaningful way. This will be necessary for large scale market adoption. From the development history of LED it is seen that the accelerating development of the technology increase the incentive to transition from traditional light sources. The introduction of LED in to general lighting can be used to achieve energy savings in both the industrialized world and in developing countries. Further, new options are available with multi channel lighting systems that can adapt to user preferences or be optimized towards various objectives.

# Chapter 2

# Light-Emitting Diodes

## 2.1 Theory of Light-Emitting Diodes

One of the problems with controlling the light output from LEDs is that the technology itself has some inherent nonlinearities. These nonlinearities stem from the way semiconductor materials behave when used in this way. Both the amount of current and the temperature of the device will change the properties of the resulting illumination.

The following gives an introduction to the physical principles behind the light-emitting diode. A more detailed description is given of the effects that influence the spectral power distribution (SPD) emitted from LEDs, such as the shape of the carrier distribution, changes in band gap energy, and the influence of quasi Fermi levels. Section 2.1.1 is an introduction to semiconductors with a discussion of the carrier distribution in equilibrium. The concept of radiative and non-radiative recombination is discussed in section 2.1.2 and 2.1.3. The p-n junction in equilibrium and with bias applied is reviewed in section 2.1.4 and 2.1.5 respectively. The effects of temperature variations are treated in section 2.1.6. Modeling of LED spectra is discussed in section 2.2. A summary is given in section 2.3.

### 2.1.1 Semiconductors

Semiconductors are materials that differ from metals and isolators in the way that electrons behave in the material. In isolators, electrons are bound very tightly in the material structure, and current cannot easily flow. In metals, the electrons are bound very lightly and therefore current will flow very easily. In semiconductors most electrons will be bound in the structure, but a small fraction are mobile, so that in some circumstances current will flow easily and in others it will not. A missing electron or electron vacancy in the structure can also move and act as a charge carrier, called an electron *hole*. In an undoped semiconductor in equilibrium the product of the electron concentration $n_0$ and hole concentration $p_0$ is constant

$$n_0 p_0 = n_i^2, \tag{2.1}$$

where $n_i$ is the intrinsic concentration.

It can be shown that only certain energy states are allowed in the crystal structure, while others are forbidden. This is done by solving the Schödinger equation for a single particle in a periodic potential, as in the Kronig-Penny Model [93, p. 166], or using various other numerical methods [93, 75]. For a review of III-V material band structure see Vurgaftman et al. [157]. The result is bands of states where free carriers can exist. For a semiconductor diode the two most interesting bands are the *conduction band*, where electrons have enough energy to move freely about in the crystal, and thus the electrons can conduct current, and the *valence band* where electrons are constricted in the valence bonds between atoms. In the latter current can be conducted by moving holes. The density of states for electrons $\rho_n(E)$ in an ideal semiconductor at a given energy $E$ is given by the parabolic relation

$$\rho_n(E) \propto (E - E_c)^{1/2} \tag{2.2}$$

and the density of hole states $\rho_p(E)$ in the valence band, is given by

$$\rho_p(E) \propto (E_v - E)^{1/2} \tag{2.3}$$

where $E_c$ is the lowest conduction band energy and $E_v$ is the highest energy of the valence band, which for convenience is often set to zero [133, p. 88]. Note that the potential that is used to find the density of states is highly simplified, giving only an approximate solution.

We now look at the probability of finding an electron in a state with energy $E$. This is given by the Fermi-Dirac distribution

$$f_e(E) = \frac{1}{1 + \exp((E - E_f)/k_B T)}. \tag{2.4}$$

where $E_f$ is the Fermi energy i.e. the energy at which state occupation probability is $1/2$, and $k_B$ is the Boltzmann constant. The probability of finding a hole with a given energy $f_h(E)$ is then equal to the probability of not finding an electron in the state giving

$$f_h(E) = 1 - f_e(E), \tag{2.5}$$

The effective electron density is then the product of the available states from equation (2.4) and the occupation probability (2.2).

$$n(E) \propto f_e(E)\rho_n(E) \tag{2.6}$$

and similarly for holes the product of (2.5) (2.23) gives the hole density

$$p(E) \propto f_h(E)\rho_n(E). \tag{2.7}$$

This means that the carrier electrons will be at the bottom of the conduction band. Figure 2.1 shows the effective carrier distribution for electrons (a) and holes (b).

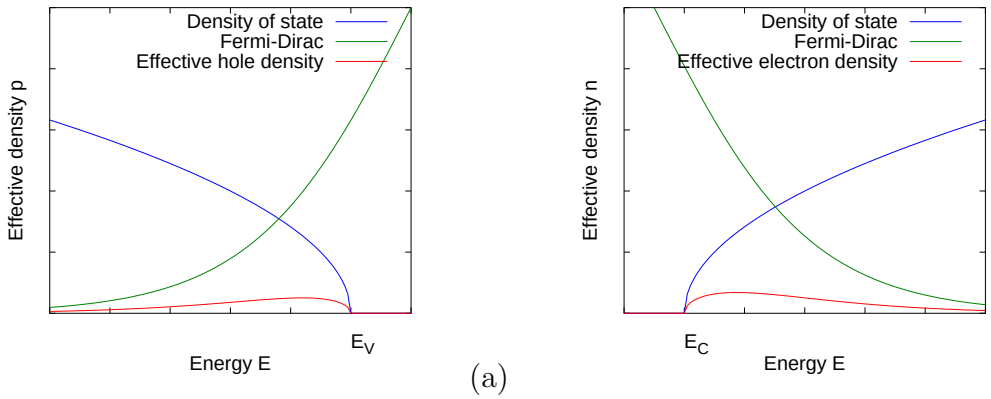


*Figure 2.1: The effective density of holes below the band gab calculated by the multiplication of the Fermi-Dirac function and the density of states (a), and similarly for electrons above $E_C$ (b)*

### 2.1.2 Radiative Recombination

In equilibrium, the carrier densities are given by the mass action law (2.1), however, we can introduce excess carriers, either by light injection or by current injection. The excess carriers can *recombine*, when an electron in the conduction band is near a hole in the valence band. In recombination the electron- hole pair combine, whereby it is eliminated and the energy difference is released. Figure 2.2 (a) illustrates a radiative recombination. The recombination rate $R$ is given as the negative change in carrier densities and is proportional to the density of electron-hole pairs

$$R = -\frac{dn}{dt} = -\frac{dp}{dt} = Bnp \tag{2.8}$$

where $B$ is the called the bimolecular recombination coefficient.

If the transition is direct i.e. without significant momentum difference between hole and electron, the energy will be released in the form of photon. If the transition is indirect i.e. with a high momentum difference the energy will be released as vibrations in the crystal, called phonons. Phonon creation is equivalent to increased heat in the crystal. Therefore non-radiative recombination is generally unwanted in light emitting devices for two reasons: The carrier pair is wasted when no light is emitted and the crystal structure is heated up. Heating of the material has adverse effects on both the light output (see section 2.1.3) and device lifetime [87].

As an first approximation we assume that photon emission transitions can occur from any energy level in the distribution of electrons in the conduction band $n(E)$ to any hole in the valence band $p(E)$. This is expressed in terms of the convolution, which can be viewed as an integral of all possible transitions

$$(n(E) * p(E)) = \int_{-\infty}^{\infty} n(E)p(E' - E)dE' \tag{2.9}$$

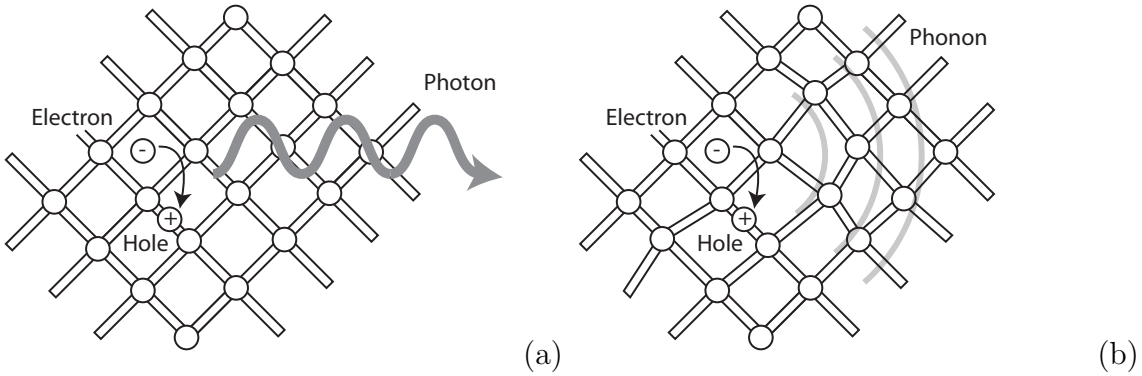


*Figure 2.2: Recombination of an electron and a hole in the lattice, releasing a photon(a). A non-radiative recombination causing energy to be dispersed as lattice vibrations, called phonons (b).*

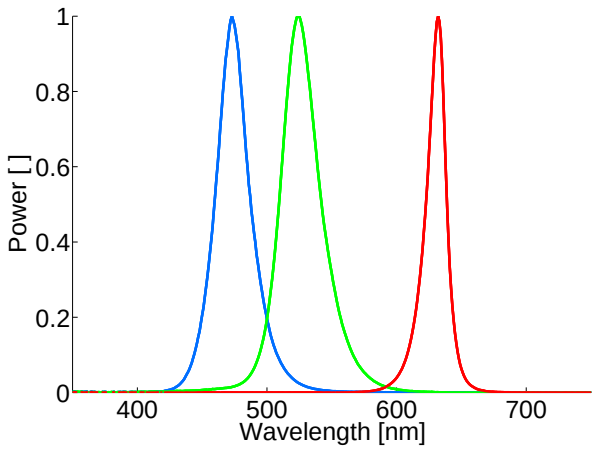


*Figure 2.3: Spectral power distributions of an RGB LED system.*

where $E'$ is a convolution variable, and the integration limits can be set near the band edge due to the exponential decrease in the Fermi-Dirac function. The energy $E$ of photons at a given wavelength $\lambda$ is given by $E = hc/\lambda$, where $h$ is Planck's constant and $c$ is the speed of light. This model produces a distribution similar to the spectral power distributions seen in spectral measurements of LEDs seen in figure 2.3. The figure shows typical examples of measured spectral power distributions of three different LEDs: Red, green, and blue. It is seen that the SPDs are narrow shapes that are slightly asymmetrical. This model is applied to measured spectra in section 5.2. If energy is introduced in the form of an incident photon or a high enough applied voltage electron-hole pair can be generated as is the case for photovoltaic cells and Zener diodes. Generation of electron-hole pairs will not be discussed in any further detail.

### 2.1.3 Non-Radiative Recombination

If no photon is emitted when the recombination occurs it is called *non-radiative recombination*. Instead of an emitted photon, the energy is dissipated as vibrations in the crystal lattice, as illustrated in figure 2.2 (b). Processes that can cause such recombination in the crystal bulk to become non-radiative are the *Auger effect* and *deep level recombination*. Deep level recombinations are caused by defects in the crystal such as foreign atoms, dislocations, interstitials, or any combination of these. The defects will in general have a different energy structure than the surrounding structure and can therefore present energy levels inside the band gab [85]. These deep levels become recombination sites, where light emission will be inhibited in the region near the defects. Single point defects are difficult to detect, but larger complexes of defects can be observed as dark spots in the radiance from the surface of an LED [134, p. 38]. With decreased photon emission defect sites will see increased heating from the phonon emission. Heating of the crystal increases the probability of migration, delocalization and other defect generation [143]. The increased number of defects will cause increased heating, creating more defects. This may create a self-amplifying process with accelerating degrading of the light output. This is consistent with results seen in lifetime tests [105]. Another way to detect degrading was reported by Pursiainen et al. who reported that changes in the number of defects could be monitored in the I-V curve of AlInGaP LED light sources [126].

Auger recombination can occur if another carrier is present at the recombination site. There is a finite probability that the recombination will transfer the energy to this third carrier, this electron will be exited to high energy states into the conduction band and similarly, holes will be transferred to low lying states in the valence band. The probability of this occurring is proportional to the carrier density cubed

$$R_{\text{Auger}} = Cn^3, \tag{2.10}$$

where $C$ is the Auger coefficient. This effect rises dramatically with current density due to the cubic relation with density and is generally considered one of the main causes for the so called *droop effect* where the efficiency decreases with increasing current density in most high power light-emitting diodes [136].

### 2.1.4 The p-n Junction

In this section the *pn-junction* will be discussed. The carrier density can be manipulated by doping a semiconductor material with dopants. In III-V materials donors come from group II, VI and acceptors from group IV. Different atoms can be used, for instance, InGaN can be doped with Zn [103] and with Si [19]. If we assume that dopants are fully ionized and disregard unintended impurities then the carrier concentration is equal to the doping concentration for n-type materials $n = N_D$ and for p-type materials $p = N_A$.

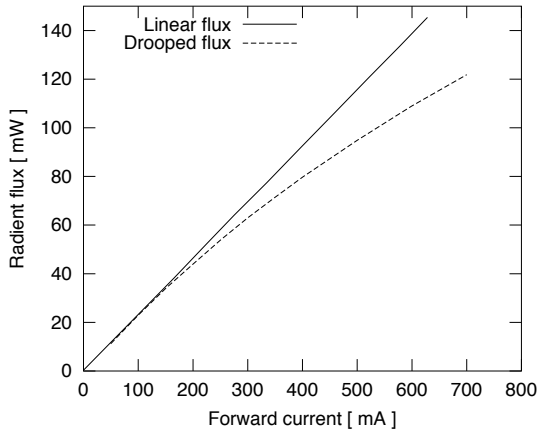


*Figure 2.4: The radiant flux, measured as a function of forward current, from a typical LED. This shows the droop i.e. the decrease from the linear behavior of an ideal device.*

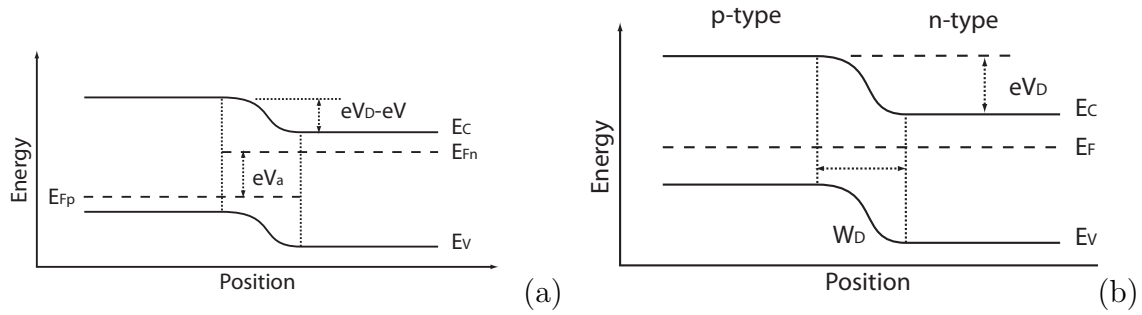


*Figure 2.5: Energy levels as a function of location in a p-n junction in equilibrium (a) and under forward bias condition (b). Showing the depletion width $W_D$ and the quasi-Fermi levels $E_{Fn}$ and $E_{Fp}$.*

When a p-type and a n-type material are joined, the *junction* between them becomes non-conductive. This is due to the fact that electrons move by diffusion from the n-type region into the p-type region and combine with the acceptors. Likewise, holes move from the p-type region to the donors in the n-type region. This leaves a region without charge carriers, where ionized donors and acceptors reside. This is called the depletion zone or space charge region. The dopants, fixed in the lattice and stripped of the carriers create an electric field that acts against the diffusion process. The width $W_D$ of the depletion zone is given by

$$W_D = \sqrt{\frac{2\epsilon}{e}\left(\frac{N_A + N_D}{N_A N_D}\right)(V_{bi} - V)}, \tag{2.11}$$

where $e$ is the electron charge $\epsilon$ the permittivity of the material and $V_{bi}$ is the built-in potential or diffusion voltage [16, sec. 4.5-4.7].

$$V_{bi} = V_D = \frac{k_B T}{e}\ln(N_A N_D / n_i^2). \tag{2.12}$$

This is the voltage produced by the space charge region, where ionized acceptors and donors have been stripped of electrons and holes.

### 2.1.5 Non-Equilibrium Conditions

When an external voltage $V_a$ is applied to the diode, the overall equilibrium is disturbed, but quasi equilibrium is assumed to hold in either material type (see figure 2.5 (b)). These equilibriums are represented by the quasi Fermi levels. The state occupancy in the conduction band is given by the Fermi distribution $f_n(E)$ in which non-equilibrium is defined by the thermal energy $k_B T$ and the quasi Fermi level $E_{fn}$, the distribution is therefore given by

$$f_n(E) = \frac{1}{e^{(E_{fn} - E)/k_B T} + 1}, \tag{2.13}$$

and likewise for the energy states occupied by holes with the quasi Fermi level $E_{fp}$.

$$f_p(E) = \frac{1}{e^{(E - E_{fp})/k_B T} + 1}. \tag{2.14}$$

The quasi Fermi levels are restricted by the applied voltage

$$E_{fn} - E_{fp} = eV_a. \tag{2.15}$$

We turn to the question of the current voltage (I-V) characteristics of a p-n junction. The relationship between current and voltage is described by the *Schockley equation*

$$I = I_S(\exp\left(\frac{eV_a}{k_B T}\right) - 1), \tag{2.16}$$

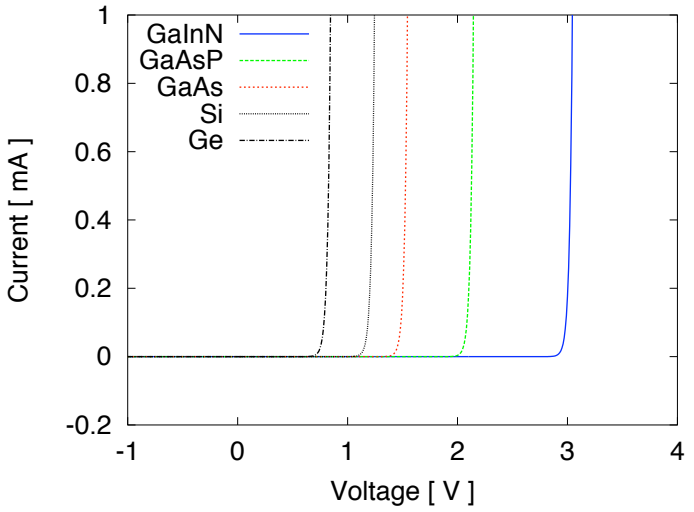


(a)

| Material | $E_g[V]$ |
|---|---|
| ZnO | 3.3 |
| GaInN | 2.9 |
| GaAsP | 2.0 |
| GaAs | 1.4 |
| Si* | 1.1 |
| Ge* | 0.7 |

(b)

*Figure 2.6: Example I-V curves for different semiconductor materials as given by equation (2.16) at 300 K (a). Band gabs of different materials (b). * Indirect band gab materials.*

where $I_S$ is the saturation current given by

$$I_S = eA\left(\sqrt{\frac{D_p}{\tau_p}}\frac{n_i^2}{N_D} + \sqrt{\frac{D_n}{\tau_n}}\frac{n_i^2}{N_A}\right). \tag{2.17}$$

where $A$ is the cross section area of the diode, $D_p$, $D_n$ are the diffusion coefficients and $\tau_p$ and $\tau_n$ are the carrier lifetimes. For the interesting case of forward bias where $V \gg k_B T$ then $(e^{eV/k_B T} - 1) \to e^{eV/k_B T}$ and equation 2.16 can be rewritten to:

$$I = eA\left(\sqrt{\frac{D_p}{\tau_p}}N_A + \sqrt{\frac{D_n}{\tau_n}}N_D\right)(\exp\left(\frac{e(V_a - V_D)}{k_B T}\right) - 1), \tag{2.18}$$

where $V_D$ is called the diffusion voltage given in equation (2.12). When the applied voltage becomes bigger than the diffusion voltage there is a sharp increase in current. This voltage is called the threshold voltage $V_{th}$ and we have that $V_D \approx V_{th}$. Figure 2.6 shows examples of the IV-curves of various semiconductors. The exponential increase in current at the threshold voltage is the reason why most LEDs systems use constant current power supplies. If the applied voltage deviates a small amount from the voltage giving the wanted current, the deviation in current will be exponentially larger, potentially either extinguishing the light or damaging the LED.

### 2.1.6 Temperature Variations

When an LED is operated with a forward voltage, heat is generated by non-radiative combination and photon absorption in the material. This injected heat increases

the temperature of the junction until the heat production is balanced with the heat transfer from the devise. When an equilibrium is reached the device will have reached its operation temperature. Raised junction temperatures have a negative effect on device lifetime, however in the following the short term effects on light emission are discussed.

The difference between the lowest energy in the conduction band $E_C$ and the highest energy in the valence band $E_V$ is called the band gab energy $E_g = E_C - E_V$. The band gab is dependent on the material composition and the temperature. By alloying different materials, the band gab can be manipulated. See the table (b) in figure 2.6 for examples of different alloys and the related band gab. For highly doped semiconductors the difference between Fermi energy and band edges is small compared to the band gab $V_{th} \approx eE_g$. The band gap energy $E_g$ changes with temperature. This dependence was found by Varshni [154] to be of the form:

$$E_g(T) = E_g(T = 0\,\mathrm{K}) - \frac{\alpha T^2}{T + \beta}, \tag{2.19}$$

where $E_g(T = 0\,\mathrm{K})$, $\alpha$ and $\beta$ are material specific fitting constants that are determined experimentally. The formula is purely empirical, but offers a good approximation for the band gab energy with.Typical values for $\alpha$ are $8{\cdot}10^{-4}\mathrm{eVK}^{-1}$ and $\beta$ range from 100 - 200 K [49] A more recent approach by O'Donnell and Chen, based on phonon coupling has found another relation

$$E_g(T) = E_g(0) - S\langle\hbar\omega\rangle[\coth(\langle\hbar\omega\rangle/2k_BT) - 1], \tag{2.20}$$

where $\langle\hbar\omega\rangle$ is the average phonon energy and $S$ is a coupling constant [112]. However, both approaches are empirically based and has similar results in the temperature regime around room temperature.

The temperature dependence of the applied voltage is derived from equation (2.16)

$$V_a(T) = \frac{k_BT}{e}\ln\frac{I}{I_S} + \frac{E_g(T)}{e}. \tag{2.21}$$

From equation (2.19) and (2.20) it is clear that the band gab will decrease with rising temperatures, while the first term in equation (2.21) will increase with temperature. The change in the band gab is the dominant effect in equation (2.21). Thus the forward voltage decreases for a given constant current for increasing temperatures.

If the junction is forward biased with a voltage well above the threshold a high current will flow and the junction is heated from non-radiative recombination and ohmic resistance from leak currents. The junction temperature will rise and stabilize at a certain point. The junction temperature is given by

$$T_J = R_\theta P + T_{amb}, \tag{2.22}$$

where $R_\theta$ is the thermal resistance between the junction and the ambient, $P = IV_a$ is the electrical power and $T_{amb}$ is the ambient temperature [55, 106].

## 2.2 Empirical Models

The preceding section describe the relatively complicated functions and how many material parameters are needed for the model based on the the solid state principles. Even more elaborate models exist, as presented by Eliseev et al. [44]. This complexity has inspired the use of empirical models to reduce the complexity and describe the behavior, using a small number of parameters. Several models have been suggested, which are based on general functions that can be fitted with some accuracy to the spectral power distributions. In this section, two models for the spectral power distributions of single color LEDs are investigated. The simplest model use a single Gaussian function as used by Chhajed et al. [18] for simulations of LED spectra. A model using a double Gaussian distribution was suggested by Man and Ashdown [92].

The convolution in equation (2.9) omits some of the physical effects that occur in a typical LED structure, such as the effects of momentum conservation for optical transitions and quantum well structures etc. To account for these effects the density of states in equation (2.2) and (2.23) may be modified by a non-parabolic function

$$\rho_n(E) \propto (E - E_g)^{(3y_n/2)-1}, \ \rho_p(E) \propto (-E)^{(3y_p/2)-1} \tag{2.23}$$

where $y_n$ and $y_p$ describe the non-parabolic energy dependence of the conduction- and valance band respectively, as suggested by Smith and Brennan [138, 139]. We assume here that the described correction of the parabolicity will approximate various other effects that can shape the SPD.

### 2.2.1 Gaussian Models

A simple way to model the SPD of an LED is a single normal- or Gaussian distribution, as it resembles most LED spectra to a certain degree [18]. The Gaussian distribution $f$ as a function of wavelength $\lambda$ is given by

$$f(\lambda) = ae^{-(\lambda-\lambda_0)^2/2c^2}, \tag{2.24}$$

where the amplitude $a$, centre wavelength $\lambda_0$ and width $c$ are functions of the junction temperature *and* current, which gives

$$f(\lambda) = a(I, T_J)e^{-(\lambda-\lambda_0(I,T_J))^2/2c(I,T_J)^2}. \tag{2.25}$$

This represents a simple symmetric distribution. However, LED spectra are not generally symmetric, which limits the applicability of single Gaussian functions. To account for this, one can use a double Gaussian function as done by Man and Ashdown [92], given by the following expression

$$f(\lambda) = a_1e^{-(\lambda-\lambda_1)^2/2c_1^2} + a_2e^{-(\lambda-\lambda_2)^2/2c_2^2}, \tag{2.26}$$

where $a_1, \lambda_1, c_1, a_2, \lambda_2, c_2$ are fitting parameters. For generality we must assume that each of these parameters are functions of $I$ and $T_J$. These two Gaussian models and model obtained from equation (2.9), can be scaled to fit the light output. The scaling factor can be modeled by the equations given in the following section. A modified double Gaussian model was presented by Ohno [114], which has not been considered in this work, but could be included in more comprehensive study of LED spectral models.

### 2.2.2 Light Output

The total radiant flux $\Phi$ from an LED is influenced by current $I$ and junction temperature $T_J$ and a number of material and device characteristics, such as the crystal defect density, dopant concentration, current leaks etc. Since the materials used might be unknown, we must use empirical models to describe the light output corresponding to a given set of $I$ and $T_J$. The emitted light power as a function of temperature $P(T)$ has been empirically determined to be an exponentially decaying function

$$\Phi(T) \propto \Phi(0)e^{(-T/T_0)}, \tag{2.27}$$

where $T_0$ is a material specific constant and $\Phi(0)$ can be interpreted as the power emitted at 0 K [133, p. 97].

We now turn to consider how the light output is dependent on the current. Assuming 100 % quantum efficiency, the light output would be directly proportional to the current, since every electron-hole pair would be converted to a photon. However, it is seen that efficiency decreases with increasing current, the so called *droop* effect. Different effects has been suggested as the cause for this efficiency decrease. Examples of such effects are Auger recombinations, surface recombinations, and defect recombinations [73]. Incorporating all these effects in a purely empirical relation between output power and current, we suggest using a polynomial description

$$\Phi(I) = A_0 + A_1 I + A_2 I^2 \tag{2.28}$$

where $A_0, A_1, A_2$ are fitting constants. The intersection $A_0$ should of cause be zero as no current will give zero light output. The proportional term $A_1$ can be interpreted as the linear relation between forward current and light output, that can be observed at low currents. The square term $A_2$ can then be used to describe the droop seen in figure 2.4. The usefulness of equation (2.28) is shown in section 5.1. Gardner et al. [50] found that the effect is unrelated to heating of the junction.

## 2.3 Summary

In the preceding sections we have seen how the theoretical background for LED technology can be used to create models for the spectral power distribution of the emitted

light. Light emission requires radiative recombination while non-radiative recombination decrease the light output. It is discussed how direct band gab semiconductors can be used as light sources by constructing a p-n junction and applying a voltage in the forward direction of the device. The emergence of the spectral power distribution and its dependence on a number of parameters has been discussed. However, the number of parameters and the complexity of these calculations has led to formulation of simplified models, approximating the spectral emission. The Gaussian models are purely empirical and based on simple similarity with the measured spectra. It is the aim of this work to compare the models presented. In Chapter 5 theses models will be studied by characterizing LED devices with respect to changes in temperature and current and compare model behavior under these changes. Other models are available, such as the ones presented by Eliseev et al. [44] and Ohno [114] which could be studied in a similar manner. Chapter 4 discusses how the spectral power distributions from LEDs presented in this work, were measured accurately while current and temperature was held varied.

# Chapter 3

# Light Quality

The subject of this chapter is light quality and the quantitative measures used for evaluation of light quality from light sources. When considering illumination for use by humans, one must consider the qualitative aspects of how the lighting is perceived. In order to characterize and optimize lighting systems with regard to perceived quality, a number of quantitative metrics, developed by lighting organizations, that are used in this work are presented in the following.

When quantifying perceptual experience there is an inherent component of subjectivity, due to both the physiological differences of individuals and the way the human visual system interprets light stimulus. Perceptual responses to light stimuli is therefore standardized from statistical analysis of several human subjects and represents an averaged approximation to general human experience. In this work, the recommendations and standards set forth by the *International Commission on Illumination* (CIE) is used. The definitions in the following sections are to be regarded as conventions, formulated by the lighting related organizations, guided by scientific measurements and theoretical considerations, but they are also based on tradition and practical feasibility. Most notable is the discussion relating to the color rendering index (CRI), where several authors have pointed out problems regarding the current color rendering metric in relation to LED light sources [131, 11, 34, 144]. Other metrics has been proposed such as the color quality scale [36] and the supplemental gamut area index [128]. Furthermore, the CIE has recommended that the CRI be supplemented by other qualitative measures, until it can be fully replaced by a more accurate and useful metric [26]. However, since no standardized method exist, this practice has not been employed in this work

When considering the light quality of a light source, there are a number of other characteristics that can be interpreted as quality parameters. The spatial distribution of light, is generally required to have a high homogeneity of intensity and color in the illuminated field, as vastly varying illumination intensities can be disturbing in for instance task lighting. In relation to time dependent phenomenon in lighting, there is the issue of unwanted low frequency visual flicker [155], glare [47], changes

over longer times in LEDs caused by heating of the junction [87] and changes in light output caused by material degradation occurring over the lifetime of the device. For clustered light sources, there is the further issue of colored shadows, occurring when the differently colored light sources, set up together, cast differently colored shadows at different angles. Attention to these issues is important when designing a lighting solution, but they will not be treated in detail in the following.

This chapter begins with a review of basic photometric concepts related to human light perception. Chromaticity and standard color maps are treated in section 3.2. Additive color mixing is reviewed in section 3.3. Color temperature and *correlated color temperature* (CCT) are discussed in section 3.4. Chromaticity difference is treated in section 3.5. The calculation of the color rendering index is discussed in section 3.6. Thresholds of visual perception are discussed in section 3.7. Lastly, a summary is given in section 3.8.

## 3.1 Basic Photometric Concepts

*Photometry* is the study of how the human visual system responds to light stimulus. The detailed structure of the eye, optic nerve, and visual cortex is beyond the scope of this work. In the following, the *human visual system* refers to the entire visual system seen as whole, from light sensitive cells, to the cognitive signal processing causing perception of colors. We consider color vision, with emphasis on spectral sensitivity, to be able to characterize spectral properties of light sources.

The following consider the visible range from around 350 to 750 nm, since radiation with wavelengths outside this range has no direct influence on visual performance. The basic unit of photometry is the unit of *luminous intensity*, the *candela*. Originally based on a standard candle, the newest definition was adopted by *General Conference on Weights and Measures* in 1979:

> "The candela is the luminous intensity, in a given direction, of a source that emits monochromatic radiation of frequency $540 \cdot 10^{12}$ hertz and that has a radiant intensity in that direction of 1/683 watt per steradian." [15, p. 116]

The definition is generalized to be applicable to any spectral power distribution by employing a generalization of the spectral sensitivity of the human eye. For a source with radiant intensity $I$ the luminous intensity at a given wavelength $\lambda$ is

$$I_v(\lambda) = 683.002 \frac{\mathrm{lm}}{\mathrm{W}} V(\lambda) I(\lambda), \tag{3.1}$$

where $V(\lambda)$ is the luminosity function defining the eyes sensitivity, also called $\bar{y}(\lambda)$. This is defined by the *CIE standard photometric observer* (CIE 1931) [21] and shown

| Quantity | Unit | Symbol | Description |
|---|---|---|---|
| Radiant flux | W | $\Phi$ | Radiated power. |
| Radiant intensity | W/sir | $I$ | Power per unit solid angle |
| Radiance | W/(sr·m$^2$) | $L$ | Power emitted from an area in a solid angle. |
| Irradiance | W/m$^2$ | $E$ | Power received per surface area. |
| Luminous intensity | cd | $I_v$ | Base unit - Perceivable light in a solid angle. |
| Luminous flux | lm(cd sr) | $\Phi_v$ | Total perceivable output of a light source. |
| Luminance | cd/m$^2$ | $L_v$ | Light emitted from an area in a solid angle. |
| Illuminance | lx (lm/m$^2$) | $E_v$ | Incident luminous flux per area. |
| Luminous efficacy | lm/W | | Luminous flux per electrical power. |
| Luminous efficiency | lm/W | | Luminous flux per radiated optical power. |

*Table 3.1: Important units of radiometry and photometry.*

in figure 3.1. The pre-factor stems from the conversion between frequency and wavelength. For a light source, the net amount of perceivable light is defined by the luminous flux, given by the integration or summation over all the spherical coordinates and $\lambda$

$$\Phi_v = \int_0^{2\pi} \int_0^{\pi} \int_{380\,\mathrm{nm}}^{730\,\mathrm{nm}} I_v(\lambda, \theta, \varphi) \sin(\theta) d\lambda d\theta d\varphi, \tag{3.2}$$

where $\theta$ and $\varphi$ are the spherical coordinates of a sphere around the light source. The integral over $\lambda$ from 380 nm to 730 nm denotes integration across the visible spectrum. When dealing with visual responses the integrals will yield zero outside the visual range and are therefore in the following given as indefinite integrals. Other useful radiometric and photometric quantities and units are given in table 3.1.

An important characteristic of an LED is its *luminous efficacy*, the ratio between luminous flux and electrical input power $\Phi_v/P_{in}$. The term is sometimes confused with luminous efficiency that describes the ratio between luminous flux and radiant flux

$$\frac{\Phi_v}{\Phi} = \frac{\int V(\lambda) S(\lambda) d\lambda}{\int S(\lambda) d\lambda}. \tag{3.3}$$

Which gives an indication of the visual usefulness of the spectral power distribution (SPD) $S(\lambda)$. The first definition is used throughout this work, as it is indicative of the possible energy savings. The second definition can be used to describe the perceptual usefulness of the emitted light.

The human eye has two kinds of light sensitive cells: The cone cells functioning in normal lighting conditions (photopic vision) which are responsible for color vision, and rod cells functioning in low level lighting $10^{-2}$ to $10^{-6}$ cd/m$^2$ (scotopic vision) and in the peripheral visual field. To be able to distinguish between different colors, an average human being has three distinct types of cone cells, responding to long, middle, and short wavelengths in the visible spectrum, corresponding to red, green, and blue, roughly speaking [166, sec. 2.2.7].

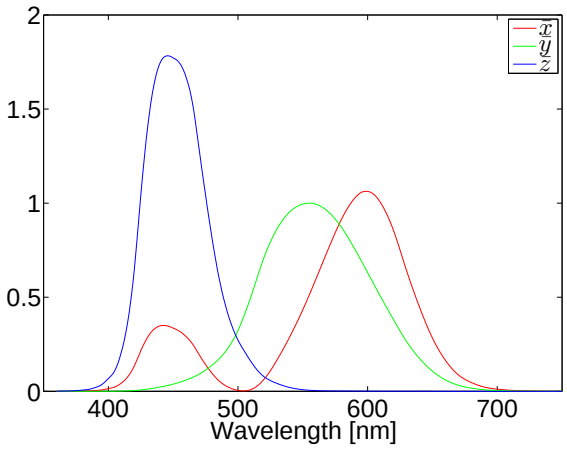


*Figure 3.1: Color matching functions of the CIE 1931 standard observer [20].*

To quantify color experience the colorimetric response to incident light has been measured by various authors by way of color matching [56, 163]. From these measurements the color matching functions (CMF) was formalized by the CIE in the standard colorimetric observer. They are valid in a 2° field of view and assumes negligible rod cell response. However, they serve as the underlying definitions used in most applied photometry [166, p. 131].

The color matching functions $\bar{x}(\lambda), \bar{y}(\lambda), \bar{z}(\lambda)$ are shown in figure 3.1. A given spectral power distribution $S(\lambda)$ incident on the eye will cause the visual system to respond and the colors perceived can then be described in the form of a set of tristimulus values defined as the inner product of the color matching function and the spectral stimuli:

$$X = \int \bar{x}(\lambda)S(\lambda)d\lambda, \tag{3.4}$$

$$Y = \int \bar{y}(\lambda)S(\lambda)d\lambda, \tag{3.5}$$

$$Z = \int \bar{z}(\lambda)S(\lambda)d\lambda. \tag{3.6}$$

A triplet of these quantities corresponds to a unique color experience and any two spectral power distributions with identical corresponding $(X, Y, Z)$ values will cause a similar experience, these are known as metamerisms[166, Sec. 3.8]. The tristimulus values can be loosely interpreted as the red, green, and blue components that human color perception is built upon.

## 3.2 Chromaticity

From the tri-stimulus values, the *chromaticity* is derived. The chromaticity is used to specify the "color" of a light source independently of the luminous intensity of the light. The tristimulus values are normalized and a dimension is removed which enables a representation in standardized two-dimensional diagram, called a *chromaticity diagram*. This intensity independence becomes invalid in cases of high light levels where receptor saturation occurs, known as glare, or in low light levels where the cone response is diminished and rod cell response is not negligible, called the mesopic and scotopic vision regimes.

Given the tri-stimulus values the CIE 1931 chromaticity coordinates $x$ and $y$ can be calculated. These coordinates uniquely describe the chromaticity of the light source and are given by

$$x = \frac{X}{X+Y+Z}, \tag{3.7}$$

$$y = \frac{Y}{X+Y+Z}, \tag{3.8}$$

$$z = \frac{Z}{X+Y+Z} = 1 - x - y. \tag{3.9}$$

To be able to visualize the colors of the chromaticity diagram an array of chromaticity points has been converted to sRGB color triplets and plotted, the resulting diagram is shown in figure 3.2 (a). Chromaticities considered white are located near the equal intensity point at the center of the diagram $x, y = \{1/3, 1/3\}$ which is also close to the daylight illuminant D65, located at $x, y \approx \{0.31, 0.33\}$. However, the general definition of white light is given by the chromaticities of black body radiation in various manifestations, which are discussed in sections 3.4 and 3.6. Moving towards the edges of the diagram constitute moving towards higher color saturation, the edge of the chromaticity diagram representing monochromatic light sources, in the figures annotated with te wavelength in nanometer. The line connecting the blue and red area is sometimes referred to as the purple line. The chromaticities along this line are combinations of red and blue and do not refer to any monochromatic light source, but is an abstraction of the color description. The CIE 1931 chromaticity diagram is non-uniform, meaning that the geometric distance between just perceptible differences in chromaticity are uneven across the diagram, as shown by MacAdam [90], also see section 3.7.

### 3.2.1 Uniform Color Spaces

The CIE 1960 uniform color space (CIE 1960) [22] is an approach to a color space where all geometric distances within the diagram are approximately proportional to

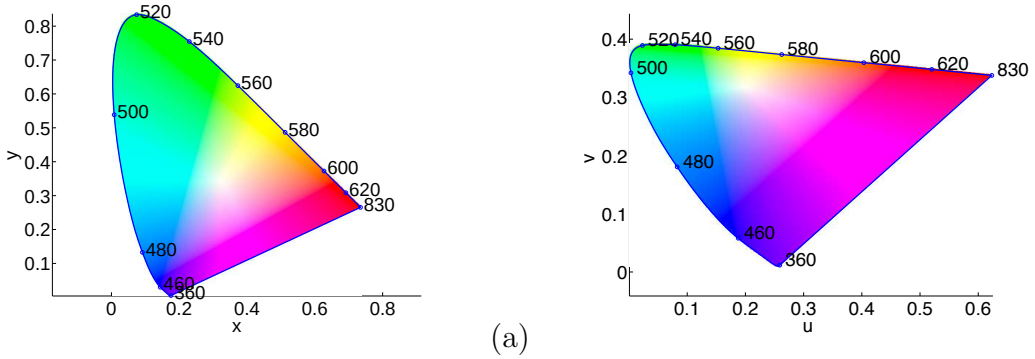


*Figure 3.2: The non-uniform CIE 1931 chromaticity diagram (a) and the CIE 1960 chromaticity diagram (b). Wavelengths of monochromatic sources annotated along the boundary locus. The plotted colors are representative within the sRGB gamut but will differ depending on the display device or printing method.*

the perceived changes in chromaticity. The CIE 1960 chromaticity coordinates $u, v$ of a light source are defined from the tri-stimulus values $X, Y$ and $Z$

$$u = \frac{4X}{X + 15Y + 3Z}, \tag{3.10}$$

$$v = \frac{6Y}{X + 15Y + 3Z}, \tag{3.11}$$

where the pre-factors were determined experimentally by Judd [69] and simplified by MacAdam [91] for the adoption of the color space as a standard by the CIE. The CIE 1960 has since been replaced by the newer recommendations of the CIE 1976 [132, 25], where the chromaticity coordinates are transformed by

$$u' = u \tag{3.12}$$

$$v' = \frac{3}{2}v. \tag{3.13}$$

The use of a uniform color space is important, when describing perceived deviations from target chromaticities in a consistent manner across the entire chromaticity diagram. However, this two-dimensional description cannot be used to describe difference in luminance. When calculating color differences for objects with varying luminance one can use the CIE 1964 uniform color space $(U^*, V^*, W^*)$ described by the transformation

$$U^* = 13W^*(u - u_0), \tag{3.14}$$

$$V^* = 13W^*(v - v_0), \tag{3.15}$$

$$W^* = 25(Y)^{1/3} - 17, \tag{3.16}$$

where $(u, v)$ are the uniform chromaticity coordinates, $Y$ is the trichromatic value proportional to the luminosity, and $(u_0, v_0)$ is the chromaticity of the white point or reference illuminant [23, 165].

## 3.3 Color Mixing

Given more than one light source with distinct chromaticities, the light can be combined by additive color mixing [166, p. 118] [133, p. 234]. Given $N$ light sources with spectral power distribution $S_n(\lambda), n = \{1, 2, 3 \dots N\}$, the tristimulus values becomes

$$X = \int \bar{x}(\lambda)(S_1(\lambda) + S_2(\lambda) + S_3(\lambda) + \ldots + S_N(\lambda))d\lambda, \tag{3.17}$$

$$Y = \int \bar{y}(\lambda)(S_1(\lambda) + S_2(\lambda) + S_3(\lambda) + \ldots + S_N(\lambda))d\lambda, \tag{3.18}$$

$$Z = \int \bar{z}(\lambda)(S_1(\lambda) + S_2(\lambda) + S_3(\lambda) + \ldots + S_N(\lambda))d\lambda. \tag{3.19}$$

These sums can then be rewritten in terms of the individual light sources with factors

$$L_n = \int \bar{x}(\lambda)S_n(\lambda) + \bar{y}(\lambda)S_n(\lambda) + \bar{z}(\lambda)S_n(\lambda)d\lambda, \tag{3.20}$$

that determine the chromaticity coordinates $x$ and $y$ from equation (3.7) and (3.8)

$$x = \frac{\sum^N x_n L_n}{\sum^N L_n}, \tag{3.21}$$

$$y = \frac{\sum^N y_n L_n}{\sum^N L_n}, \tag{3.22}$$

where $x_n, y_n$ is the chromaticity coordinates of the $n$th light sources. The area in the chromaticity diagram defined by all possible chromaticities is the *gamut* of the system. Within the gamut, any chromaticity can be replicated by adjusting the light output of individual light sources. Figure 3.3 shows an example of three-color mixing within the gamut. The CIE 1976 chromaticity of a set of SPDs is then give by equations (3.21), (3.22), (3.12), and (3.13).

## 3.4 Correlated Color Temperature

The human visual system has evolved to adapt to naturally occurring light sources, such as the sun, reflected light from the moon, and combustion of organic material etc. This means that our sensory system is finely tuned to illumination from the phenomenon of incandescence, where heated objects radiate energy according to the temperature of the object. A body of atoms, heated to an absolute temperature $T$

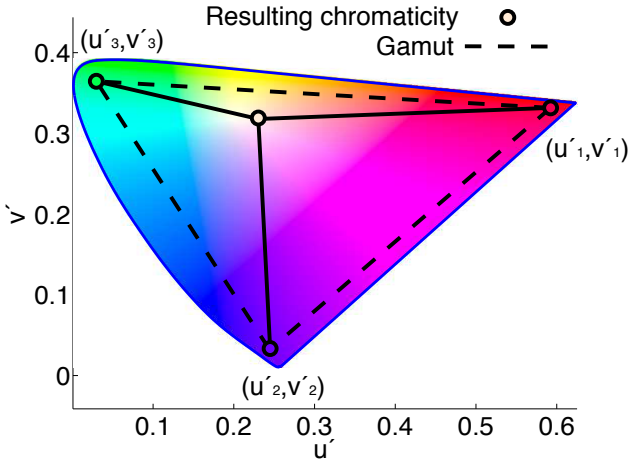


*Figure 3.3: Color mixing of three light sources with chromaticities $(u'_n, v'_n)$ within the gamut of the three light sources.*

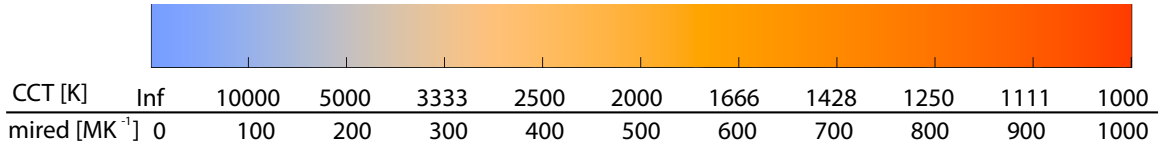


*Figure 3.4: A representation of the chromaticities of light sources along the Planckian locus, shown with associated color temperatures and the perceptible uniform color temperature scale mired $MK^{-1}$.*

will radiate electromagnetic radiation known as the blackbody radiation. Planck's law gives the spectral power distribution of this radiation. Here $I$ is the radiant intensity from an object with temperature $T$, which is given as a function of wavelength and temperature

$$I(\lambda, T) = \frac{2hc^2}{\lambda^5} \frac{1}{e^{hc/\lambda k_B T} - 1}, \tag{3.23}$$

where $h$ is Planck's constant, $k_B$ the Boltzmann constant and $c$ is the speed of light. For temperatures above 500 - 600 °C, a significant portion of the radiation becomes visible to the human eye as a red glow, and for increasing temperatures the color will tend towards a bluish white, as shown in figure 3.4. Spectral power distributions of Planckian radiators can be seen in figure 3.7 (a).

Using equations (3.23), (3.4),(3.5), (3.6), (3.10) and (3.11), the chromaticity of the blackbody radiation for a range of temperatures can be calculated. Each of these chromaticities are then designated with the corresponding *color temperature* $T_C$ commonly given in Kelvin. These chromaticity points constitute the Planckian locus. In figure 3.5, the locus is plotted in CIE 1960 chromaticity diagram for a range of temperatures. The familiarity of such light sources and the temperature scale means that comparing

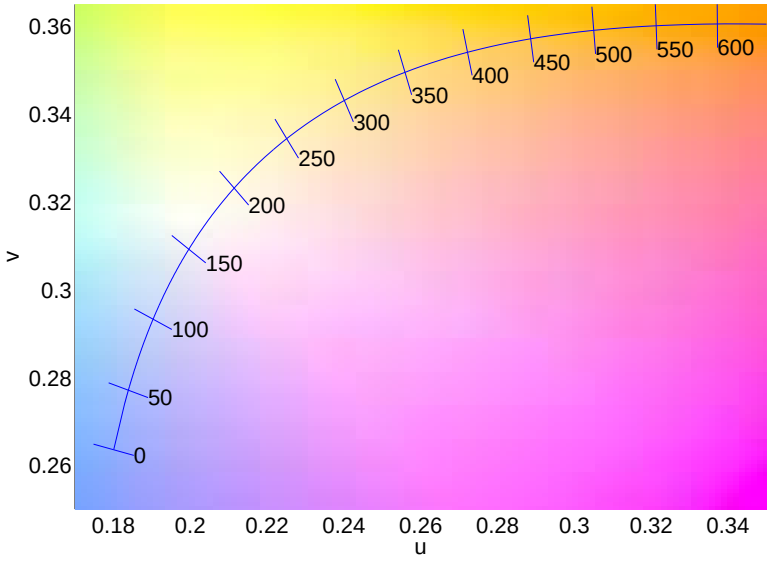


*Figure 3.5: A section of the CIE 1960 uniform color space, showing the isotherms along the Planckian locus marked with the corresponding mired values. Examples of isothermal lies are marked at 50 mireds intervals.*

a given light source to a Planckian radiator can be intuitively used to classify light sources from their resemblance to a black body radiator with a similar chromaticity. The method of describing a perceptual qualitative aspect of a light source by its equivalent temperature radiator was first described by Priest in 1923 [124].

For light sources that are not Planckian radiators, the color temperature cannot be used directly, instead the correlated color temperature is used. It is used to describe white test light source and it is defined as the temperature of a blackbody radiator with a spectrum, that has its associated chromaticity point closest to the chromaticity of the test light source in the CIE 1960 uniform color diagram. This causes chromaticities with similar CCT to be located on straight isothermal lines perpendicular to the Planckian locus in the CIE 1960 diagram. The lines perpendicular to the Planckian locus with chromaticites $(u_T, v_T)$, have the slope

$$t_T = -\frac{du_T}{dv_T}. \tag{3.24}$$

The isotherms and the relevant section of the CIE 1960 color space can be seen in figure 3.5. Although replaced as the standard color map, the CIE 1960 color map was kept as the uniform chromaticity coordinate system in relation with CCT calculations to ensure consistent results [166, p. 225]. The values of $c$ and $h$ have been measured with higher accuracy following the issuing of the standard in 1931. The change, however, is of small practical importance in this context [166, p. 226].

The CCT has the drawback that a change in temperature and the perceived change in chromaticity is reciprocally related [125]. Consequently, smaller numeric differences in CCT at high CCT values may be difficult to intuitively compare with similar numeric differences at lower values. Changes in the color temperature is related to the human perception of the change by

$$M = \frac{10^6}{T}, \tag{3.25}$$

where $M$ scales uniformly across the temperatures of interest, is measured in $\mathrm{MK}^{-1}$ and is commonly referred to as mired. The mired scale is uniform in the same way as the CIE 1960 color space, so that a change of one mired is equal to the same perceived change across the range of temperatures [166, p. 224].

## 3.5 Chromaticity Difference

The qualitative issue that humans react negatively to illumination that significantly deviates from the Planckian chromaticity curve (see figure 3.5) is quantified by the *chromaticity difference* $\Delta_{u,v}$ [24]. It is calculated as the distance between the chromaticity of the test light source and the chromaticity of a reference light source with the same CCT. It is given by the Pythagorean distance in the CIE 1960 chromaticity diagram.

$$\Delta_{u,v} = \sqrt{(u_t - u_r)^2 + (v_t + v_r)^2}, \tag{3.26}$$

where $(u_r, v_r)$ and $(u_t, v_t)$ are the chromaticity of the reference and test illuminant respectively. The chromaticity difference, also called $DC$, is a measure of how "white" the light is. If the chromaticity of a test light source is too far above the reference locus, the light will appear to have a greenish tint (high values of $v$ and low values of $u$ in figure 3.5). Similarly, if the chromaticity is below the Planckian locus, the light will seem pinkish for high $u$ values and $v$ low values. From this we see that $\Delta_{u,v}$ should be minimized for increased light quality. By using the $Duv$ defined by ANSI C78.377-2008 [4] the position above or below the Planckian locus is noted by applying a sign to the distance. However, the $Duv$ has not been approved by the CIE, and has therefore not been used in this work.

The color rendering index specification contains a recommendation for the maximum value of $\Delta_{u,v}$ for the illumination to be considered white. The light test light source is recommended to maximally deviate from the chromaticity of the reference by $\Delta_{u,v} < 5.4 \cdot 10^{-3}$, corresponding approximately to 15 mireds along the Planckian locus [166, p. 173]. If the chromaticity difference is higher, there is a greater possibility that observers will find the light tinted with green, yellow, or magenta. In the following, the recommendation is used as a limit in a stricter sense, so that light sources outside the allowed area are considered non-white and unusable for general illumination. The

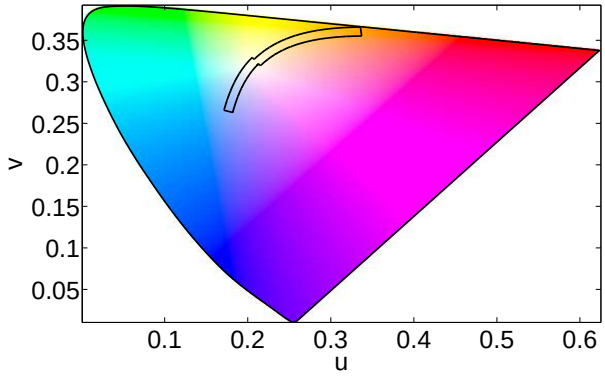


*Figure 3.6: The area of recommended chromaticities under the CRI for correlated color temperatures from 1515 K to $\infty$ K in the CIE 1960 chromatic diagram.*

area where $\Delta_{u,v}$ is below the threshold is shown in figure 3.6. The kink in the curves defining the area is caused by the shift in reference light source (see section 3.6.1).

When working in CIE 1964 uniform color space, where $U^*, V^*, W^*$ are calculated from equations (3.15), (3.16), (3.16) the color difference is also calculated from the geometric distance

$$\Delta E = \sqrt{(U_r^* - U_t^*)^2 + (V_r^* - V_t^*)^2 + (W_r^* - W_t^*)^2}, \tag{3.27}$$

where the subscripts $r$ are for the reference illuminant and $t$ denotes the test illuminant. The color difference $\Delta E$ is not independent on the luminosity.

## 3.6 Color Rendering Index

Given a light source, used for lighting in relation to human visual activity, one of the key quality criteria is how well it renders colors of illuminated objects for the observer. The most widely used standard for quantifying this is the *color rendering index* (CRI) specified by the CIE [24]. The CRI of a white light test source is calculated by comparing the color rendering of a reference light source with the test light source. The spectral power distribution from the test light source is reflected off a set of standard test color samples (TCS) and the difference in the color, in the $U^*, V^*, W^*$ color space, of the reflected light is compared to the corresponding color from the reference light source reflected of the color samples. The purpose of this is to test how much the spectral composition of the illumination from the test source resembles the illumination from a corresponding reference, which is either a blackbody radiator or a daylight simulator. To increase the intuitive understanding of the index by laypersons the maximum rating is defined to be 100 for the reference. Color deviations are

scaled by a factor and subtracted from 100, so that light sources differing from the corresponding reference has indices lower than 100. The following is an overview of the calculation of the CRI for a light source with known spectral power distribution.

### 3.6.1 Reference Illuminants

Due to the historic prevalence of blackbody radiators for lighting, they have been used to define the reference for color rendering. The Planck distribution in equation (3.23) is very similar to the spectrum of incandescence from filament based light bulbs. The spectral power distribution of blackbody radiation from sources at varying temperatures is depicted in figure 3.7 (a). The reference light source is selected by calculating the CCT of the test light source and then use a reference with the same CCT. For correlated color temperatures below 5000 K, the corresponding Planckian radiator of temperature $T = T_C$ described by equation 3.23 is used as a spectral reference light source.

Incandescence spectra from arbitrarily high temperatures have not been realized in any practical way. Therefore the reference light sources for higher color temperatures were chosen to be related to measured spectral distributions of daylight. The daylight simulator which is used as a reference in the CIE CRI for color temperatures above 5000 K is the *Standard illuminant D*. There are various other standardized illuminants [166, section 3.3.4-5], however, some are obsolete and/or fall outside the scope of this investigation.

#### Standard Illuminant D

The sun is, to a large extent, a blackbody radiator with most of the radiation in the visible range, given that it has a surface temperature of approximately 5800 K. However, atomic absorption lines of various chemical elements present in the sun and different phenomenon in the atmosphere of the earth, such as Rayleigh scattering of blue light, causes the light received on the surface of the earth to be different from the ideal blackbody radiation. Due to the naturally occurring variations in daylight, the standard illuminant for temperatures above 5000 Kelvin has been chosen to be different phases of daylight. It is described by the daylight simulation called the D illuminant. It was found by Judd et al. [67], that the chromaticity of daylight follows a simple parabolic function

$$y_D = -3.000x_D^2 + 2.870x_D - 0.275, \tag{3.28}$$

where $x_D, y_D$ are CIE 1931 coordinates of the D illuminant. The chromaticity of a D illuminant with a given color temperature $T_C$ is then located at the intersection between the particular isotherm with $T_C$ and the curve defined by (3.28). The daylight SPD can then be approximated by the linear combination of three vectors $S_0(\lambda)$, $S_1(\lambda)$

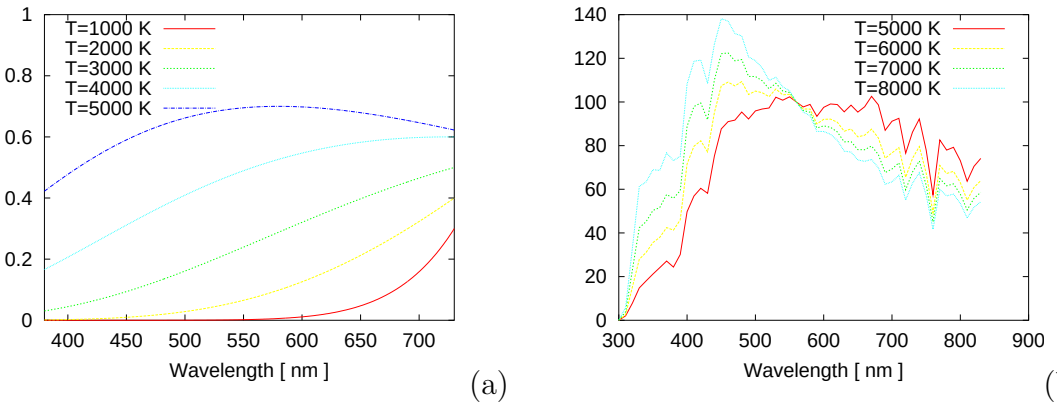


*Figure 3.7: Standard illuminants at correlated color temperatures from 1000 to 8000 K. The Planckian radiators (a) and standard illuminant D (b).*

and $S_2(\lambda)$ found by Judd et al. [70] from measurements by Henderson and Hodgkiss [59, 60]

$$S(\lambda) = S_0(\lambda) + M_1 S_1(\lambda) + M_2 S_2(\lambda), \tag{3.29}$$

where, $M_1$ and $M_2$ are scalars defined by

$$M_1 = \frac{-1.351 - 1.7703 x_D + 5.9114 y_D}{0.0241 + 0.2562 x_D - 0.7341 y_D} \tag{3.30}$$

$$M_2 = \frac{0.0300 - 31.4424 x_D + 30.0717 y_D}{0.0241 + 0.2562 x_D - 0.7341 y_D}, \tag{3.31}$$

where $x_D, y_D$ are found from equation (3.28). Examples of the D illuminant at different temperatures are shown in figure 3.7 (b) [166, p. 146]. The simplest way to find the corresponding reference distribution for a given SPD is then to find the point on the curve given by equation (3.28), which is closest to the relevant point on the Planckian locus. This gives $(x_D, y_D)$ which can be used to calculate the reference SPD. It should be noted that the D illuminants are located above the Planckian locus in the chromatic diagram. This causes a kink in the curve where $\Delta_{u,v} = 0$ at $T_C = 5000$ K, as seen in figure 3.6.

### 3.6.2 Chromatic Adaptation

When viewing a sample with a certain chromaticity, the visual response is affected by the surroundings and pre-exposed stimuli. The phenomenon is known as *chromatic adaptation* and is responsible for humans being able to distinguish and recognize colors in vastly different lighting conditions. Von Kries [79] suggested that the adaptation of one part of the retina would affect the overall trichromatic sensitivity represented by a linear transform so that stimuli exposed under condition $A$ and stimulus exposed

under viewing condition $A'$ are related by

$$\begin{pmatrix} X \\ Y \\ Z \end{pmatrix} = T_{AA'} \begin{pmatrix} X' \\ Y' \\ Z' \end{pmatrix}, \tag{3.32}$$

where $T_{AA'}$ is an invertible matrix relating condition $A$ and $A'$ and $X', Y', Z'$ are the transformed tri-stimulus values. Several experimental studies have found problems with this assumption [166, sec. 5.12.2]. However, the transform is still used to compensate for the effect of the difference between the test and reference illuminant in the color rendering index calculation. The chromaticity $u_{c,i}, v_{c,i}$ of light reflected off samples numbered $i$ under a reference illuminant with chromaticity $u_r, v_r$ is given by

$$u_{c,i} = \frac{10.872 + 0.404(c_r/c_t)c_{t,i} - 4(d_r/d_t)d_{t,i}}{16.518 + 1.481(c_r/c_t)c_{t,i} - (d_r/d_t)d_{t,i})}, \tag{3.33}$$

$$v_{c,i} = \frac{5.52}{16.518 + 1.481(c_r/c_t)c_{t,i} - (d_r/d_t)d_{t,i}}, \tag{3.34}$$

where $c_r$ and $d_r$ are related to the reference illuminant in the following way:

$$c_r = (4 - u_r - 10v_r)/v_r, \tag{3.35}$$

$$d_r = (1.708v_r - 1.481u_r + 0.404)/v_r. \tag{3.36}$$

### 3.6.3 CRI Calculation Procedure

The determination of the CRI by measuring the reflected light from physical samples, although interesting for illustratory purposes, has today been replaced by the more practical calculation using mathematical descriptions of color samples and illuminants implemented in a computer program, which is used to analyze spectral radiometric measurements. Below is a discussion on the procedure for calculating the CRI by analyzing the data directly from spectroscopic measurement of the spectral power distribution emitted from the white light source.

1. The chromaticity of the test light source is calculated. The chromaticity difference between the test source to the reference of the same CCT is calculated in the CIE 1964 color coordinate system. $\Delta_{u,v}$ should be less than $5.4{\cdot}10^{-3}$ for the light to be considered white light (See section 3.5).

2. The CCT is determined for the test light source to select a reference illuminant with the same color temperature. If below $T_C = 5000$ K, a Planckian radiator is selected, if above a D illuminant.

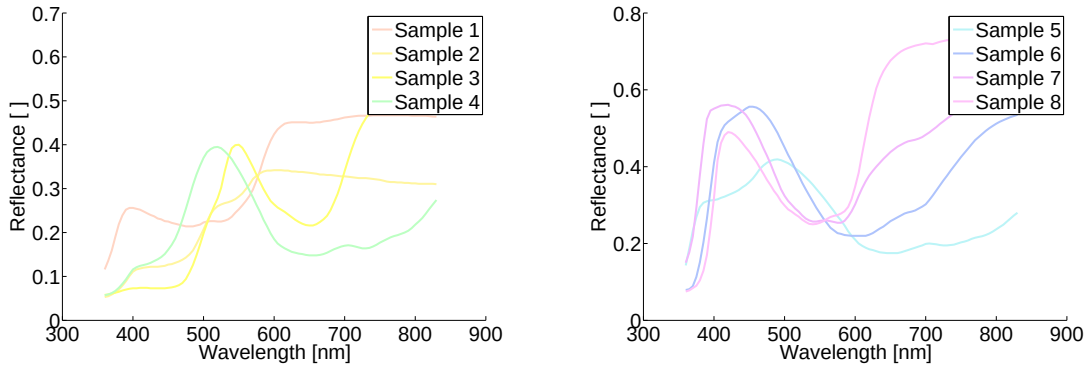


*Figure 3.8: The reflectance curves of the standard samples used in the CIE color rendering index.*

3. The chromaticity of the light reflected off the 8 first standard samples shown in figure 3.8 from the reference and test respectively is calculated from table values.

4. The Von Kries transformation from equations (3.33) to (3.36) is applied to the sample chromaticities to compensate for the chromatic adaptation caused by the shift in illuminant.

5. The color difference $\Delta E_i$ between the sample $i$ under reference and test illumination is calculated using equation (3.27).

6. Individual indices $R_i$ for the different colored samples are calculated from

$$R_i = 100 - 4.6\Delta E_i. \tag{3.37}$$

7. The average of the indices is calculated to give the general color rendering index

$$R_a = \frac{1}{8}\sum_{i=1}^{8} R_i. \tag{3.38}$$

It is important to note that $R_a$ and $\Delta_{u,v}$ are not related in any trivial way. A lowering of $\Delta_{u,v}$ will not necessarily result in an increase in CRI. This is illustrated by ignoring step 1 in the procedure and simulate spectra well outside the recommended chromaticities. The simulation of LED spectra by Bretschneider [13] show relatively high CRI can be achieved for the high values of $\Delta_{u,v}$ with $R_a \approx 60$ at $\Delta_{u,v} \approx .05$.

From the above, it is shown that $R_a$ only gives an indication of the perceived resemblance between objects illuminated under the reference and test source. The choices of samples, numeric pre-factors, and Von Kries transformation have a strong impact on the result. Parts of the specifications included in the CRI definition can be viewed as being arbitrary to some extend, having mostly historical background. However, the metric is standardized and the only one used widely, and has therefore been chosen

for this work. As indicated in the introduction to this chapter, replacements of the CRI is under development, due to various shortcomings of the metric. For a review addressing these issues see Guo and Houser [57].

## 3.7 Visual Thresholds

We now consider human sensitivity to small changes in illumination especially the wavelength discrimination and chromatic sensitivity, which are relevant for spectral light quality. If a property is varying with increments smaller than the *just noticeable difference* (JND), human observers will not be able to perceive the variation. In lighting this becomes important, for instance, when assessing homogeneity of an illuminated field or comparing the illumination from different light sources. Wavelength discrimination describes the ability of human beings to distinguish single wavelengths. This must be considered since the wavelength shifts of LED spectra related to temperature and current effects can exceed the just noticeable difference.

Figure 3.9 (a) shows the wavelength discrimination as found by Wright and Pitt [164]. From the figure it is seen that wavelength discrimination is most accurate at 500 nm and at 600 nm with $\Delta\lambda \approx 1$ nm, and a local maximum of $\Delta\lambda \approx 2$ at 540 nm. The accuracy is diverging at each end of the visible range, where the sensitivity vanishes. Wavelength discrimination is somewhat dependent on the observing conditions with the uncertainty becoming larger for smaller viewing angles [8].

The ability to distinguish small differences in chromaticity has been investigated by MacAdam [90], who found that chromaticity discrimination could be described in terms of ellipsoids in the chromaticity diagram. Figure 3.9 (b) shows the *MacAdam ellipses* in the CIE 1960 diagram, for illustration purposes the ellipses are enlarged by a factor of ten, noramlly called ten-step MacAdam ellipses. From the figure it is apparent that the CIE 1960 color space is only approximately uniform, as the MacAdam ellipses would be equally sized circles in a completely uniform color space. The CIE 1976 $u', v'$-chromaticity map that is stretched in the $v$-direction offers a slightly more uniform coordinate system. To achieve higher uniformity non-linear transforms has been proposed [45]. However, using non-linear color maps introduces practical problems with intuitive understanding and increased complexity in calculations of, for instance, color mixing. When regarding correlated color temperature, the just noticeable differences were investigated by Judd [68] who found it to be 5.5 $\mathrm{MK}^{-1}$ [166, p. 574]. This is equivalent to $\Delta T_C = 40$ K at 2700 K and $\Delta T_C = 240$ K at 6500 K.

## 3.8 Summary

In the preceding section we have reviewed the following light quality concepts: Correlated color temperature, chromaticity difference, and the color rendering index. For

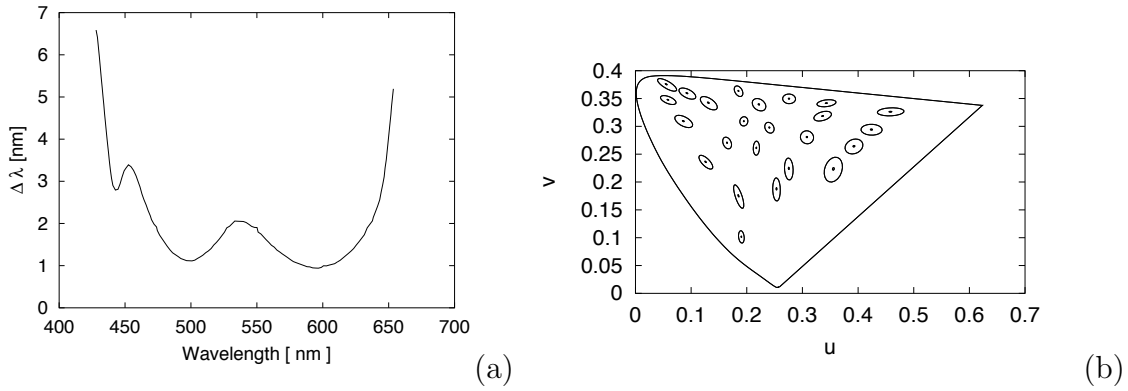


(a) (b)

*Figure 3.9: Wavelength discrimination based on measurements by Wright and Pitt [164] (a). MacAdam ellipses in the CIE 1960 chromatic diagram magnified by a factor of 10 (b).*

a given light source these characteristics can be calculated from a measured or modeled spectral power distribution, Furthermore, visual thresholds have been discussed in relation to changes in the spectral and chromatic characteristics of a given source of illumination. The presented methods of characteristics is used in the model analysis in Chapter 5 and the simulations in Chapter 6.

Due to the fact that user preference concerning CCT differs among individuals and is dependent on the time of day, prior adaptation and the use of the light source, the use of the CCT as a quality characteristic is therefore highly application specific. However, if a specific CCT is desired, quality can be measured by how close the CCT from the specific test light source is from the desired value. The chromaticity difference shows how much the test light source resembles the reference light source in terms of chromaticity. It is not clear that a high chromaticity difference in itself is a problem, however, when visually comparing different light sources the difference may become apparent as a color tint to the illumination. The color rendering index, while being somewhat arbitrary, still gives a useful indication of the ability of the light source to replicate the color rendering from the corresponding reference light source. The CRI can thus be used as a general guideline, but applications where color perception is critical, other measures should be considered, for example in section 7.1 where individual $R_i$ are considered to ensure for instance faithful highly rendering of saturated colors.

In order to determine these characteristics for a given light source it is most practical to measure the spectral power distribution. Chapter 4 reviews the new experimental setup that was developed and used in this work, to measure spectral emissions from LED light sources.

# Chapter 4

# Measurement Setup

The purpose of this work is to characterize LED light sources with respect to light output and light quality. To do this the spectral power distribution (SPD) must be measured, either from the average SPD of the total light emission or in limited solid angles depending on the situation. *Radiometry* is the study of electromagnetic radiation from light sources in terms of emitted energy as a function of wavelength and spatial distribution of the radiation. Radiometric quantities such as total radiant flux and irradiance requirer absolute measurement of the spectral power distribution in the relevant configuration. Therefore rigorous calibration must be preformed, to ensure accurate and reproducible spectral radiometric results, for evaluation of test light sources. *Photometry*, the study of human visual response to light stimuli, also often requirer absolute measurement of the various quantities. Photometric quantities such as luminous flux, chromaticity, correlated color temperature, etc. are calculated from the spectral power distribution and the mathematical descriptions of the color response of the human visual system. This is for instance done by weighing the spectral power distribution by the color matching functions $\bar{x}, \bar{y}, \bar{z}$ and applying the various calculations used to quantify estimates of human color and light perception, as described in Chapter 3. The following is a description of the techniques used for radio- and photometric characterization of light sources applied in this work. The use of integrating spheres for measurement of total radiant flux measurements is discussed in section 4.1. Spectral calibration, calorimetric calibration, and absorption correction is discussed in section 4.2. An new automated setup for measurement of multiple settings of current and environment temperature, which was developed as part of this work is described in section 4.4. A short summary is given in section 4.5.

The general method for characterizing light sources, here especially LED light sources, is the following: The light source is placed in a controlled environment where ambient temperature and electrical input are controlled. The light source must be stabilized in order to yield reproducible results for long term operation. To produce comparable measurement results we have used the recommendations of the IES LM-79 [64]. In this work, total luminous flux is measured by placing the light source

inside an *integrating sphere*, and extracting a small portion of the light for spectral measurement. Light sources can be investigated in either a forward flux or total flux configuration. Other methods include estimating the total luminous flux from goniometric measurements of the irradiance from a number of different angles. These methods will not be used in this work. Radiant intensity is measured by placing the light source at a controlled distance to a detector with a know aperture, such that the measurement solid angle can be found. The detector could be an integrating sphere system, using an input port as the aperture.

From the input device a portion of the light is transferred to a spectrometer typically via a multimode optical fiber. The spectrometer uses a grating for diffraction, to measure the light power according to specific wavelengths. The spectral power distribution of the light is converted to digital signals by a charge-coupled device (CCD) array. The data from the spectrometer can then be used for the relevant calculations.

## 4.1 Integrating Spheres

An important characteristic for a light source used for illumination is the total luminous flux $\Phi_v$, i.e. the total amount of emitted radiant flux weighted by the response of the human eye. This is used to determine the luminous efficacy and general applicability of the light source. The total luminous flux is given by the integration of the intensity $I$ over a sphere surrounding the light source modified by equation (3.1)

$$\Phi_v = \int_V I_v dV = \int_0^{2\pi} \int_0^{\pi} \int_\lambda 683.002 \frac{\text{lm}}{\text{W}} \bar{y}(\lambda) I(\theta, \phi, \lambda) \sin(\theta) d\theta d\phi d\lambda, \tag{4.1}$$

where $\theta$ and $\phi$ are the spherical coordinates and $\bar{y}$ is the luminosity function. When measuring the total radiant flux of a light source it is practical to use an *integrating sphere*, also called an Ulbricht sphere. The principle of an integrating sphere is that the light is emitted inside a hollow sphere with a diffusing and highly reflecting coating on the inside. The multiple diffuse reflections of the light cause the light inside the sphere to be uniformly distributed, such that the irradiance at any part of the inner surface of the sphere is directly proportional to the total luminous flux of the light source. However, if a surface element is directly illuminated this homogeneity is not present on this element. To avoid direct illumination baffles are used to block direct light on the measurement ports. The uniformity is increased when the inside surface of the sphere is increased compared to other elements such as ports and baffles. However, the irradiance also decreases proportional to the area. Choosing the right size for the sphere is therefore a tradeoff between uniformity and irradiance. The irradiance on the surface inside the sphere is given by

$$L_s = \frac{\Phi_v}{\pi A_s} \frac{\rho}{1 - \rho(1 - f)}, \tag{4.2}$$

where $A_s$ is the inner surface area of the sphere and $\rho$ is the reflectance of the inside surface. The second dimensionless term is due to the multiple reflections on the inside of the sphere. The multiple reflections cause the irradiance on the sphere wall to be much greater than if a flat surface had been illuminated by the same light source. The term is called the *sphere multiplier* and is defined as

$$M = \frac{\rho}{1 - \rho(1 - f)}, \tag{4.3}$$

where $f$ is the sphere surface to port area ratio [83]. For a sphere with a highly reflecting coating with a reflectance of 97 % in the visible range, an inner radius of 1 m and a port aperture with a diameter of 20 cm, the sphere multiplier is 43.7. While a 6 inch sphere with 0.5 inch port has $M = 36.7$. As $M$ is related to the number of diffuse reflections in the sphere the number can be used to evaluate different spheres and port configurations with respect to the achievable homogeneity.

In certain situations it is necessary to increase the diffuse reflection from a given area. Examples are support structures inside the integrating sphere or lamp reflector screens with low loss and a high degree of diffusion. In an integrating sphere surfaces with high absorption should be coated to decrease this absorption. It is seen from equation (4.3) that the multiplier rises linearly with the reflectivity $\rho$ of the sphere wall. This is the reason why the inside of the integrating sphere is usually coated with a highly reflecting diffusing material such as barium sulfate ($BaSO_4$). We have, for instance, used the coating *Avian-D White Reflectance Coating*, which is based on $BaSO_4$ [7], on the reflectors for the light sources mentioned in section 7.1.2. It is used to increase the diffuse reflection from surfaces where this is needed. To achieve high reflectance, multiple layers of coating are applied. The diffuse reflectance has been measured using an 8° input - 8° output setup where the diffuse light is captured in an integrating sphere (Ø2 inch). To prevent the non-diffused specular reflections from contributing to the measured distribution, a strongly absorbing patch is placed at the 8° output port. The light source is a fiber coupled *Mikropack Halogen light source HL-2000-FHSA*. It is fiber coupled to the integrating sphere. The coated surface to be measured is set to cover the port of the integrating sphere. The spectral difference between the sphere with the sample mounted and with an *Avantes WS-1 white reference tile* has been measured. The reflectance is then calculated as the ratio between data from the mounted sample and with the white sample. Figure 4.1 (a) shows the diffuse spectral reflectance of the coating with different numbers of coatings. Figure 4.1 (b) shows how the mean reflectance increases for increasing number of layers of coating. From figure 4.1 (b) it is seen that saturation of the reflectance has not be reached with 5 coatings. To increase reflectance further, more layers could be added although the effect seems to be diminishing. The relatively high amount of noise seen in figure 4.1 (a) at short wavelengths is due to the low radiant emission at these wavelengths from the halogen light source used for measurements. With application of 5 layers

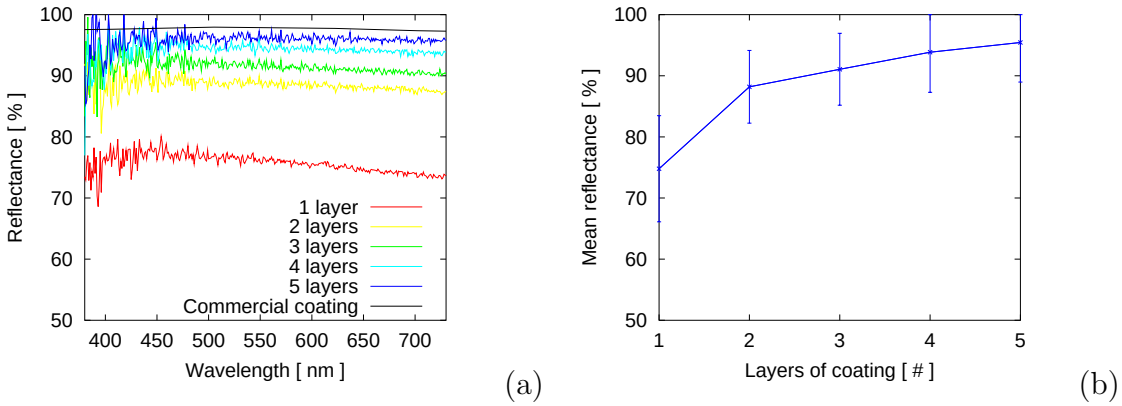


*Figure 4.1: Diffuse reflectance of a surface coated with 1-5 layers of Avian-D White Reflectance Coating, as a function of wavelength in the visible range. This is compared to a commercial coating with data from product sheet [82] (a). The mean reflectance as a function of the number of coatings applied (b).*

a reflectance of 95 % is obtained which come close to the example of a commercial product [82].

In the following two different measurement configurations will be discussed. Lighting systems emitting light in approximately all directions are characterized in a full sphere configuration ($4\pi$). Lighting systems that only emit light in the forward direction can be characterized in a $4\pi$ configuration. However an easier way is to use a "half-sphere" forward flux ($2\pi$) configuration. Figure 4.2 show the two configurations for total flux (a) and forward flux (b) measurements. In the total flux setup the test light source is placed in the center of the integrating sphere. Direct light from the light source, that has not been diffused can contain a large portion of the emitted light. Therefore, baffles are put in place to prevent direct light from hitting the absorbing surfaces such as test light sources and open ports. For light sources that radiate in a half sphere, such as most SSL products, it can be practical to insert the light source through one of the ports of the integrating sphere, as shown in figure 4.2 (b). This ensures that the changes in absorption and reflection contributed by changes of light source, heat sink, wiring, etc. can be minimized. Additionally, excess heat from the cooling mechanism will be emitted outside the integrating sphere. This will prevent the problems associated with raised temperatures inside the integrating sphere. For detailed reviews of the effects of integrating spheres baffles and port apertures, see Ulbricht [153], Walsh [160], Keitz [72].

Another method to determine total luminous flux is to use goniometric measurements. Where the luminance is measured in all solid angles around the light source and equation (4.1) is used to determine the total flux. However, goniometers that are suitable for large light sources are very large compared to the light source. Due to

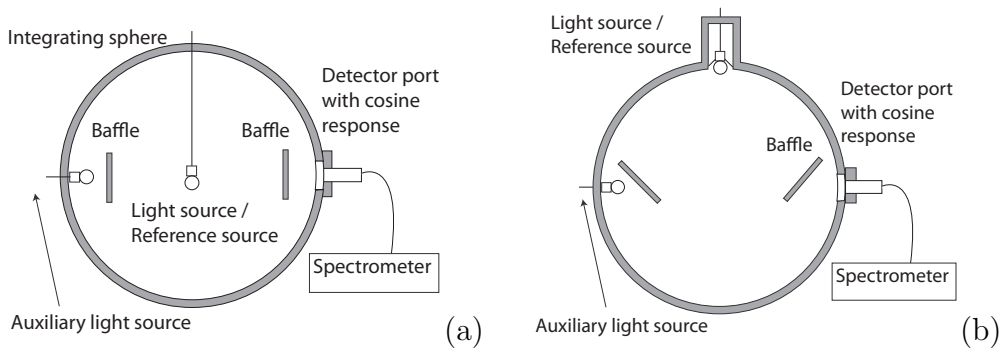


*Figure 4.2: Integrating spheres used for total radiant flux measurement of a source illuminating a full sphere ($4\pi$ geometry) (a) and similar for a forward flux light source ($2\pi$ geometry) (b).*

spatial constraints in the laboratory, such a setup has been unfeasible, and hence these methods will not be discussed further.

## 4.2 Calibration

To make radiometric and photometric measurements it is necessary to calibrate the measurement apparatus. In this work spectral power distributions are measured using grating spectrometers with CCD arrays. Both a spectral and a calorimetric calibration are needed for this characterization setup.

The spectral calibration discussed in section 4.2.1 ensures that the individual pixels are mapped to corresponding wavelengths. This is done using an atomic emission line lamp with known spectral peaks. The calorimetric calibration described in section 4.2.2 determine the sensitivity of each pixel to incident light at a given wavelength, and is made by measuring the response of the system to a standard lamp of spectral irradiance over the visible wavelength range. This is done by relating the response of the system to the standard of irradiance light source with the tabulated output of the reference. The system is calibrated as one component, where the calibration gives the response of the entire system. This method of apparatus calibration encompasses the response of the integrating sphere, the loss from fiber coupling and transmission, grating loss and CCD response. In this work spectrometers with fixed gratings are used. A spectrometer with changeable grating can be used if varying sections of the spectrum needs to be examined. However, when the grating is moved or changed the setup has to be re-calibrated, due to the changed geometry and variable response and sensitivity of the different parts of the apparatus.

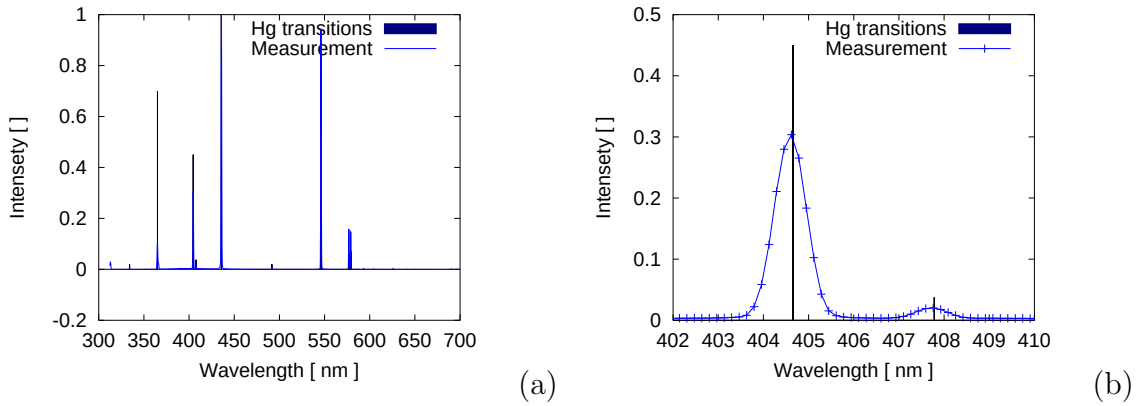


*Figure 4.3: The SPD of the NeHg lamp, with the table values [127] for center wavelengths, overview (a) and zoomed in on an example(b).*

### 4.2.1 Spectral Calibration

To calibrate the spectral response of the spectrometer, the narrow band radiation from atomic transitions is used to determine the scaling of the ($\lambda$)-axis. The Avantes spectrometers used widely in this work feature an internal calibration. This calibration was tested for accuracy using the stable atomic transition lines from a gas discharge lamp. The light from a *Pen Ray* NeHg lamp was measured using the spectrometer. The measurement result was compared to tabulated transitions taken from NIST Atomic Spectra Database [127]. The measurement and tabled values are shown in figure 4.3 (a). In the example seen in figure 4.3 (b) the measured peaks are plotted together with the tabulated center wavelength of the transition. The difference in wavelength between measured peak center and tabulated center wavelength is 0.03 nm. The wavelength discrimination of the human eye are at least an order of magnitude larger than this error, namely from 1 nm to around 5 nm, as seen in figure 3.9 (a). This means that the spectral calibration of the spectrometer is precise beyond what is required for photometric measurement. However, figure 4.3 (b) shows a large spread in wavelength around the transition lines. The full with half maximum value around the peak is $\Delta\lambda \approx 1$ nm. As this broadening is much larger than the linewidth of the atomic transition it must be caused by the measuring apparatus. This means that this equipment is not suited for resolving details in spectra less then 1 nm. It should be noted that this broadening is close to the accuracy of the wavelength discrimination of human eyes. However, the tristimulus curves ($\bar{x}, \bar{y}, \bar{z}$)) are so smooth that spectral details of this size will have negligible influence on photometric proprieties. In the following it is assumed that this spread will have consequences that are below the just noticeable difference threshold for visible stimuly.

### 4.2.2 Calorimetric Calibration

In order to make absolute measurements of energy output from light sources as a function of wavelength the calorimetric response of the measurement system must be calibrated. This is done using a calibration reference source for which the spectral energy output is known. For a given light source the signal $S(i)$ from each pixel in the spectrometer numbered $i$ with sensitivity from $\lambda_1$ to $\lambda_2$ is given by

$$S(i) = \Omega\tau \int_{\lambda_2}^{\lambda_1} L(\lambda)\alpha(i)d\lambda, \tag{4.4}$$

where $L(\lambda)$ is the radiance from the source on the detector aperture, $\Omega$ is the solid angle of the detector aperture, $\tau$ the exposure time and, $\alpha(i)$ is the response of the apparatus at this particular pixel. If the light source is inside the integrating sphere $\Omega = 4\pi$ and the radiance . Here the broadening effect seen in section 4.2.1 is neglected, as it will have negligible effect on photometric characteristics. Using the calibration light source with a given $L_r(\lambda)$ in a known geometry, $\alpha(i)$ can be found and used to find $L(\lambda)$ from $S(i)$ obtained from a test light source. For the calibration we can use the fact that the luminance $L(\lambda)$ times the exposure time $\tau$ of the measured signal $S(\lambda)$, as function of wavelength, is related to the reference luminance $L_r(\lambda)$ times the reference exposure time $\tau_r$ and the reference measurement $S_r(\lambda)$ in the following way:

$$\frac{L(\lambda)\tau}{S(\lambda)} = \frac{L_r(\lambda)\tau_r}{S_r(\lambda)}. \tag{4.5}$$

The relation between the signal as a function of wavelength $S(\lambda)$ and the signal from individual pixels $S(i)$ is discussed in section 4.2.1.

To isolate the relevant results and make precise measurements the background noise in the measurements must be minimized. The sources of noise are electrical noise in the detector system and stray light from the environment. These errors can be removed from the results by taking a measurement with the test light source powered off and simply subtract the background signal $B(i)$ from the test signal. With the reference radiance $L_r(\lambda)$ the radiance of the test source becomes

$$L(\lambda) = L_r(\lambda)\frac{S(i) - B(i)}{S_r(i) - B_r(i)}\left(\frac{\tau_r}{\tau}\right), \tag{4.6}$$

where $S_r$ and $B_r$ are the signal and background of the reference measurement. It should be noted that variations in the ambient light, for instance from daylight will be difficult to remove with this method. Therefore, such light sources should be obscured. Stray light from the test light source that is reflected off surfaces in the surrounding should be avoided, as it will create an erroneous increase in the signal. Nearby surfaces are therefore painted with low reflection paint.

As the standard of spectral irradiance a 1000 W (FEL) quartz halogen tungsten lamp is used. This can be traced to the NIST FEL 1000-Watt Standard of Spectral

Irradiance for the relevant wavelengths [54]. The reference radiance $L_r$ of the source is given with a precision around 1%. However, the propagation of uncertainty has not been calculated for this measurement setup. For a review of uncertainty in spectral measurement of LEDs see Pousset et al. [123] and Csuti et al. [31]. The reference lamp is rated for 8.000 A, which is provided by a calibrated *Newport 69935 digital radiometric power supply*. The filament of the calibration lamp has a length of approximately 1 cm and can generally not be considered a point source. Therefore the radiance in a given direction varies with orientation of the source. To ensure the highest attainable precision in this respect, the calibration source is placed on an adjustable platform. The platform can be adjusted with five degrees of freedom, using two linear stages, a rotation stage, and a two dimensional yoke stage. The alignment is made using the alignment jig, which has been used to align the reference when the calibration was done initially. By aligning the alignment jig with the measurement setup, the conditions under which the reference was made can be duplicated. The alignment jig is fitted with a cross hair engraved on a glass plate. The alignment is done by setting up a laser beam as seen figure 4.4. The 40 inch integrating sphere is too big to practically align, so it is anchored to the floor for stability. The rest of the setup then has to be arranged accordingly. A glass plate is mounted parallel to the port opening of the integrating sphere. The mirrors in front of the laser are adjusted such that the beam is centered on the cross hair on the alignment jig. The part of the beam that is reflected from the cross hair must then be aligned such that the beam aligns with the beam from the laser. The transmitted part of the beam has to be centered on the glass plate on the sphere port. The setup must now be adjusted such that part of the beam that is reflected of the port plate is coinciding with the beam coming from the laser. When all reflected laser beams are centered and reflected directly back towards the laser the sensor and the calibration source has the right orientation. The precision of this alignment is constricted by the uncertainty matching the laser spots. These are approximately 1 mm of in size in the current setup. With length scale of 500 mm, this causes the uncertainty on the angles to be on the order of 0.1°. A potentially larger uncertainty stems from the fact that the standard of irradiance is give for a small point at the described distance and angle from the emitter. Using larger ports will cause the uncertainty to rise due to the inhomogeneity in the radiation field. The irradiance data for the standard lamp is given for a distance of 500 mm. The distance is measured using a metal ruler. This method gives an uncertainty in length on the order of 1 mm. This uncertainty could be decreased by placing the reference mount on a linear precision stage.

When performing a calibration of the entire system it is important to note that small changes in the setup may cause changes in the response of the system. Changes in the bending of optical fibers or mounting and unmounting of fibers coupling can change the response of a system dramatically. Standard deviation around 30 % in the

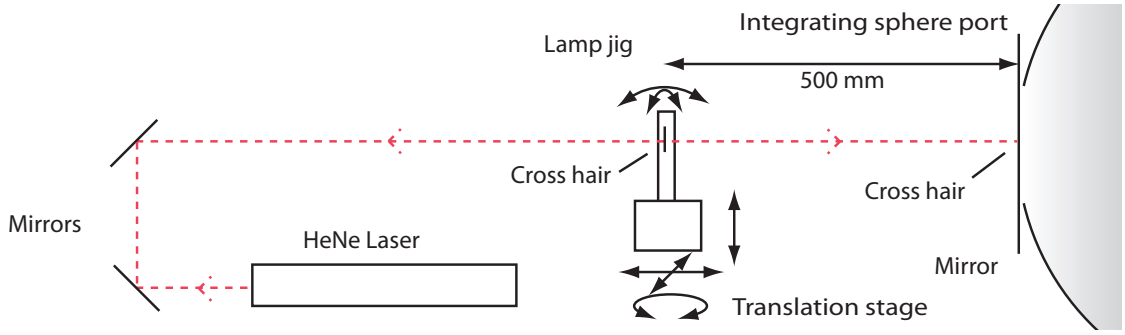


*Figure 4.4: Alignment setup for the calibration lamp and the integrating sphere. Laser beams are used to control the orientation of the calibration lamp in relation to the static integrating sphere.*

response has been observed over a 2 year period in a non-critical system. When greater care is taken the deviations can be decreased to under 2 % in the visible range. Figure 4.5 (a) shows calibration curves from the same system, measured at different times. As seen the figure 4.5 (b) the calibration curves vary over time. It should therefore be noted that the calibrations be made whenever a change has been made to the system.

### 4.2.3 Absorption Correction

If the test light source is inside the integrating sphere, or some part of the test lamp is obscuring the input port, the materials that make up the source will absorb and reflect a portion of the light. Different light sources have different designs and holders etc. that absorb light differently. The absorption from a test light source will be different from the reference light source. Therefore a self-absorption correction must be applied to measurements, on every new sample light source. This is done by mounting an auxiliary light source inside the sphere. By measuring the SPD from the sphere, where the axillary lamp lit, with the sample mounted $S_m(\lambda)$ and compare the result with spectral measurement without the sample $S_0(\lambda)$

$$A(\lambda) = S_m(\lambda)/S_0(\lambda), \tag{4.7}$$

the ratio $A(\lambda)$ can be used to correct the measurement. For large fixtures absorption has been seen as high as 50 %. When using the forward configuration light is reflected from the LED mount giving an increase in reflection in the sphere. The auxiliary light source must be stable and have a high light output across the visible spectrum. It is possible to use halogen bulbs for this purpose, however the low light output in the blue and near UV range can cause problems in this range.

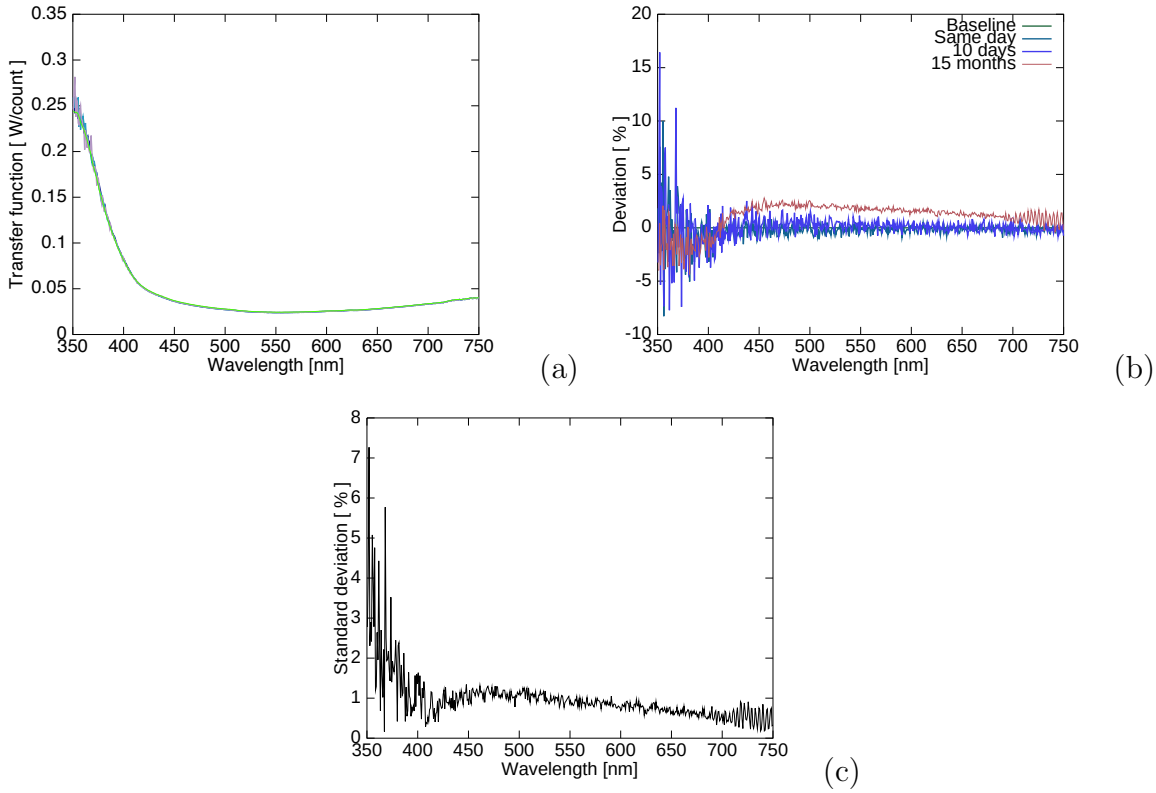


*Figure 4.5: Calibration curves for similar systems measured at different times. A typical transfer function (a). Deviations from the baseline result over time(b). The standard deviation on the calibration measurements over one year (c).*

## 4.3 Temperature Control

Due to the variations in spectral power distribution caused by changes in the junction temperature (see sections 2.1.6 and 2.2.2) it is important to keep the junction temperature of the LED constant during measurements. The most common way of characterizing LED devices is with an ambient temperature of 25°C, using a very short current pulse. Due to the small width of the active region and the high current density, it must however be expected that a rapid temperature change will occur even over short time spans. This characterization method can be used to compare performance between different LED devices, but it will not be applicable in situations where an LED is operated continuously at a higher junction temperature.

A typical change in dominating wavelength is on the order of 0.05 nm/°C [89]. With an operation temperature of 120 °C, the shift becomes 5 nm. This change is above what must be considered perceptible in some wavelength domains (see figure 3.9). Within the same temperature span the LED might loose between 5 % and 30 % of the luminous flux [28].

To be able to maintain and control a stable temperature for measurement of the LED, the LED is mounted on a surface, which is thermally connected to a *Peltier element*. The Peltier element is driven by a controller using the input from a temperature sensor, placed between the LED and the Peltier element. This gives a system where the device temperature $T$ is required to be stabilized around a certain value $T_0$. The sensor gives the temperature $T_s$ and the Peltier element is powered by a voltage $V_P$. The relation between cooling voltage $V_P$ and $T_s$ is not generally well known, therefore it will be beneficial to use a feedback control scheme. In this work we have used a control scheme called a *proportional*, *differential* and *integral* (PID) controller [113]. In this case the PID controller is used to minimize temperature oscillations and the amount of time used for the temperature to stabilize. Given the sensor temperature $T_s$, the set point temperature $T_0$, the control output voltage $V_P$ from the controller is given by the sum of the proportional $P$, integral $I$ and differential $D$ part

$$V_P = P + I + D = K_p(x(t) - x_0) + K_p \int_0^t (x(\tau) - x_0)d\tau + K_d \frac{d}{dt}(x(t) - x_0) \quad (4.8)$$

where $x$ is the *error signal*, given by $x = T(t) - T_0$, $t$ is the time, and $K_p, K_p, K_d$ are control parameters. The proportional or gain term responds directly to the error signal however using only this term will result in an oscillation around the set point. The integral term responds to the accumulated error and accelerates the process towards the set point, but increase overshoot. The differential term can be used to dampen the overshooting oscillations, but is sensitive to noise due to the nature of differentiation.

For temperature stabilization we use a *TEC 2000* controller. Here the temperature set point can be set manually or using an external voltage. The temperature is monitored with an AD 590 sensor. The control voltage $V_P$ and the temperature $T$

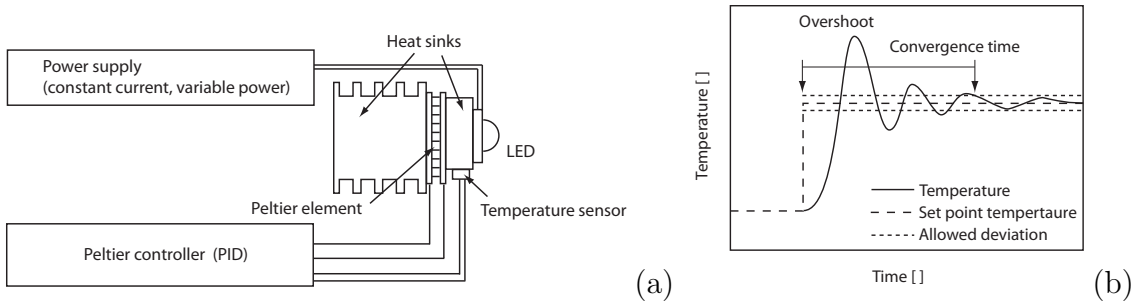


*Figure 4.6: The temperature stabilization setup. showing the LED, LED mount (primary heat sink), Peltier element, secondary heat sink and the LED and Peltier drivers (a). Illustration of the resulting temperature evolution controlled by the PID controller (b).*

is related by a simple first order expression $T_{set} = aV + b$ where $a$ and $b$ has been determined to be $a = 20$ °C/V and $b = 0.5$ °C [161]. This temperature controller is equipped with a PID circuit and a power supply for the Peltier element. The $P$, $I$ and $D$ terms must generally be adjusted manually to achieve the lowest stabilization time. This is due to the fact that individual heat sinks vary in size and shape, giving different responses to the system. Due to the variation in response of the various LED components, heat sinks etc. it could be of interest to apply adaptive control [162, 6], such that the manual configuration of control parameters could be eliminated.

If stabilization time is too long, measurements with respect to a high number of temperatures become impractical. It is therefore of interest to decrease the stabilization time. The response of the stabilization setup is influenced by the size of the heat sink on both sides of the Peltier element. The platform where the LED is mounted will be named the primary heat sink, its role is to conduct the heat from the LED to the Peltier element. The secondary heat sink conducts the heat away from the Peltier element to the surroundings. The size and shape of both influence the performance of the temperature stabilization system. We use a configuration where the primary heat sink is made from solid cylinder aluminum, 1 cm in diameter and 2 to 4 cm in length, with a 5 mm thick base covering the 1 inch Peltier element. The AD 590 temperature sensor is mounted on the primary heat sink with low thermal resistance to the LED. This gives a convergence time of around 5 min for a change from room temperature to 10 degrees below room temperature. If the thermal resistance between temperature sensor and the Peltier element is large, the response will be delayed in time, causing the PID controller to overshoot, this can significantly increasing stabilization time.

Since LEDs can be damaged by high junction temperatures it should be ensured that the LED does not reach temperatures where the rated maximum junction temperature is exceeded, which could be the case if the overshoot is too large. This can be remedied by placing the sensor on the primary heat sink close to the Peltier element.

To ensure that the heat from generated from the LED creates a fast response the thermal resistance between LED and sensor should also be low. Another method is to ramp up the temperature in smaller steps with equalization time at each step.

To be able to effectively control the temperature of the LED, it should be noted that the TEC 2000 supports both heating and cooling, by reversing the voltage across the Peltier element. This can be used to characterize LEDs, at elevated temperatures, where ambient temperatures and not self heating is the main contributor to the raised temperature.

An aspect of dynamic temperature control related especially to LED, is the way heat dissipation from the LED is temperature dependent (see section 2.2.2). As the LED backside temperature increases the junction temperature increase. This causes the efficiency of the LED to decrease, this again causes increased heat dissipation. The increased heat load will cause the efficiency to decrease and so on and so forth. Similarly a decrease in temperature will cause an increase in efficiency and have the opposite effect. Therefore an LED that is forward biased above the threshold voltage will have an amplifying effect on temperature fluctuations caused by the temperature stabilization setup. This effect will increase for increasing currents.

Peltier elements generally have a low *coefficient of performance*, meaning that the amount of heat generated at the hot side is significantly higher than the heat removed from the cold junction. This causes the temperature difference between hot and cold junction to increase. If the secondary heat sink behind the Peltier element is too small, the temperature difference will rise, leading to a situation where sufficiently heat cannot be transferred and a target temperature cannot be reached. The problem increases with decreasing set point temperature, due to the increase in dissipated power from the Peltier element. The effect can be observed as a decreasing of the slope of the temperature signal with time for decreasing temperature. If the secondary heat sink is not able to dissipate enough heat from the Peltier element the temperature signal will level out and the set point cannot be reached.

## 4.4 Automated Setup

Forward current and junction temperature are the primary operation parameters, affecting the spectral power distribution of an LED, when age deprecation is disregarded. Therefore an automated characterization setup for LED components with respect to both current and temperature has been set up. The setup can be used for automated measurements of many settings of current and temperature that otherwise would require many hours of manpower. The following is a description of forward flux measurement setup seen in figure 4.7. The LED is mounted on an aluminum heat sink with screws and thermal paste to facilitate easy removal and increased heat transfer. A temperature sensor is mounted on on the primary heat sink. The output from

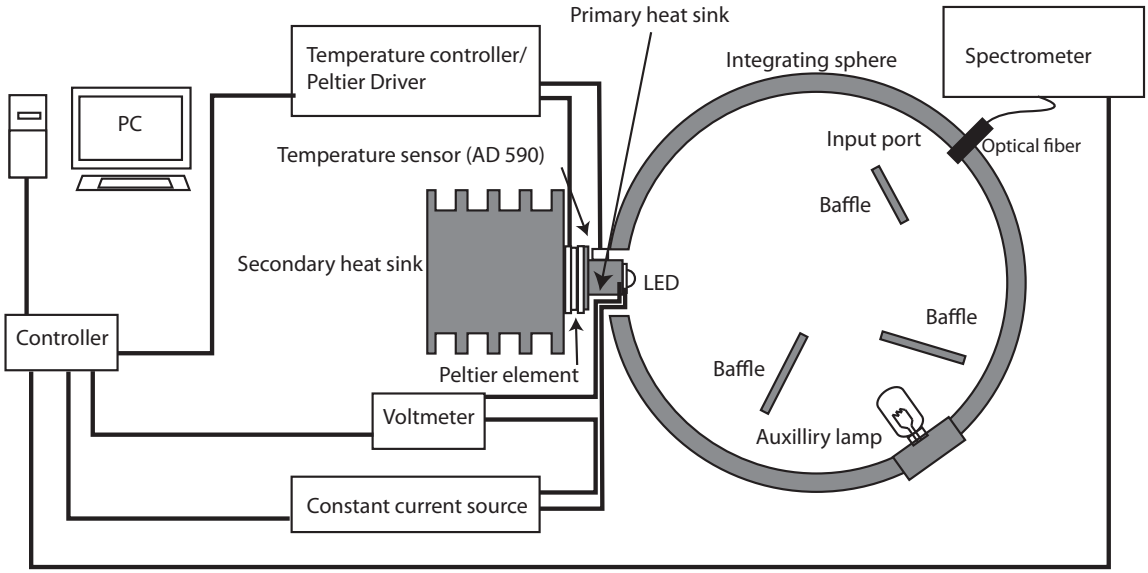


*Figure 4.7: Illustration of a typical $2\pi$ automated setup with an automated control for characterization of single LED devices.*

this sensor is connected to the TEC 2000 temperature controller that also powers the Peltier element. The secondary heat sink is made of black anodized aluminum with an area of approximately 700 $cm^2$.

The LED mount is inserted into an integrating sphere (Ø 6 inch). The light is coupled to the spectrometer with a *Thorlabs FTO38MM*, 600 micron multimode fiber. The LED is connected to a constant current power supply *LDC 2000* and *Keithley 2701* with a 7706 module acting as a voltmeter or alternatively a *Keithley 2400 SourceMeter* The drift of the voltage measurements is $\pm 0.035$ % over a year according to the data sheet [71].

The temperature controller current supply and voltmeter is monitored and controlled from a PC running a custom made *LabVIEW* PC program, such that the changes in the input parameters and data acquisition is fully automated. An AD 590 temperature sensor, is used as input to PID amplifier to stabilize the temperature. A voltage proportional to the temperature is read from the TEC 2000 and monitored by a computer. The forward voltage across the diode is measured using the Keithley multimeter which can convey the data to the computer. The computer can trigger the measurement of the spectral power distribution is then measured using an *Avantes AvaSpec 3648* spectrometer. The spectrometer has a wavelength range of 300 nm - 830 nm covering the visible range.

### 4.4.1 Automated Spectrometeric Measurements

Given an LED, driven at different values of forward current and junction temperature, the radiant flux might differ by large amounts, and this needs to be addressed by the measuring setup. This is done by adjusting the integration time or exposure time of the spectrometer.

The integration time $\tau$ determine the amount of time the measurements apparatus is open, for the light to be measured. If the integration time is too low the signal is going to be too small and the signal to noise ration (SNR) is going to be high. If the integration time is too long the spectrometer will saturate and clip the signal where the saturation occurs. Finding an integration time that gives a strong signal without saturation is therefore of interest.

A LabVIEW program has been developed to facilitate automatic setting of the integration time. A clipped signal gives very little indication of the size of overshoot in $\tau$ so it is preferable to make a fast reduction of $\tau$ in the case of saturation. This is done by reducing $\tau$ by a large percentage until clipping is avoided, and similarly to increase $\tau$ if the signal is below a threshold.The integration time is adjusted via an iterative process where $\tau_1$ is the initial integration time and $\tau_2$ is the adjusted integration time. We define the $S_{max}$ and $S_{min}$ as maximum and minimum signal strengths defining a high enough resolution. The maximum of the measured signal is $S_{peak}$. Now if $S_{peak} \leq S_{min}$ then

$$\tau_2 = (S_{max}/S_{peak})\tau_1, \tag{4.9}$$

and if $S_{peak} \geq S_{max}$ then

$$\tau_2 = \alpha\tau_1 \tag{4.10}$$

where $\alpha > 1$. With this algorithm the $\tau$ converges fast enough for this purpose, usually within a few iterations given a reasonable initial value. The signal resolution rise linearly with $\tau$ until saturation where the signal suffers clipping distortion. So as high values for $S_{max}$ and $S_{min}$ as possible without clipping distortion are preferred to get high resolution and decrease signal to noise ratio.

### 4.4.2 Measurement Procedure

The following is a description of the procedure that has been used for radiometric measurements in this work. The procedure can be changed to accommodate differences in LED systems.

1. The integrating sphere is calibrated as described in section 4.2.2. This is especially important if changes have been made to the measurement setup.

2. A spectral measurement is made of the empty sphere using the auxiliary lamp.

3. The test light source is placed in the port of the integrating sphere, such that the operating parameters can be controlled. Fixtures must be placed in a realistic setting with regards to orientation and surrounding structure. Single LED components are placed on a temperature controlled primary heat sink.

4. With the test light source unpowered the auxiliary light source is used to make a spectral measurement. This measurement is compared to a measurement from the setup without the test light source and the absorption correction is applied using equation (4.7).

5. A spectral measurement is made to determine the background light level.

6. The power supply for the test LED is turned on. If the measurement is of a device in continuous operation a waiting period is inserted. This will device must be equalized with respect to case or fixture temperature, such that the light output is stable.

7. When the temperature of the device is stable the spectral measurement can be made and the SPD can be calculated from equation (4.6), and the total flux can be calculated from equations (4.4) and (4.1).

When several measurements with variations in the parameters are performed the procedure is controlled by the computer program and altered in the following way: The current is set to the designated value and a 30 second pause is inserted to equalize the heat transfer from LED to the temperature sensor. As a large temperature difference between LED sensor can cause an overshoot in the PID controller. The temperature setting procedure is initiated for the set point temperature and terminated when the set point temperature is reached and the variation in temperature is below 0.1 K. The forward voltage across the diode is measured and the result is transmitted to the computer. The signal from the spectrometer is recorded using a fixed or automatically adjusted exposure/integration time. The spectral power distribution is calculated using the calibration and absorption data as described in section 4.2. The procedure is repeated for varying settings of temperature and forward current, from a lookup table on the controller PC. The setup has been used for characterizations of various LEDs and the measurements described in sections 5.1 and 7.2 have been obtained using this setup.

## 4.5 Summary

The preceding sections have described the measurement techniques and apparatuses used for radiometric characterization of LED light sources. The use of integrating spheres has been discussed, and a characterization of a useful coating with high diffuse

reflection has been presented. Total luminous flux measurement for evaluation of overall energy efficiency and luminous efficacy of LED light sources has been discussed.

The calibration of the measurement setup is critical to the reliability of the measurements. We have found that the spectral scaling calibration of the spectrometers is precise beyond what is needed for colorimetric purposes. However, the uncertainty of the spectral measurements is approximated to $\Delta\lambda \approx 1$ nm. The uncertainty on the calorimetric reference transfer function is $\pm 1$ %, and the uncertainty in calibration is also $\pm 1$% for long and midrange visible wavelengths. For short wavelength the uncertainty rises to 2-3 % towards the near UV region. The compound uncertainty from these factors are largely determined by the largest source of error, which is estimated can be found from the variations in the calibration measurements. However, the compound uncertainty of the measurement setup has not been calculated. This calculation would be required a precise evaluation of the uncertainty on all the elemets of the setup as well as on the resulting photometric characteristics. For details on uncertainty in radiometric and photometric measurements subject see Nimeroff [110], Pousset et al. [123], Ohno and Kranicz [115].

Compensation for absorption is presented due to the need to measure LED systems in various implementations. For configurations where reflectors and other structures need to be taken in to account i.e. where the LED cannot be isolated from the LED system.

Since LED components and devices are affected by self-heating, temperature control is important. The use of Peltier elements and PID control schemes have been discussed. In this project an new automated measuring setup has been developed to allow precise and extensive characterization of LED devises by measure the resulting SPD of a large number of settings of current and temperature. This is used to determine illumination properties of LEDs in applications within lighting where the LED devices will be operated with varying junction temperature, caused by variations in forward current and/or changes in the ambient temperature. The influence of current and temperature can then be accounted for, in applications where stability in color rendering and chromaticity is critical, such as described in 7.1 and 7.2.

# Chapter 5

# Current and Temperature Characterization

In general lighting applications using LED technology a key question is: How will a given LED device be affected by the injected forward current and junction temperature? This chapter discusses the results of characterizations of individual LED components, which was done as a part of this work. The influence of operating temperature and forward current on the spectral power distribution, has been investigated. The spectral power distribution has been measured for varying values of both forward current and thermal pad temperature in order to investigate the models presented in Chapter 2. The models of the spectral power distribution, has been investigated with regards to correlation with experiments, the derived physical values and the resulting chromaticities. Additionally, a method for measuring the junction temperature using the temperature dependence of the band gab is tested, using the same setup. The results of the characterizations are compared to the theoretical considerations from Chapter 2 and the perceptible characteristics are evaluated using the relevant photometric concepts discussed in Chapter 3.

LEDs from two different manufactures have been subjected to characterization. The LEDs are from *Cree* and *Philips Lumileds*. The Lumileds LEDs have been characterized radiometrically for use in the project described in section 7.2. Three colored Rebel LEDs: red, green, and blue, were characterized for use in plant illumination

From the results it is found that the decrease in quantum efficiency with increasing forward current

The results were obtained using the setup described in Chapter 4, can be seen in section 5.1. For evaluation of the spectral emission models presented in Chapter 2, Cree X-Lamp LEDs were tested at higher junction temperatures. The results can be seen in section 5.2. A method for non-contact electrical thermal characterization and junction temperature measurement of LEDs is presented in 5.3. A summary is given in section 5.4.

## 5.1 Current-Temperature Plane Characterization

In many LED lighting applications the spectral power distribution has to be determined with a high degree of precision. The forward current and thermal pad temperature are the dynamical factors that can be controlled externally by adjustments to the power supply and the cooling mechanism. In the project described in section 7.2 it was necessary to characterize light output of the Luxeon Rebel LEDs, which was to be used as light sources. The characterization was made with respect to the thermal pad temperature and the supplied current. Using the automated test setup that was developed as part of this work and is described in section 4.4, the spectral power distributions, corresponding to varying values of forward current and operation temperature, was measured. This was done due to a need for high light output and minimal energy usage for electrical power and cooling. The measurement data is visualized in current-temperature plane graphs. The models are fitted to the data in the columns and rows presented in these graphs. The resulting parameters presented are the mean and standard deviation of the fitting results across all rows and all columns.

The measurements presented in the following are used to investigate the empirical models presented in section 2.2.2. The model parameters has been fitted to the measured data. The light output power as a function of temperature is fitted to the exponential equation (2.27) using the MATLAB fitting routine `lsqcurvefit` which uses the least square method. From the fitting, the parameters $\Phi(0)$ and $T_0$, which associate light output and temperature, can be acquired. The polynomial function (2.28) describing light output as a function of forward current is fitted to the measured data, using the MATLAB function `polyfit`, which also uses the least square method. Here an extra data point $\Phi(I = 0\,\mathrm{mA}) = 0$ mW, has been added to the data sets to guide the fitting routine towards results with high correspondence with data. This is justified by the fact that zero current gives zero energy output.

To be able to grade the quality of the models the *coefficient of multiple determination* $r^2$ is used to find correlation between model and measurement. The various models have very high correlation with the measured LED spectra, which gives $r^2$ close to 1. The coefficient of multiple determination is a relative measure which depends on the data range, number of data points etc. Therefore, one can only compare results using data in the same format. In some cases it is useful to use $1 - r^2$ to clearly distinguish the small differences in the correlation. The colored spectral power distributions shown in the following are used to illustrate the position in the visible spectrum. The colors in the SPD plots are produced by converting tristimulus values $(X, Y, Z)$, of monochromatic light sources along the visual range, to sRGB triplets [63]. The shown colors are therefore to be regarded as approximations.

The rebel LEDs surface-mount devices (SMD) are normally soldered directly on to the surface of the printed circuit board (PCB). This is done to facilitate smaller size and lower thermal resistance. However, to enable the testing of several devices

the LEDs were mounted on the heat sink with bolts, such that devices can be easily exchanged on the heat sink. Thermal resistance in the interface between LED and heat sink were decreased using thermal paste. When using this technique it should be noted that bubbles or gabs in the thermal paste might decrease the heat transfer. To ensure that this issue did not affect the measurements the red Rebel LED (LXML-PR01-0275) was tested in two different configurations. One with the LED mounted with thermal paste, and one where the LED was reflow soldered on the PCB. This was done to test if the thermal resistance was affected significantly by the different configurations. Comparing the two methods, the results did not show any significant difference in heat transfer. The LEDs have been characterized for thermal pad temperatures from 20 - 35 °C, that would be typical temperatures in the relevant setup where active cooling is employed. The thermal pad temperature is the temperature of the primary heat sink, measured approximately 3 mm from the LED. For the blue and green LED the forward current is regulated in the high power regime between 200 mA and 1000 mA. The red LED is supplied with current from 200 mA to the rated maximum of 700 mA.

The results for the Lumileds royal blue Rebel LED (LXML-PR01-0275) are shown in figure 5.1. Two bins have been measured are: E4D (Radiometric flux at 750 mA: 425 - 500 mW, peak wavelength: 445 nm - 450) and C5D (Radiometric flux at 750 mA: 275 - 350 mW, peak wavelength: 450 - 455 nm) [89]. Examples of the spectral power distributions at forward current of 1000 mA and 975 mA and a thermal pad temperature of $T_{pad} = 20$ °C are shown for the two bins, in figures 5.1 (a) and (e). It can be seen that the two bins in figures 5.1 (a) and (e) have different light output for approximately the same forward current, with a difference of approximately 30 %. This is inside the data sheet values. From the data exemplified in figure 5.1 (b) we have the following fitted parameters: The intersection $A_0$ is on the order of $\pm 20$ mW. This is possibly caused by the fact that the data is from the high power region with no data for low input power. This could cause a low precision near the intersection point. The proportional coefficient is $A_1 = 1.554 \pm 0.0072$ mW/mA and $A_1 = 1.187 \pm 0.011$ mW/mA for the two bins respectively. This is taken over the range of temperatures that have been investigated. The second order term $A_2 = -0.330 \pm 0.0058 \cdot 10^{-3}$ mW/mA$^2$ and $A_2 = -0.5019 \pm 0.0044 \cdot 10^{-3}$ mW/mA$^2$. The second order term $A_2$ or $A_2/A_1$ coefficients can be interpreted as describing the decrease in light output in response to increased current, also known as droop. These coefficients could then be used to characterize LEDs regarding droop. The coefficient of determination of the fitted models is very high $r^2 = 0.9997$ and $r^2 = 0.9992$ respectively, which shows that the model has a high correlation with the measured results. The output power as a function of the thermal pad temperature $T_{pad}$ for the selected current of 350 mA is shown figures 5.1 (c) and (g). The fitted values for the data in these figures are $\Phi(0) = 520$ mW, $T_0 = -100$ K and $\Phi(0) = 400$ mW, $T_0 = -500$ K for the two bins respectively. The negative fitted values for $T_0$ is obviously difficult to interpret as characteristic

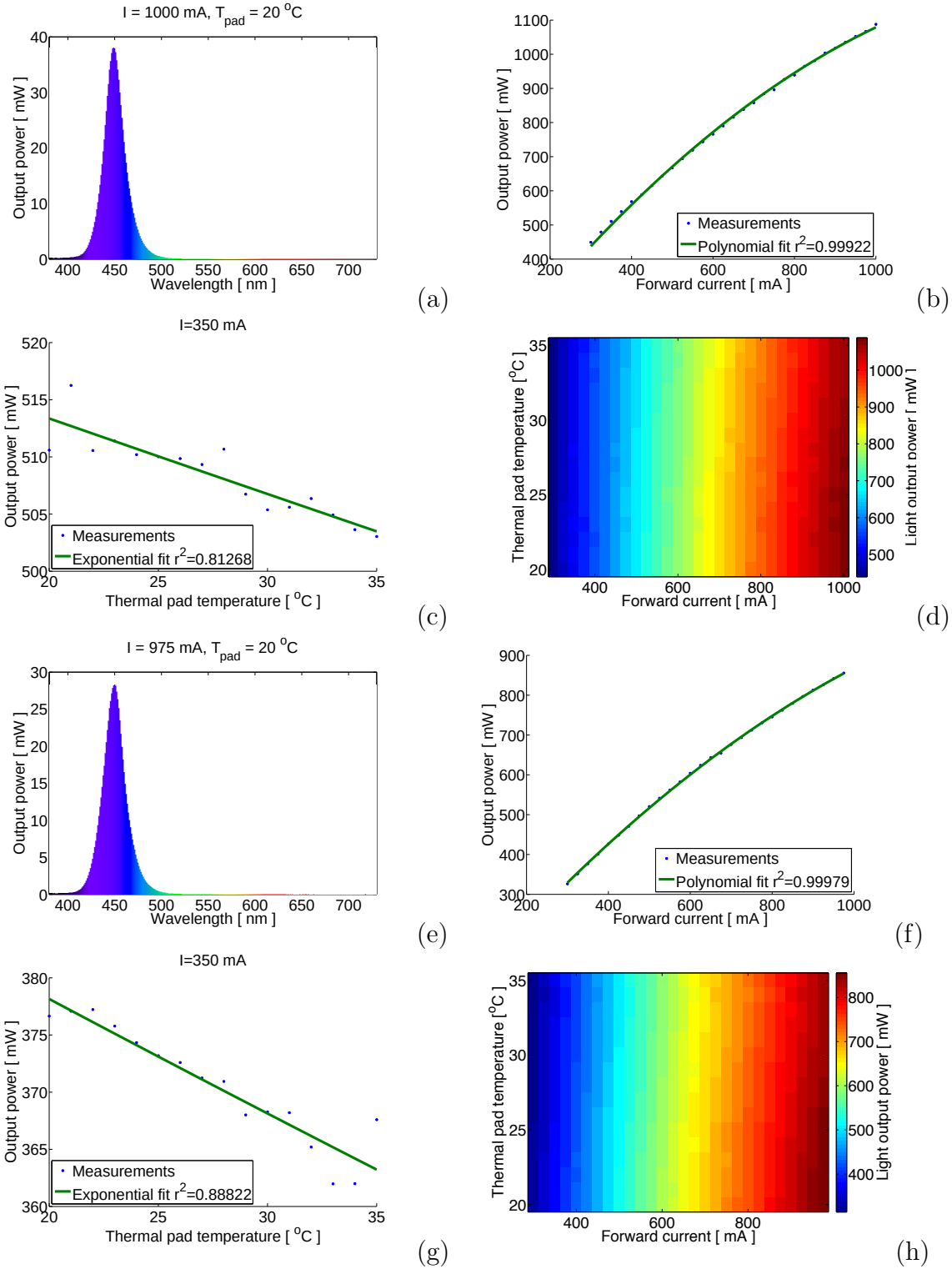


*Figure 5.1: Results of the characterization of the Lumiled Rebel LED LXML-PR01-0275 Bins E4D and C5D. The SPD of Bin E4D (a) and bin C5D (e). Light output as a function of temperature (c) (g). Light output as a function of current (b) (f) and light output as a function of current and temperature (d) (h).*

temperatures, and the model can not be used to extrapolate the light output beyond the measured interval. However, it is seen that coefficient of determination between model and data is low, $r^2 \approx 0.85$, due to the spread in the measured data within the interval. This means that the fitting parameters have a high degree of uncertainty. The decrease in light output in the investigated temperature range for both bins are 3 %. which seems to be somewhat higher then the approximately 1 % from the datasheet [89, p. 13]. The light output is shown in the current-temperature plane in figure 5.1 (d) and (h). It can be seen from the figures that the light output decreases slightly for increasing temperatures, such that a given light output will require a higher current for increasing temperatures. Typical application of this data would be to search for a particular power output at the highest possible thermal pad temperature, in order to decrease energy consumption for the cooling mechanism.

The results obtained from the green Rebel LED LXML-PM01-0080 are presented in the following.. The bin is: M2C (Photometric flux 90 - 100 lm, dominant wavelength 525 - 535 nm) [89]. Figure 5.2 shows the results for the characterization with regard to forward current and thermal pad temperature. Figures 5.2 (a) and (b) shows the spectral power distribution of the LED with a current set to $I = 1000$ mA and $T_{pad} = 20$ °C. Figure 5.2 (b) shows the radiant power as a function of forward current. The polynomial model gives the following results: The proportional term is found to be $A_1 = 0.8730 \pm 0.0025$ mW/mA The intersection point is at $A_0 = 13.23 \pm 0.22$ mW. Which is 2.4 % of the maximum light output. The droop parameter is fitted to give $A_2 = -3.742 \cdot 10^{-4} \pm 1.3 \cdot 10^{-6}$ mW/mA$^2$. The fitness given by the coefficient of determination, $r^2 = 0.997$, is in this case lower than for the blue LEDs presented in figure 5.1. The curvature of the droop curve is deviating from the model by a few percent. This could present a problem if the curve is to be used for prediction of light output. However, the parameter is still a useful description of the overall decrease in the efficiency of the LED. When regarding light output as a function of thermal pad temperature, the variation is very small in the measured interval. The characteristic temperature from equation (2.27) is found to be $T_0 = -1120 \pm 191$ K. Again this temperature does not give meaning in any physical sense. From the data shown i figure 5.2 (d) it is seen that the light output from this LED varies very little within the measured temperature interval. From these measurements predictions outside the temperature measured interval will have large uncertainties.

The test procedure have been applied to the Lumileds red LED LXML-PD01-0040. The bin is G4C (Photometric flux 40 -50 lm, dominant wavelength 620 - 630 nm). Figure 5.3 (a) shows the spectral power distribution. Figures 5.3 (b) and (d) shows clearly how the light output decreases for currents higher than 620 mA at all temperatures. This is in contrast to the data sheet which does not show this dip in light output [89, p. 15]. Figure 5.2 (c) show that the light output is reduced with 5 % over a 20 K interval. This is somewhat smaller than the decrease shown in the datasheet

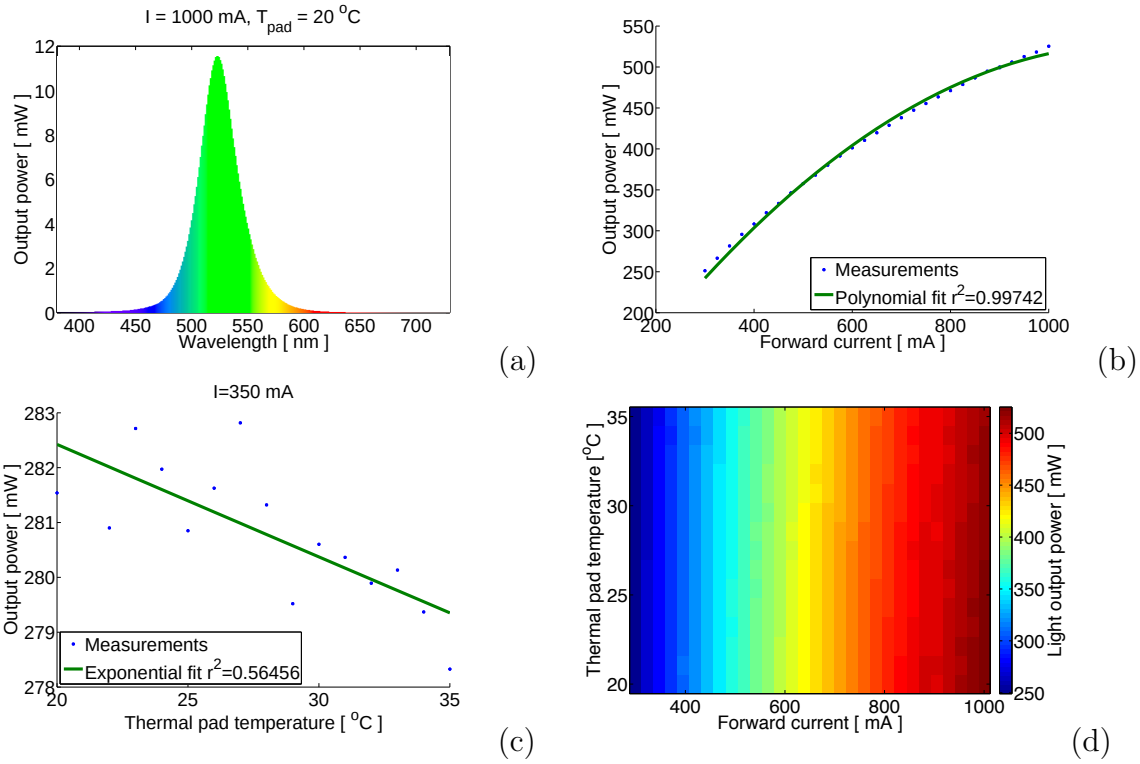


*Figure 5.2: Results of the characterization of the Lumileds Rebel green LED LXML-PM01-0080 Bin M2C. The SPD the LED (a). Light output as a function of current (b). Light output as a function of temperature (c) function of current and temperature (d).*

[89, p. 13]. The polynomial fit gives the following results: The intersection term is found to be $A_0 = -7.43 \pm 0.43$ mW. The proportional term gives $A_1 = 1.4846 \pm 0.0070$ mW/mA. The droop term is found to be $A_2 = -0.00110 \pm 3.4 \cdot 10^{-5}$ mW/mA$^2$, which is drastically larger for the this LED compared to the previously mentioned. The fitness ($r^2 = 0.983$) of the model on this data is evidently less suited to describe a decrease in light output power for increasing current. Figure 5.3 (c) shows a decrease in light output 5.5 % on the 20 - 35 °C range. This is significantly higher then the datasheet, which shows the value to be approximately 2.7 %.

From these measurements we also have the forward voltage and spectral power distribution as function of the forward current and heat sink temperature. From the voltage readings we see a drop for increasing temperatures and a slow increase from the threshold voltage for increasing current, which is expected. For the blue and green diode we see a monotone increase in light output as a function of current and a slight decrease in light output with increasing temperature. This is expected from theory. However, for the red LED shown in figure 5.3 (b) a peak is seen in light output around 620 mA. Several LEDs of the same bin where tested in a similar way, with similar results, of peak flux around 600-700 mA. This is unexpected, and is not mentioned in the product data sheet [88]. The red LED has 20 % higher thermal resistance than the others, and this lead to decreasing efficiency if there is lack of thermal contact, heating the diode excessively. The measurement was repeated with the LED soldered to the heat sink, however the same behavior was repeated.

## 5.2 Spectral Models

When using LEDs in applications where precision in color is required, it is useful to have models of the spectral power distribution. In the following three different models are investigated. The purely empirical model using single and double Gaussian functions, described in section 2.2.1, and the model using the solid state physics principles, described in section 2.1.2. In the following the latter model is called the quasi Fermi level (QFL) model. It is furthermore of interest to study how the perceived color is affected by the changes in the spectral power distributions, caused by changes in the junction temperature. It is investigated how well the models, are able to predict the results of measurements. The LEDs used in this study are the Cree XLamp [29]. The spectral measurements presented in the following are relative, and does not include absolute quantities of emitted energy. This provides only the shape of the distribution. The reason for this is that the experimental setup used for these measurements did not include a standard of spectral irradiant flux, such that absolute measurements could not be preformed. Examples of the measurements can be seen in figure 5.4. It can be seen how the spectral power distribution changes and decrease for increasing temperatures.

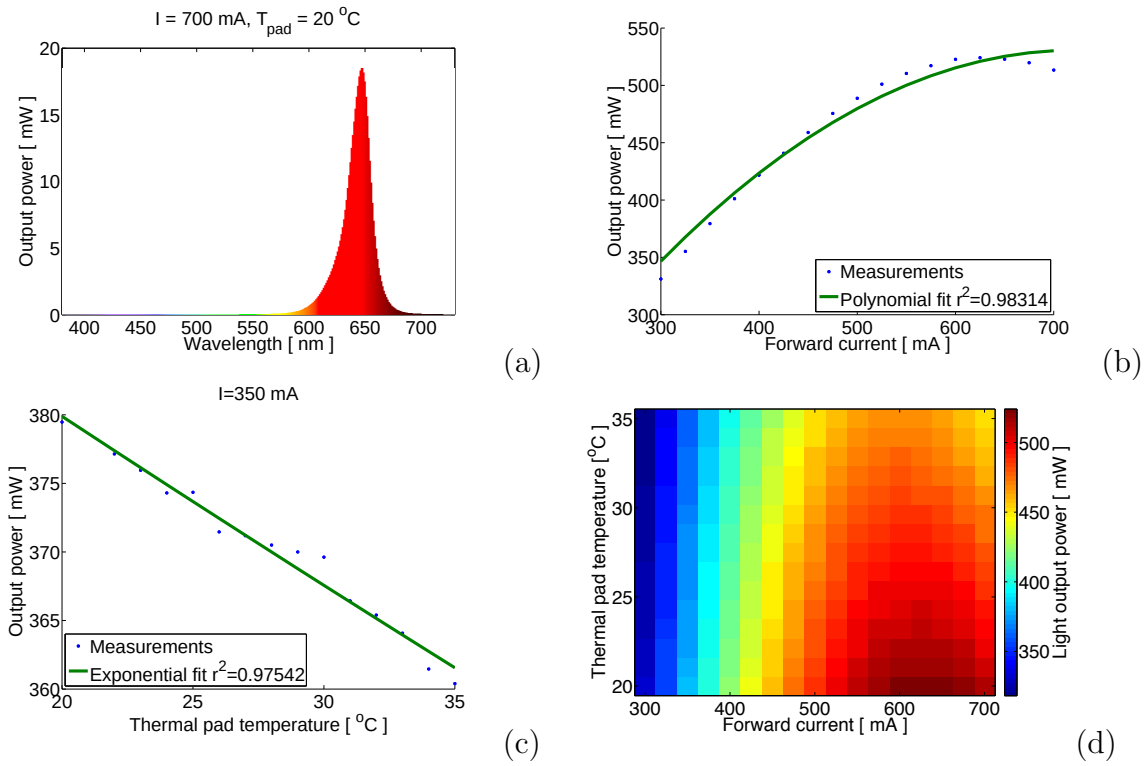


*Figure 5.3: Results of the characterization of the Lumileds Rebel LED LXML-PD01-0040 bin G4C. The SPD the LED (a). Light output as a function of current at $T = 20$ $^{\circ}C$ (b). Light output as a function of temperature at $I = 350$ $mA$ (c) and light output as a function of current and temperature (d).*

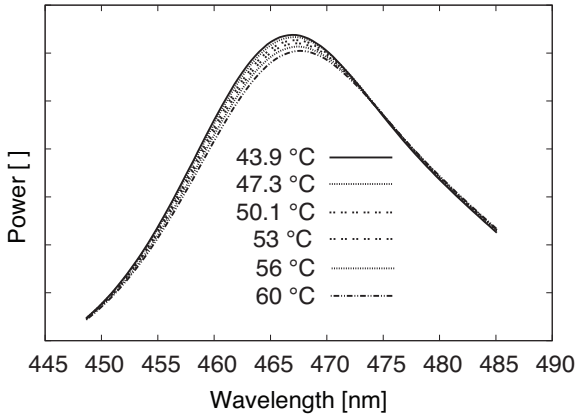


*Figure 5.4: Example of the measurement results, spectral changes with increasing temperature with a 300 mA current. Note the decrease in net output with increasing temperature.*

The models that have been fitted to the measured distributions are: The Gaussian distribution given by equation (2.25), the double Gaussian given by equation (2.26), and the quasi Fermi level model given in equation (2.9). The parameters in the models are fitted to the measured SPDs of the using *Levenberg-Marquardt* least squares method, included in the GNU Octave `leasqr` [101] without any further restrictions, and the fitting parameters were recorded. The results of the fitting of the models to measured spectra are described qualitatively below. Figure 5.5 shows examples of fits for the blue LED with the associated $r^2$ value.

From figure 5.5 (a) it is clear that a single Gaussian has several problems as a model for the blue LED. The peak wavelength is off by several nanometers, the maximum value of the fit is off by several percent and the slopes of the long wavelength side of the profiles do not match. Even with a relatively high correlation between data and model, key features of the SPD are noticeably mismatched.

The double Gaussian model seen in figure 5.5 (b) match the measured data very closely compared to the single Gaussian. This model has a much higher correlation. Looking at $1 - r^2$ we find an order of magnitude lower value compared with the single Gaussian. The slopes and peak match within the resolution of the spectrometer.

The Quasi Fermi level model exemplified in figure 5.5 (c) has a correlation close to that of the double Gaussian, however we see a mismatch around the peak wavelength both in amplitude and peak wavelength. A practical aspect of using this model is that the exponential functions inside the convolution exhibit large fluctuations in the maximum values, with small changes in parameter values. This means that optimal fits are not easily obtained due to a fast divergence of the least square method.

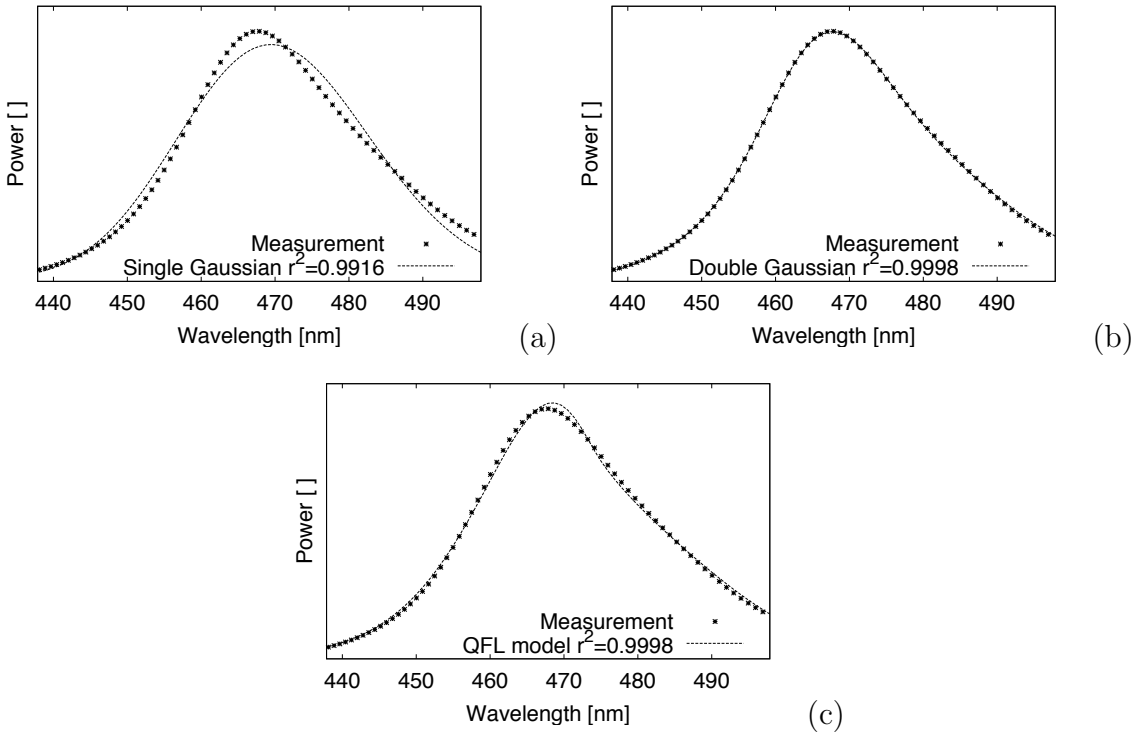


*Figure 5.5: Examples of the different models fitted to the measured data. It is clear that the single Gaussian has a significantly different shape than the measurement.*

### 5.2.1 Temperature Dependence

The performance of the models at varying temperature is investigated in the following. Equation (2.22) is used to calculate the junction temperature from the constant current $I = 350$ mA, the measured ambient temperature $T_{amb}$ and voltage $V$, and using the thermal resistance value from the datasheet [29]. With this, the measured spectra can be associated the with a specific junction temperature. The full width half maximum (FWHM) and peak wavelength of the different fitted models and the measured SPDs are shown as a function of junction temperature in figure 5.6 (a) and (b). The changes in these parameters are near the resolution of the spectrometer, so the resolution of the data has been improved by interpolating the SPD with a spline function. It is clear from figure 5.6 (a) and (b) that the model that best replicates these characteristics is the double Gaussian. The quasi Fermi level model fit to within one nm from the measurements, while the single Gaussian is off by several nm.

The parameters obtained by fitting the QFL-model to spectral power distributions is investigated in the following. The temperature induced change in the band gap $E_g(T)$ were obtained from fitting equation (2.9) to the spectral measurements. The values are plotted as a function of temperature and the Varshni relationship (2.19) is fitted to these results (see figure 5.7). The fit provides a high correlation with measurements $r^2 = 0.996$.The parameters in the equation was found to be: $E_g(T =$

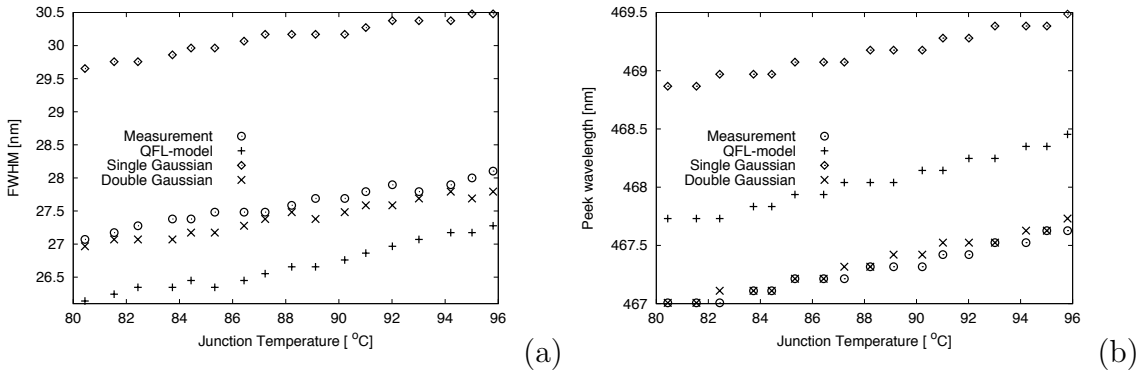


*Figure 5.6: Full width half maximum (a) and peak wavelength values (b) for the measurements compared to the different models. Spline interpolation of the SPDs have been used to increase the resolution.*

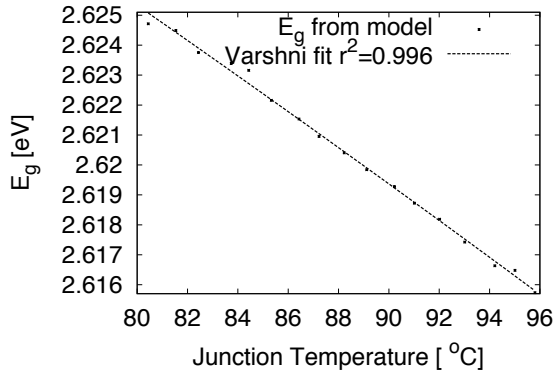


*Figure 5.7: Temperature dependence of the band gap $E_g(T)$ found from fitting model parameters for the blue LED as a function of temperature. The Varshni relationship is fitted to the measuremnt.*

0) = 2.72 with $\alpha = -0.0011$ eV K$^{-1}$ $\beta = 1490$ K. However, the short temperature interval limits the accuracy of this fit, since the features of the Varshni curve vary very little in this interval.

The quasi Fermi levels extracted from fitting the model to the measurement data are shown in figure 5.8. As seen in figure 5.8 (a) the variation in $E_{fp}$ is very small and could be approximated by a constant on this interval. $E_{fn}$ have a significant trend, but still the relative change is small. The parabolic adjustment parameters $y_p$ and $y_n$ seen in figure 5.9, exhibit a clear rising trend with higher temperature within the measured range.

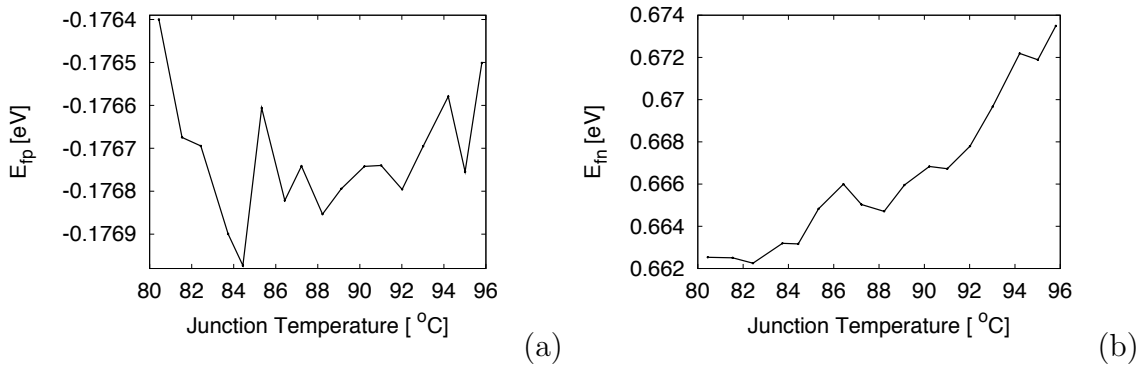


*Figure 5.8: The quasi Fermi levels $E_{fn}$ (a) and $E_{fp}$ (b) extracted from the data fitting as a function of junction temperature, for the blue LED.*

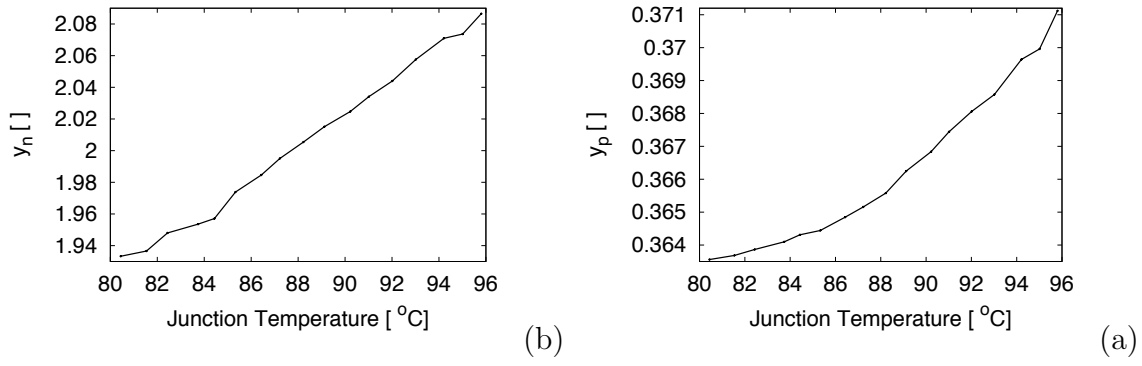


*Figure 5.9: The parabolic adjustments $y_n$ and $y_p$ as function of temperature for the blue LED. $y_n$ rises nearly linearly with temperature on the measured interval with an increase is 0.009 1/K. For $y_p$ there is a clear tendency of rising values for rising temperature (b).*

### 5.2.2 Chromaticity Replication

When considering LEDs for illumination and signage, it is of interest to look at the colorimetric predictions by models of the LEDs. In the following the chromaticietis of the presented models are compared to measurements. The chromaticities are found from the closest fits of the models for varying temperatures. The spectral power distributions of the measurements and corresponding models are converted to chromaticities in the uniform CIE 1976 color coordinate system. The distributions are converted to tristimulus values using equation (3.4) to (3.6). The chromaticity values are found by inserting the tristimulus values into equation (3.10) and (3.11), and finally transform the values to $(u', v')$ using equation (3.12) and (3.13). Figure 5.10 shows chromaticities of the measurements and the models in the CIE 1976 u'v' coordinate system. To evaluate the visual perceptibility of these changes the curves are shown together with MacAdam ellipses. The MacAdam ellipses used in figure 5.10 are generated by translating the nearest MacAdam ellipses to the measurement point corresponding to the lowest temperature, and then test within how many MacAdam steps the corresponding model is located within. It can be seen that there is a significant deviation between the measured data and the models. All models appear to have approximately similar slope and length, but the chromaticities are shifted in the color space in various directions. The double Gaussian is shifted to within a 5-step ellipses, the QFL-model is shifted to within an 8-step ellipses and the single Gaussian is shifted to within a 12-step ellipses. Using this methodology, we find that the discrepancies are well above the noticeable level of human perception. In the ANSI specification [4] 7-step ellipses are specified as acceptable, however this is for white light, with chromaticities around the Planckian locus and not

With the approximate linear shift of chromaticities it might be possible to adjust the chromaticity resulting from the model by applying a suitable linear transform.

## 5.3 Thermal Characterization

When an LED is operated with a forward voltage, heat is generated by non-radiative combination and photon absorption in the material. This heat increases the temperature of the junction until the heat production is balanced with the heat transfer from the devise. When an equilibrium is reached the device will have reached its operation temperature. The operation temperature affect the light output and lifetime of the device. Therefore heat management is a critical aspect of high power LED systems, and with that the capability to measure the junction temperature. A method for measuring the junction temperature and the thermal resistance of an LED is presented in this section, along with the results of a measurement that has been done as part of this work. As seen in section 2.1.6 the electrical properties of the LED change with temperature, this can be utilized to measure the junction temperature of an LED in

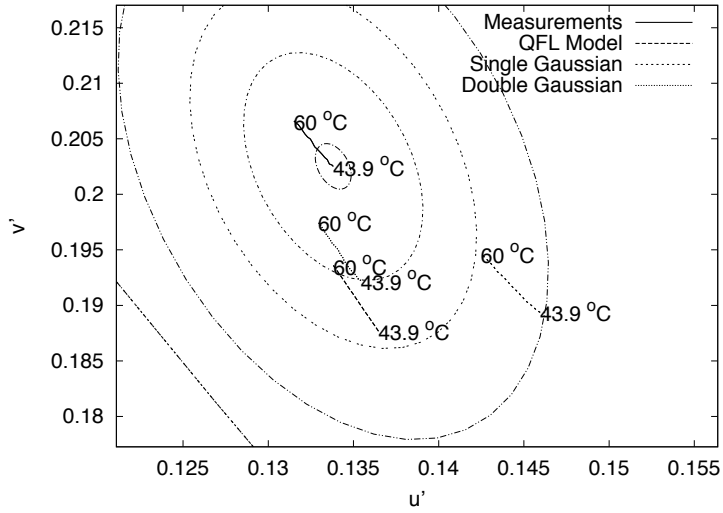


*Figure 5.10: The chromaticity coordinates of the test LED for varying temperature in the CIE 1976 u'v' coordinate system, along with the chromaticies of the best fits for the different models. Additionally the nearest MacAdam ellipses [90] has been displaced and centered on the chromaticity of the lowest measured temperature, 1, 5, 8, 12-step ellipses are plotted.*

a non-destructive way. When the junction temperature can be measured for known power

### 5.3.1 Forward Voltage vs. Junction Temperature

The junction temperature is of critical importance when dealing with LED devices, however this quantity is not easily measurable. Under normal circumstances the junction itself is inaccessible for standard temperature measurement. Thermal probes and thermal imaging are not practical due to the junctions position inside the solid state structure. Furthermore, the packaging with lenses etc. may present difficulties for traditional temperature measurements. An indirect method for measuring the junction temperature of an LED is to measure the electrical characteristics of the LED at known temperatures, and then determine unknown temperatures using these characteristics. For a review of methods for determining the junction temperature see Blackburn [10]. The following is a description of a method to do this measurement and the results obtained for a test LED.

Rearranging the terms in Shockley's equation (2.16) and inserting Varshnis equation (2.19) we find the following relation between junction temperature $T_J$ and the applied voltage $V_a$:

$$V_a(T_J) = \frac{k_B T_J}{e} \ln \frac{I}{I_S} + \frac{E_g(T_J)}{e} = \frac{1}{e}\left(k_B \ln\left(\frac{I}{I_S}\right) T_J + E_{g,0} - \frac{\alpha T_J^2}{T_J + \beta}\right). \qquad (5.1)$$

For large values of $T_J$ compared to $\beta$ in equation (2.19) the change in band gap with respect to temeprature will be proportional to $\alpha$ ie. $\frac{dE_g(T_J)}{dT_J} \approx \alpha$. From this we have that the applied voltage at a constant current $I = I_C$ and sufficiently high temperature will be linearly dependent on the junction temperature.

$$V_a(T_J) \approx \frac{1}{e} k_B \ln\left(\frac{I_C}{I_S}\right) T_J + \frac{E_{g,0}}{e} - \alpha T_J + \alpha\beta = K_1 T_J + K_2, \tag{5.2}$$

where $K_1$ and $K_2$ are constants.

### 5.3.2 Experimental Procedure

To test this method a setup was built and a LabVIEW program interface was constructed to preform this measurement. The following is a description of the developed setup. The LED is mounted on a temperature stabilizing platform as described in section 4.3. The test LED is powered from a constant current source *Keithley 2400 SourceMeter* which also monitor the voltage. The constant $K_1$ and $K_2$ are found in the following way: The LED is driven by a constant current at a small reference current (1mA). If the forward current is small compared to the rated maximum current, the dissipated power will negligible. Using the thermal resistance equation (2.22) and assume an approximate value for $R_\theta$ of 10 °C/W we find that self heating will contribute to a temperature difference of 0.02 C °. The set point of the temperature controller is set to an appropriate value. The temperature is now monitored by the computer. The temperature stabilization routine is set to return when the temperature oscillations are below 0.1 °C. When this is achieved the forward voltage is measured and the temperature is recorded. At this point the temperature set point is changed to the next value, and the process is repeated. The resulting $V_a(T)$ curve can then be established. The linearly result expected from equation (5.2) is seen in figure 5.11 (a).

Using the same experimental components the LED is now driven with a higher current corresponding to significant self heating. Here the forward currents applied are 300 mA, 500 mA and 700 mA. Upon stabilization of the temperature the constant current controller is set to the reference current and the forward voltage is monitored from a voltmeter within the power supply. The voltage is measured as a function of time. An example of the results is shown in figure 5.11 (b).

Since the forward voltage is related to the junction temperature at the low reference current, the starting point of the curve in figure 5.11 can be translated to the junction temperature - immediately after the voltage is changed. For varied values of the power $P = IV_a$ the calculated temperature is shown in figure 5.12. The slope of this curve gives the thermal resistance $R_\theta$ from equation (2.22). The figure shown is for the Lumileds red Rebel LED (LXML-PD01-0040). The thermal resistance of the LED is measured to be $R_\theta = 9.8 \pm 2.1$ °C/W. The data sheet value for the test LED is 12 °C/W. The data sheet value is outside the uncertainty of the measurement.

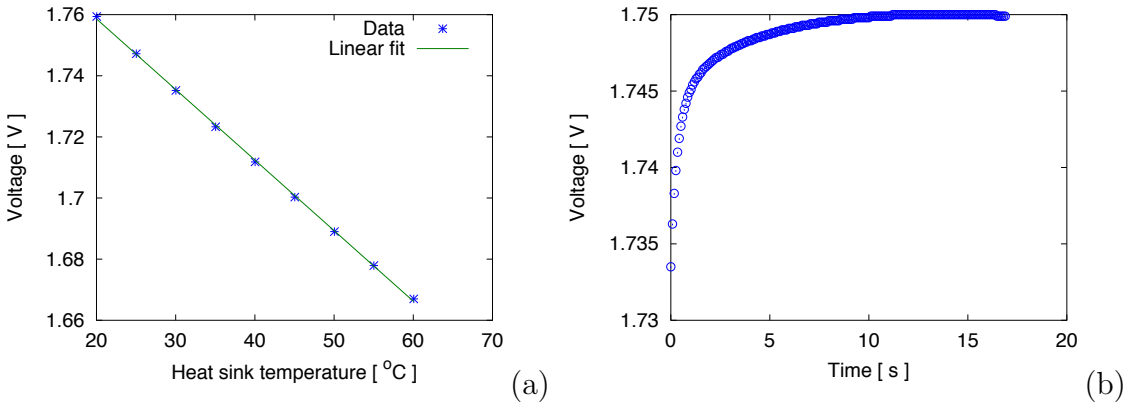


*Figure 5.11: Low current calibration curve, with the forward voltage as a function of heat sink temperature (a). Example of cooling curve, showing the forward voltage as a function of time from the switch from high to low current (b).*

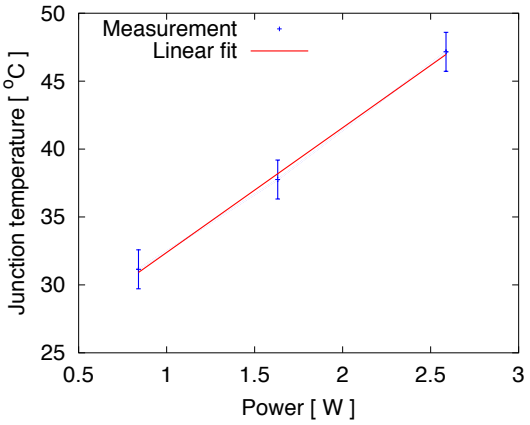


*Figure 5.12: Junction temperture as a function of input power. The slope of the curve signifies the thermal resistance of the test LED.*

However, the spread on the measurement of the starting voltage is relatively high, as seen from the error bars, signifying the standard deviation of the readings. The critical problem is that the heat capacity of the junction is very low, due to the small size of the depletion width, and that the thermal resistance to the substrate is very low. Therefore, the heat dissipates vey quickly, causing the temperature to fall quickly from the operating temperature. To make more accurate measurements, the time resolution in the voltage measurements should therefore be improved. As the setup is currently constructed, this measurement requirer some manual intervention. It would be of interest to incorporate this method in the setup described in section 4.4, such that the junction temperature could be measured in an automated way, together with radiometric or photometric quantities.

## 5.4 Summary

In order to utilize LED for illumination and optimize light quality, it is of importance to be able to determine the operational parameters that should be used with the regarded LEDs. In this chapter experimental results have been presented that has been achieved in the course of this work. In section 5.1 the automated setup described in section 4.4 has been used to measure commercial LED light output in a current-temperature mesh. Three different colored LED from the same manufacture have been tested. The mesh can be used to identify ideal configurations of forward current and thermal pad temperature. It is shown how the decrease in the efficiency of the LED for increasing current or *droop* can be approximated by a second order polynomial dependent on the current. It is suggested that the polynomial pre-factors can be used to numerically characterize this dip in light output efficiency. Within the measured temperature range it is seen that the square term or curvature is not greatly affected by the temperature, which is consistent with the work Kim et al. [73], which shows that the droop is independent of the junction temperature. However, within the limited temperature range the temperature dependence of light output can not be effectively evaluated. Larger temperature intervals have to be measured to determine the temperature dependence. A special case where the light output of an LED device decreases with increasing current, within the rated current interval, does not fit the model very well and this characterization method is is therefore not well suited for this device or others with similar response.

A comparison between the theoretical models for the spectral power distribution that was presented in Chapter 2 has been presented in section 5.2. The three models: The quasi Fermi level model, single Gaussian and double Gaussian models, which are presented in sections 2.1.2 and 2.2.1. By comparing the coefficient of determination $r^2$ for the different models we find that a double Gaussian function performs best with regards to reproducing the SPD, the single Gaussian model give the results least correlated to measurements. The QFL-model generally has a $r^2$ value between the double and single Gaussian. The temperature dependence that has been found from fitting parameters in the quasi Fermi level model are presented in section 5.2.1. Although the changes are small, relative to the values of the parameters, some clear trends are seen. As the model is semi empirical, the results are difficult to interpret in a strict physical sense. However, the model uses relatively few parameters and could possible be used to make useful predictions, if it is applied to larger temperature intervals and for varying values of the current. In this respect it could be of interest to use the newly developed automated setup to further explore these relations. The color replication of these models has been investigated by comparing the chromaticity of the models for changing temperatures. From this, it is seen that the chromatic deviations of the models follow a similar trend to the $r^2$ characteristic. The smallest chromatic deviation is within a 5-step MacAdam ellipse for the double Gaussian, and the largest deviation

is 12 step MacAdam ellipses for the single Gaussian. This means that the predicted and measured chromaticities will be distinguishable by human observers. It is possible that a linear transform will be enough to correct these discrepancies. These deviations are interesting in the context of color mixing due to the fact that the inaccuracies of the models may hinder

Other models for the spectral power distribution exist, both purely empirical such the modified double Gaussian presented by Ohno [114] and more complex models based on the detailed analysis of the composition of the active region by Eliseev et al. [44]. However, given the simplicity of the QFL-model and the absence knowledge of the composition of the commercial LED, it is interesting that this simpler model perform as well as it does.

With regards to thermal characterization, a method for measuring the junction temperature has been tested, using the thermal stabilizations setup described in section 4.3. This method can also be used to find the thermal resistance between the LED and thermal pad. The found thermal resistance show a lower value then the datasheet value. The underestimation of the junction temperature and thereby also the thermal resistance. It is possible that this is due to an incapability to measure the initial fast cooling of the junction. In order to improve the method the time resolution needs to be refined.

The time consuming part of these experiments is the temperature stabilization, which has been a limiting factor on the number of measurements. To further investigate the usefulness of the described models, larger temperature intervals should be investigated with monitoring of the junction temperature. This could be achieved implementing the procedure described in section 5.3, in the automated setup described in section 4.4, and control the Peltier element with an adaptive control scheme.

# Chapter 6

# Optimization of Light Quality

The subject of the chapter is optimization of light quality for lighting systems, consisting of differently colored light-emitting diodes. With the increased use of LED technology for lighting, the spectral quality of the light becomes increasingly important. Using different colored LEDs in a cluster configuration, and varying the light output of individual light sources, the spectral characteristics of the light source can be modified to fit different needs. If LED lighting is to be used in applications where color rendering or other measures of spectral quality is important, then it would be useful to map the possible lighting characteristics of a given light source. An LED cluster light source is defined as follows: A set of distinct LED components, with distinct spectral power distributions, that can be supplied individually by a controlled power source. A typical LED cluster consists of individual LED components placed at a distance comparable to the extent of the components. Several LED chips can also be placed on a single component enabling smaller distances between the individual light source [117]. A 7-color LED cluster setup that has been characterized as part of this work is seen in figure 6.1 (a). Another approach to clustered LED light sources is the combination of many white LEDs of different bins, collected on the same chip to avoid large production bins. Such a device is exemplified in figure 6.1 (b).

When applying additive color mixing (see section 3.3) the problem of metamerisms arises. A given chromaticity can be realized using a multitude of light sources, except along the boundary of the color map, where monochromatic light sources are required. In case of LEDs a given chromaticity can be replicated by appropriately adjusting the forward current applied to three LEDs of distinct chromaticities, as long as it is within the gamut of the LEDs. Adding a fourth LED will enable a given chromaticity to be realizable by an infinite number of current settings. This freedom can be used to adjust the current settings to increase the light quality of the illumination. As spectral light quality remains a highly subjective characteristic, with no single candidate for an fully optimized illumination spectrum, it is necessary to find several configurations that offer what is viewed as high quality lighting, which are suitable for various situations. In this work multi-objective optimization has been employed to find multiple optimal

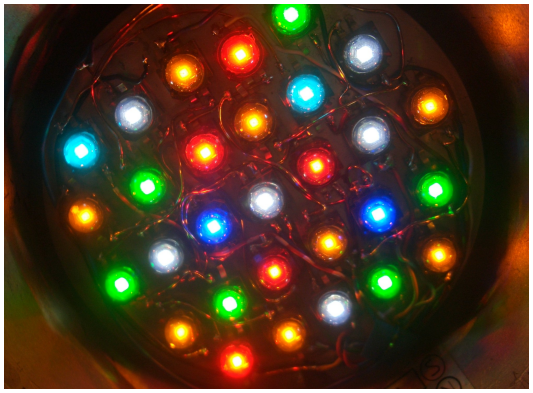
(a)
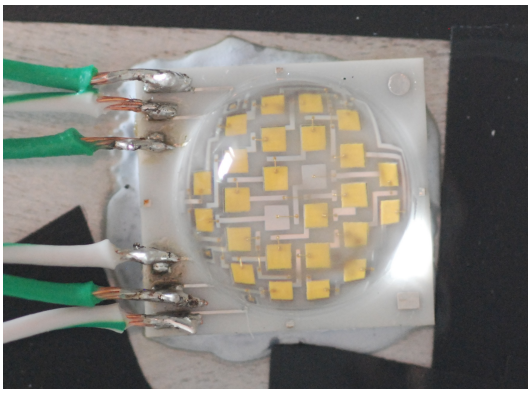
(b)

*Figure 6.1: Examples of clustered LED systems: Closeup of the seven color LED lighting system used for characterization and optimization (a). The Philips Lumileds K2 LEDs are glued to the aluminum heat sink with thermally conducting glue and connected via wires. Closeup of the Cree XLamp MPL EasyWhite (b), which employ color mixing of light from LEDs of deviating chromaticities, to achieve smaller bins sizes of $\Delta_{u,v}$ and CCT (b).*

configurations for correlated color temperature, color rendering index and chromaticity difference.

To ascertain which light quality characteristics can be realized, by a given clustered LED light source and in order to optimize these to the highest attainable level a suitable algorithm has been developed. In the following the principles behind the algorithm is presented and the results obtained for various clustered light sources. The results show how high color rendering indices can be obtained from red, green, blue, white LED systems with maxima around the CCT of the white LED. Additionally it is shown how the high CRI can be obtained by using chromaticities removed from the Planckian locus.

For more precise simulation of the spectral power distribution, from a set of LEDs it could be useful to consider temperature and current effects on each LED. This could be done by employing the models presented in Chapter 2 or the comprehensive measurements of the automated setup presented in section 5.1. Furthermore, other lighting quality metrics could be tested using this method.

The characteristics used for assessment of spectral light quality will be reviewed in section 6.1. The optimization methods and concepts used in the multi objective optimization is discussed in sections 6.2.1 and 6.2.2. The implementation of the algorithm is reviewed in section 6.2.3, along with possible improvements in section 6.2.3. The results are presented and discussed in section 6.3. A summary is given in section 6.4.

The problem can be stated as follows: Given a set of differently colored LEDs in a cluster, how well can this system reproduce a target characteristic. By treating spectral quality characteristic as optimization parameters, a simple randomized hill climber

algorithm has been developed and used to search for desired results. By varying the target values across an interval of values it is shown how accessible characteristics can be mapped with respect to each other. Previous research in the field, has only used a very limited number of light sources. Light quality optimization using traditional light sources and filters has been addressed by Eklund [43]. LED light sources has been optimized with regard to efficacy and CRI by Žukauskas et al. [158]. For systems with up to four LEDs optimization of CRI has also been done by Ohno [114], Chhajed et al. [18], Bretschneider [13]. The approach put forward in this work can be used for any number of different LEDs and any set of quality characteristics that can be calculated from the spectral power distribution. Further work in this field could incorporate optimizing more than one color rendering metric, searching for global maxima for several spectral quality characteristics or test various settings on human subjects

## 6.1 Optimization Characteristics

Light sources for lighting have several figures of merit or quality characteristics. The characteristics are quantities that can be calculated from the spectral power distribution. In the following light quality is defined by the following concepts: Correlated color temperature, chromaticity difference and color rendering index, which are reviewed in sections 3.4, 3.5, and 3.6. A short rationale for the use of theses characteristics is given below.

The correlated color temperature of a light source is one of the key characteristics of light quality, it is described in detail in section 3.4. Human beings can perceive this quality directly as “cold” and “warm” white light, although these labels are opposite to the actual color temperature. Humans are also indirectly affected, for instance by the content of blue light in regard to the circadian cycles [46]. The preference for color temperature is a highly subjective matter that is not easily formalized. Therefore, it is not possible to argue quantitatively that one color temperature is preferable to another. If constraints are introduced, such as preference of certain groups or special application, an optimal CCT can be found but not in general. The implication of this is that a dynamic light source for general lighting should be equipped with a possibility for controlling the CCT, this will increase the usability of the light source. An example of an application could be a lamp or fixture, that would use the signal from a chromaticity detectors to calculate the CCT, and then use the daylight simulator from section 3.6.1 to dynamically replicate the changing CCT of daylight, while preserving a high color rendering index.

A given CCT value is located on the isothermal lines emanating from the Planckian locus (see figure 3.5). However, not all chromaticities along the isotherms can be considered as white light. The chromaticity difference $\Delta_{u,v}$ along these isotherms must

be decreased in order to increase light quality as per section 3.5. If $\Delta_{u,v} < 5.4 \cdot 10^{-3}$ the light will not be considered white.

The color rendering index, described more thoroughly in section 3.6, is the most widely used metric used for estimation of light quality. Even though the measure is debated, it remains a standard indicator of how well a light source renders colors. In the following we therefore assume that CRI should be optimized, to values as close to the maximum value of 100 as possible for maximization of light quality.

## 6.2 Multi-Objective Optimization

In a clustered LED light sources the discrete LED light sources can be combined to create any chromaticity within the gamut of the combined system. If the gamut encompasses a section of the Planckian locus the combined light source will be able to form a composite white light source with a chromaticity corresponding to the correlated color temperatures within this section. If the chromaticity difference is within the threshold $\Delta_{u,v} < 5.4 \cdot 10^{-3}$ the light can be considered white and the CRI can be used for characterization. For a system with two or three light sources, the solutions will be unique, with a given combination corresponding to one and only one chromaticity. If the number of distinct light source $N > 3$ any given chromaticity within the gamut becomes possible with a set of combinations of light sources. Within these sets of combinations the SPD can be optimized with respect to any single relevant spectral characteristics. Adding light sources, that cover perviously uncovered parts of the visible spectrum can contribute to increase color rendering. The addition of more light sources may also extend the gamut of the system, but for the purpose of this investigation this will only have significance if the extension encapsulates a larger part of the Planckian locus. It is important to note that if the target chromaticity is on the boundary of the gamut, only the light sources residing on this particular boundary segment can contribute to the SPD. This is referred to as the gamut boundary problem and it is discussed further in section 6.3.1.

Clustered light source can be mixed such that one quality characteristic can be optimized to a maximum value or near a target value. However, it is often needed to have several of these characteristics optimized for a light source, such that for instance both the CRI and chromaticity difference is optimized. For this we need to consider multi-objective optimization. The characteristics define a fitness landscape illustrated in figure 6.2. The method used in this work is a steepest decent hill climber algorithm, the application of which can reveal Pareto optimal parameters for the system. The following sections will describe these concepts in more detail.

In this work we have used standard metrics for evaluation of light sources. The CIE standard Color Rendering Index (CRI) $R_a$ to quantify the quality of color rendering [24] (See section 3.6). The chromaticity of the light is evaluated using the color

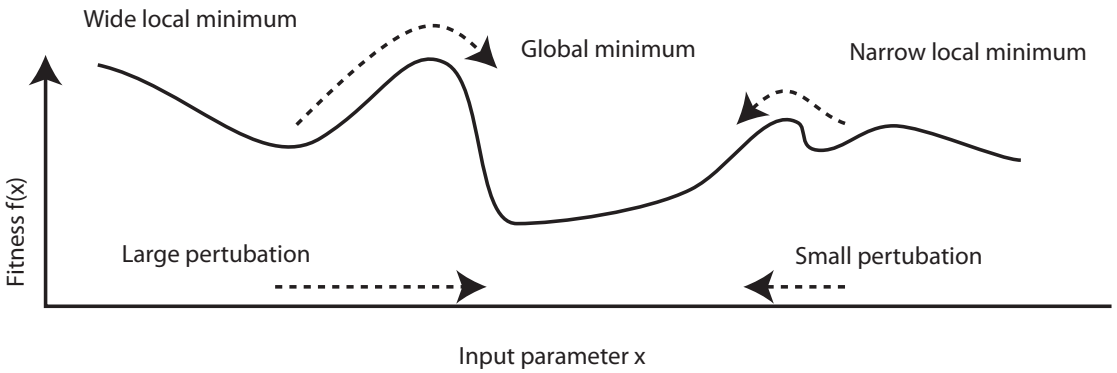


*Figure 6.2: Illustration of different features of a 1-dimensional optimization landscape where $x$ is an input parameter and $f(x)$ is the fitness with regard to $x$. Escaping from shallow local minima to the global minimum requirer small perturbations, while deep local minima requirer larger perturbations.*

matching functions of the CIE 1931 2° standard observer $(\bar{x}, \bar{y}, \bar{z})$. The correlated color temperature (CCT) and the chromaticity distance $\Delta_{u,v}$ to the blackbody locus calculated in the equidistant CIE 1960 chromaticity coordinate system. See Chapter 3 for details on these metrics.

The objective of this work is not to discuss the quality or usefulness of the currently used metrics within photometry and lighting, we have used standard evaluation schemes regardless of any shortcomings of these. However, the method is general enough that any other formalized quantity may be optimized in a similar fashion. This could become useful with the development of improved light quality metrics.

### 6.2.1 Hill Climber Search

Given a vector function $\vec{y} = f(\vec{x})$. We wish to find $\vec{x}$ such that the entries in $\vec{y}$ are minimized. A simple and general way to solve this optimization problem is described in the following: First a starting state is initiated: $\vec{x}(n = 0)$ where $n$ is the number of the state. The initial state can be a specific or random state. From this we calculate $\vec{y}(n = 0)$ and $m$ surrounding values $f(\vec{x} + \vec{\delta}_m) = \vec{y}$ where $\vec{\delta}_m$ are small perturbations. When a vector $\vec{\delta}_m$ is found that causes the length of the new vector to be less than the initial vector i.e. $|f(\vec{x})| > |f(\vec{x} + \vec{\delta}_m)|$, this vector $(\vec{x} + \vec{\delta}_m)$ is chosen as a new initiation point $\vec{x}(n + 1)$ and the process is repeated. When no $\vec{\delta}_m$ is found such that $|f(\vec{x})| > |f(\vec{x} + \vec{\delta}_m)|$ a local minimum is found. This method is called a *simple hill climber*, in this simple case it is assumed that the scale of the solution space is similar in all direction.

In this case vector indices represent quantities of very different scale. This can cause changes in one dimension to outweigh changes along other dimensions when preforming

an optimization. This could cause the optimization of one variable to be dominant. In the present problem we have multiple objective functions, that cannot easily be translated to one objective function. Scaling of the parameters are complicated by the different characteristics. The CRI, for instance, is not bounded at zero but can take arbitrary negative values, while the CCT goes to infinity when chromaticities approach the end of the Planckian locus at 0 mired. This can be simplified by dealing with the indices separately. To solve these issues we use the *steepest decent method*, where a number of surrounding states are examined and graded after whether the individual objective functions have been decreased or increased. The state with the highest grade is chosen as the next point in the iteration. If we define $y_{CRI} = 100 - R_a$ and $y_{CCT} = |T_{CT} - T_C|$ where $T_{CT}$ is the target color temperature while $y_\Delta = \Delta_{u,v}$ The problem can be stated in terms of a vector $\vec{y} = (y_{CRI}, y_{CCT}, y_\Delta)$ that is to be minimized with respect to the vector $\vec{x} = (c_1, c_2, c_3 \dots c_N)$ where $N$ is the number of LEDs and $c_n$ are control parameters.

This method does not guarantee the finding of the global minimum of the function. If the function has local minima it is clear that, given a random initial condition, there is a certain probability the search will end up in a local minimum. There are several methods to avoid ending up in a local minimum. Presently we have used two methods: Firstly, if a local minima is surrounded by a "hollow" of small width, a perturbation can be selected such that the search algorithm may escape the hollow. This can be accomplished by randomizing the step size. To avoid local minima with "hollows" occupying larger volumes of the state space another method must be used. By initiating the search in several random locations whereafter the result with the most favorable result can be selected, the problem should be minimized. The two situations are illustrated in figure 6.2.

This method will work poorly if the fitness landscape has many local minima of large widths. However, the functions used for the calculations such as $(\bar{x}, \bar{y}, \bar{z})$ and the CRI spectral test color samples have relatively smooth reflectance curves with few local maxima and largest derivatives below 0.02 $\text{nm}^{-1}$ (See figure 3.8). This indicates that the solution landscape is relatively smooth and that the above method should be applicable.

### 6.2.2 Pareto Optimal Parameters

Optimizing with respect to several fitness characteristics, often causes the optimization to reach a point where one fitness characteristic cannot be increased without decreasing another, such a point is called a *Pareto optimal* point. If these points make up a line or region of fitness space, this border is called the Pareto optimal front, defining a boundary for the optimization. The problem is also known as the maximal vector problem and has been treated in greater detail by Godfrey et al. [51] and Kung et al. [80].

This concept applies to the problem of light quality of a multicolor light sources in the following way: When examining the possible configurations of an LED cluster, adjusting the control parameters, it is possible to increase the CRI, retaining the target CCT until the CRI can only be increased by letting the CCT move away from the target value. Similarly the chromaticity difference might only be decreased by lowering the CRI or changing the CCT. The definition of isothermal lines in the CIE 1960 chromaticity diagram (see figure 3.5) cause $T_C$ to be constant for chromaticities in directions parallel to the Planckian locus. Thus, for any given CCT, other characteristics can be optimized by increasing the chromaticity difference, while keeping the CCT constant. In itself, this causes the light quality to decrease as the color of the light will become increasingly tainted for increasing $\Delta_{u,v}$.

The Pareto front signifies the boundary for the capabilities of the system to reproduce certain characteristics, in this case light quality characteristics. By mapping the Pareto optimal front for multicolored LED systems the capabilities of the systems can be determined, with regard to the quality characteristics. The settings with desirable characteristics can then be saved and tabulated for use in dynamic control system for the clustered light sources maintaining the highest attainable quality.

### 6.2.3 Implementation

The optimization routine is implemented in MATLAB using the lighting analysis software libraries developed at DTU Fotonik by the Diode Lasers & LED Systems group. The following is a description of the implementation of algorithm.

In the method target values for the characteristics are selected along with other parameters such as maximum number of iterations. The spectral data of the LEDs are loaded from data measured on single LEDs or single channels controlling multiple LEDs of the same color. The latter approach has the benefit that individual performance differences among LEDs in the particular system and absorption from the reflector or other features of the fixture, are accounted for directly in the measurement. The individual control parameters $c_i$ can correspond to either a fraction of the rated maximum forward current or the duty cycle for a PWM current supply. If the control parameters represents the forward currents, an accurate model of the effect of the current on the spectral power distribution must be used. To simplify the calculations we have used used the more linear PWM method and assumed linear behavior of radiant flux with respect to PWM signal [81]. The control parameters for the individual channels can then be used to calculate the compound SPD from the individual measured spectra $S_i(\lambda)$ using the linear approximation

$$S(\lambda) = \sum_{i=1}^{N} S_{i,}(c_i, \lambda) \sim \sum_{i=1}^{N} S_{i,}(\lambda) c_i. \tag{6.1}$$

This is with the limitation that for some PWM systems linearity will not hold for the low values of the duty cycle.

The method is the following: Using random initial parameters the SPD is calculated by super-positioning the spectra of individual LEDs using equation (6.1). The quality characteristics are calculated from this SPD. A perturbation value is selected at random between 0 % and 10 % which is applied to all control parameters in succession. The SPDs are then calculated for the new control parameters. The resulting characteristics are now compared and each perturbation associated with a score. If a characteristic is increasing in fitness or within the target interval the score for this perturbation is increased. If several characteristics are increased the score is increased further by simple addition. The perturbation with the highest score is now used as the next iteration point. If several perturbations have equal score, one among these is selected by random. Using this combination as initiation, the process i repeated until the target characteristics is reached or the maximum number of iteration is reached. When the maximum number of iterations is reached without reaching the target characteristic, the calculation is repeated using a new set of initial parameter values. The resulting combinations are saved to memory for further processing.

An example of the convergence of the algorithm is shown in figure 6.3. The figure shows how the algorithm approaches the target interval in color rendering index $R_a$ (a), chromaticity difference $\Delta_{u,v}$ (b), and correlated color temperature $T_C$ (c) as a function of the number of iterations. In 6.3 (a) it is seen that $R_a$ value converge quickly towards a high value, while the chromaticity difference $\Delta_{u,v}$ is converging slowly towards CRI threshold at $\Delta_{u,v} = 5.4 \cdot 10^{-3}$. In the example the CCT is near the target interval at initiation, however the algorithm searches both inside and outside the interval for usable solutions.

Solutions where the distance to the reference illuminant is above the threshold value of $5.4{\cdot}10^{-3}$ are removed, since CIE does not recommend using CRI for light sources that fall outside this domain. All valid solutions are kept and by selecting the maximum values of one characteristic in small intervals of another characteristic the Pareto optimal fronts can be found.

One problem regarding the chromaticity difference is due to the use of the Pythagorean distance measure, which removes information on whether a specific chromaticity is above or below the Planckian locus. The stochastic nature of the method means that the chromaticity difference of solutions can fluctuate within the allowed threshold. Since the highest acceptable chromaticity difference correspond to 15 mireds [166, p. 173] and solutions can be found on both extremes the chromaticity difference between adjacent solution could be as high as 30 mireds, which is a factor of 5.5 larger than the least noticeable difference (See section 3.7). This issue could be addressed by using the measure *Duv* defined in ANSI C78.377-2008 [4], which requirer a sign according

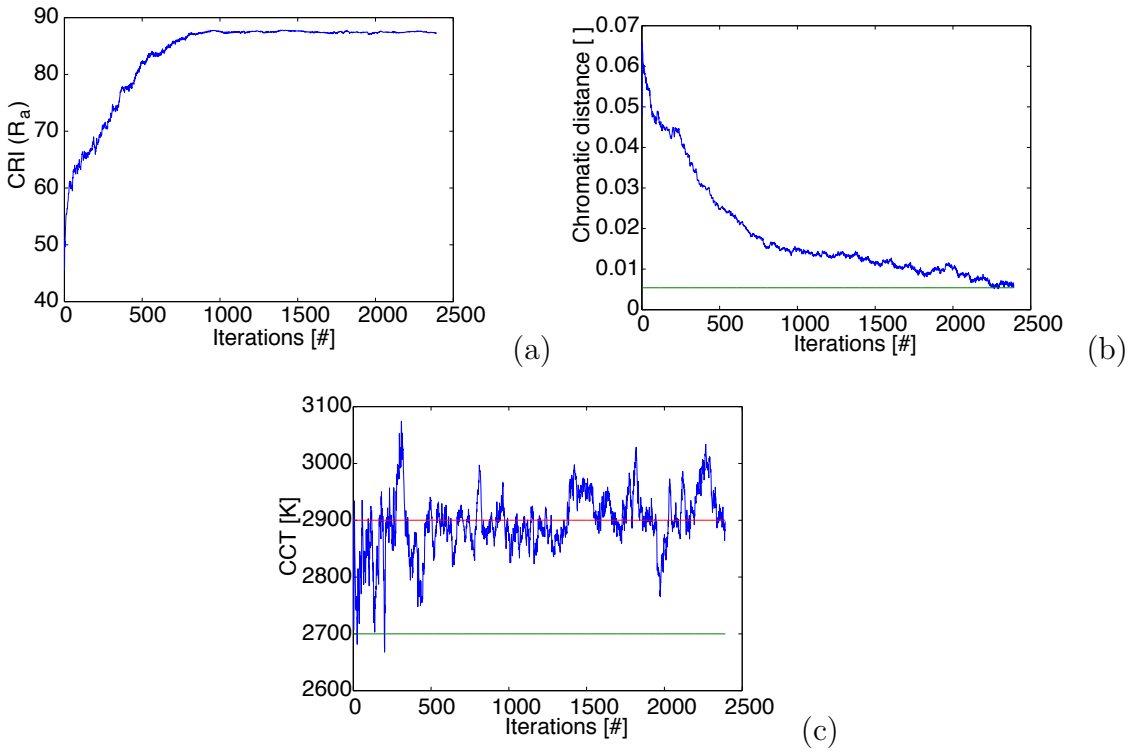


*Figure 6.3: Examples of the progression of the algorithm with $R_a$, $\Delta_{u,v}$ and CCT plotted as a function of number of iterations.*

the position of the chromaticity above or below the Planckian locus. This also enables the unique determination of a chromaticity given only by the CCT and $Duv$.

### 6.2.4 Possible Calculation Improvements

The calculations take a considerable amount of time, which could decrease usefulness of the method. The following is a discussion of the implementation, improvements to the analysis will be discussed in the summary. The focus of the work has been to find the most optimal solutions, while the efficiency of the computation has been a secondary consideration. It is therefore highly possible that faster approaches exist, such that the number of iterations or calculations needed for convergence can be reduced. The size of the of the permutations is important for the speed of converging. Smaller steps has been seen to converge slower, while the search will be able to reach solutions closer to the optimum. Larger steps will cause the iterator to converge faster, but has been seen to circle around the optimum. Scaling the step size with the distance to the target could be used to circumvent this issue.

The most computationally demanding task is the calculation of the integrals in equations (3.4), (3.5) and (3.6) and the chromaticities of the reflectance spectra in the calculation of $R_a$. In MATLAB these calculations requirer the sum of all entries in a vector `v` by the function `SUM(v)`, and individual entry multiplication of vectors `v1` and

`v2` by `(v1.*v2)`. It is possible that a pre-compiled implementation written in C or another low level programming language would increase the speed of the calculations.

A way to decrease the number of calculations needed is to decrease the resolution of the spectral data. The resolution used in the this work is 1 nm. If resolution was decreased with a factor it is likely that computation time would decrease with a similar factor. However, the approximation errors will increase with lower resolution. Another aspect is that the problems is highly parallel in nature, meaning that one optimum search does not necessarily depend on the next. This means that the optimization can easily be split in sections and calculated on multiple processors. It is however, unclear whether it will be practically possible to include calculations like this in a dedicated micro processor for real-time optimization.

It is possible to calculate the spectral characteristics of the entire state space as done by Chhajed et al. [18], Bretschneider [13], for a small number of LEDs, but for a large parameter space this is not possible, since the number of states is given by $r^N$ where $r$ is the resolution of $c_n$ and $N$ is the number of light sources. For our system of 7 different LEDs using a medium resolution for $c_i$ of 1/100 for each LED yields on the order of $100^7 = 10^{14}$ calculations of spectral characteristics. Calculations of this magnitude might be possible today using high performance computing systems. However, it is clear that this is not a viable option for many practical application and increasingly problematic for higher number of color channels.

## 6.3 Results

In the following the results of the optimization are presented. LED systems with a varying number of color channels are tested and a range of configurations with high $R_a$ indices are found using the method. The approach used here is to start with a simple RGB system and add more LEDs to show the effect of the increased coverage of the visual spectrum. For each configuration the normalized spectral power distributions is shown together with the found configurations.

In the tests the target values of $T_C$ are set to go from 2000 K to 7000 K in 500 K steps. Each individual search is limited to 2500 iteration. Due to the stochastic nature of the search, some possible configurations may not be found. Configurations outside the search area may be obtained, but they will be excluded here.

The optimization has been applied to an RGB system. This could seem redundant, as all configurations of $T_C$ and $\Delta_{u,v}$ are unique in terms of control settings. This mean that the $R_a$-index can have only one value for any given chromaticity. However, the chromaticity can vary within the chromatic difference threshold, with varying $R_a$ as a result. An RGB setup is also one of the simplest lighting system and the result gives some insight into the tradeoffs between the light quality characteristics.

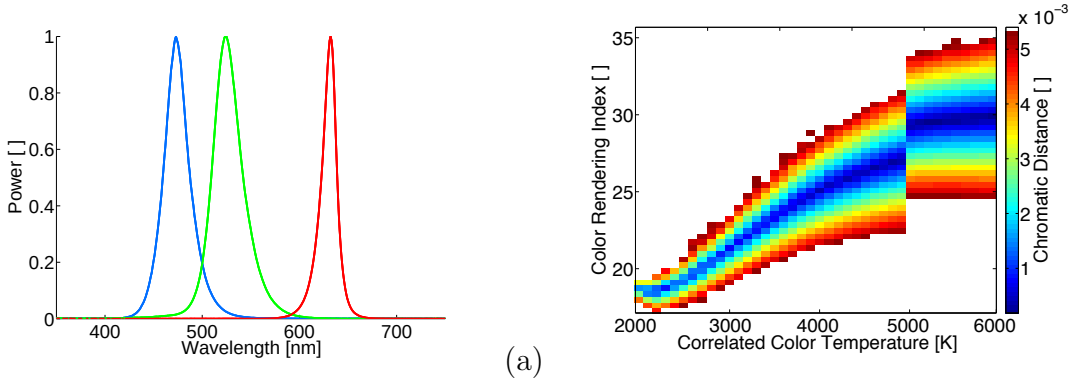


*Figure 6.4: Spectral power distributions of the tested RGB LED cluster (a). The $R_a$-index is show versus the CCT for different output configurations of the three LED source, where the chromaticity distance is allowed to change within the $\Delta_{u,v}$ threshold. White areas signify states of non-white light or states has not been reached by the search algorithm (b).*

Figure 6.4 (b) show the results with $R_a$ versus $T_C$ with fields color coded with $\Delta_{u,v}$, white areas signify $\Delta_{u,v} > 5.4 \cdot 10^{-3}$. The area with low $\Delta_{u,v}$ is the configurations that have chromaticities near the Planckian locus. The figure shows how higher CRI can be obtained by moving away from the Planckian locus. The sharp jump seen at 5000 K is due to the change in reference illuminant. The very low color rendering indices between 20 and 35 will make the light unsuitable for general illumination purposes. By supplementing the RGB system with a white LED, sometimes abbreviated RGBW, a dramatic increase in color rendering can be seen. In figure 6.5 (a) an LED with the low CCT of 2660 K is used. The effect can be seen in figure 6.5 (b) showing $R_a$ as a function of $T_C$ and $\Delta_{u,v}$. An overall increase in $R_a$ can be seen and a broad ridge or band of high values around 3000 K. It is seen that color rendering is approximately constant in bands going out from the locus of reference chromaticities. Selecting a white LED with a higher CCT causes the ridge to shift the higher CCT. The effect is seen in figures 6.5 (d) and 6.5 (e) where white LEDs with CCT of 3750 K and 5070 K has been used instead of the 2660 K white LED.

The ridge of high CRI values can be seen to slant or broaden for increasing values of $\Delta_{u,v}$. This means the increased color rendering indices can be obtained by moving away from the Planckian locus. Whether this can be regarded as an increase in light quality would be a matter of debate. However, it is clear that tradeoffs can be found between various characteristics.

In white LEDs there is usually a significant dip between the peak from the blue LED and the wavelength converted section of the spectrum. This is a clear deviations from the black body spectrum, which can cause low $R_a$ values. To remedy this a cyan LED with dominating wavelength at 500 nm is added to the cluster seen in figure

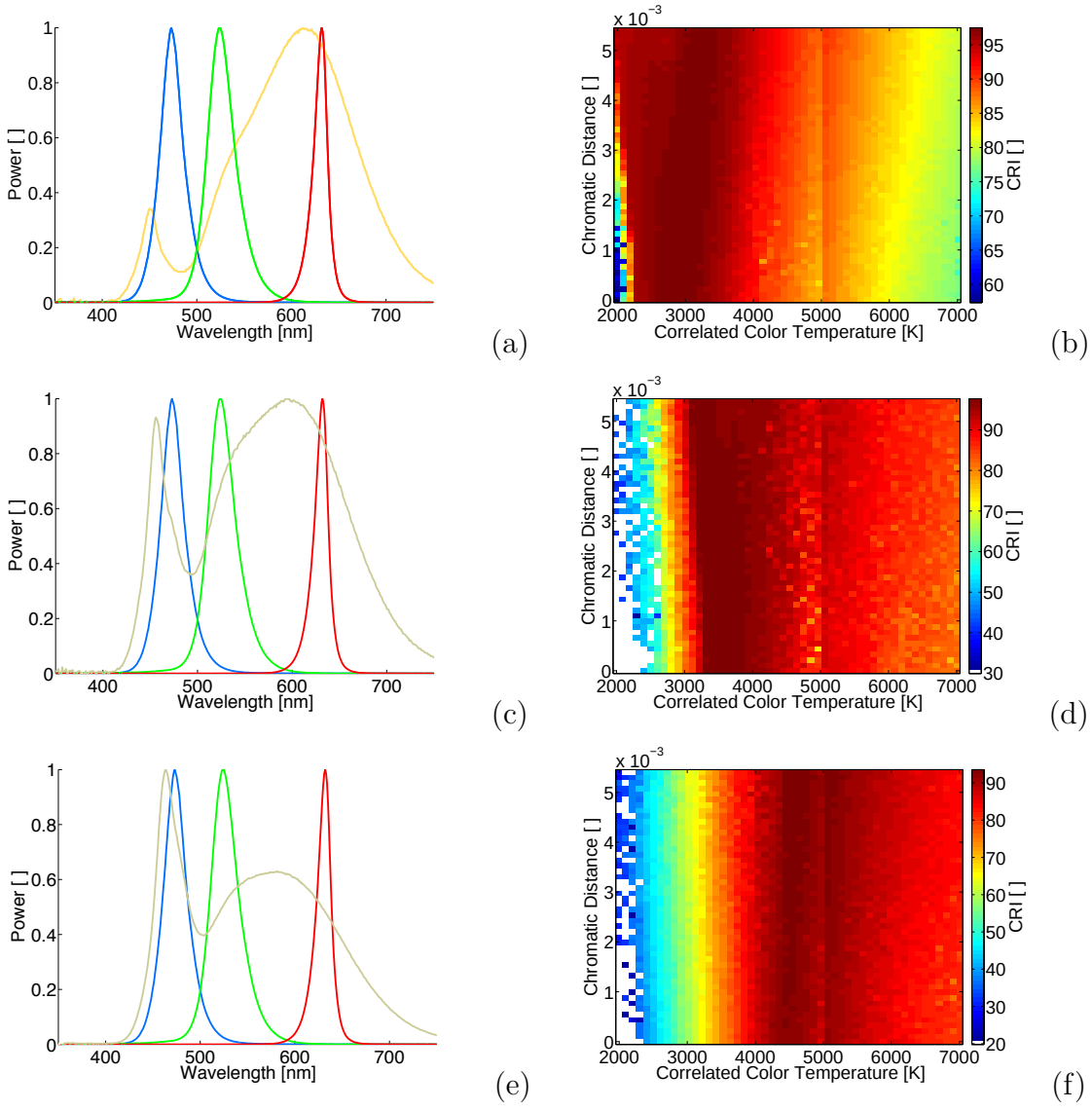


*Figure 6.5: Spectral power distributions of the used RGBW, white LED clusters. The white LEDs have CCT of $T_C$=2660 K (a), $T_C$= 3750 K (c), $T_C$= 5070 K (e). The found configurations of $\Delta_{u,v}$, $T_C$ with $R_a$ shown, for each system respectively (b), (d), and (f).*

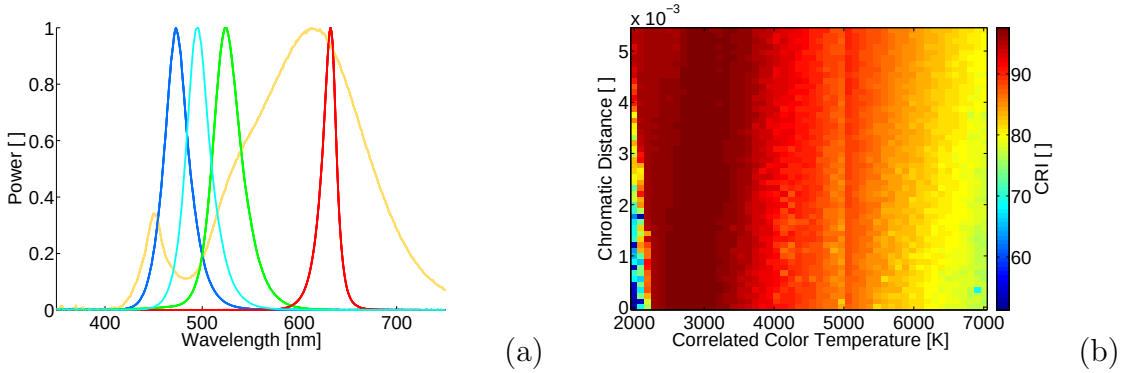


*Figure 6.6: Spectral power distributions of an RGB, white, cyan LED cluster (a). The possible configurations of $\Delta_{u,v}$, $T_C$ with $R_a$ found using the optimization (b).*

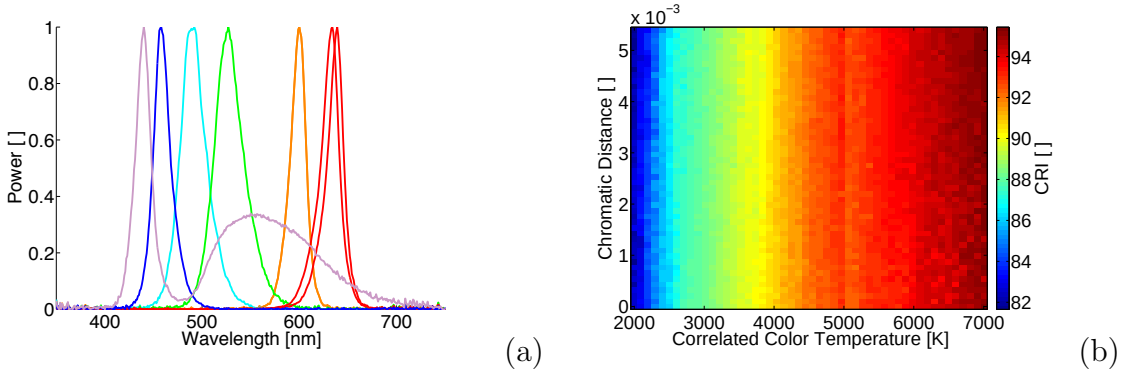


*Figure 6.7: The seven channel LED system (a) with the optimized configurations plotted (b)*

6.5 (a). The result is a rise in $R_a$ in the high CCT range as seen in figure 6.6 (b). Comparing the two results, it is seen that the CRI is increased mostly for high CCT. This could indicate that as the CCT increase the significance of the short wavelength part of the spectral power distribution becomes more pronounced in the CRI. The spectral data presented in figure 6.7 (a) is from a seven LED system demonstration system built at DTU Fotonik. The close spectral spacing of the LEDs result in very high $R_a$ across the CCT range.

### 6.3.1 Gamut Boundary Problem

As seen in figure 6.4 the CRI of the trichromatic light source is very low. The increase in CRI for increasing color temperature, is caused by the fact that the blue LED must be set to a very low setting for low CCT, this causes the tricolor system to approach the behavior of a dichromatic system, causing the CRI to fall for decreasing CCT. This is also seen for the result shown in figure 6.5. A sharp decrease in CRI below a certain CCT. To reproduce a certain chromaticity with an LED cluster system we

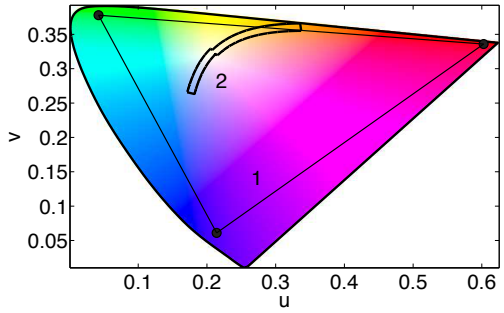


*Figure 6.8: Illustration of the gamut boundary problem. Chromaticities of red, green, and blue LED are marked with •. The lines between the points (1) encompasses the gamut area. The area of white light sources is marked (2). The intersection of area (1) and (2) are then the possible chromaticities.*

must consider the gamut of the system. If a specific chromaticity is outside the gamut of the system it cannot be reproduced. It is seen from figure 3.5 and 3.6 that the low color temperatures lie very close to the visual gamut i.e. the boundary of the chromatic diagram. The problem is illustrated in figure 6.8. In the example some of the Planckian locus is outside the gamut, which will cause the problem to occur around the intersection between Planckian locus and gamut boundary.

For low color temperatures, only light sources with chromaticities near this chromatic boundary defined by the chromaticity line $1 = x + y$, or $v' = -\frac{3}{20}(u' - 4)$ can contribute to the SPD. Light sources with chromaticities further away from this line would only "draw" the chromaticity away from the low CCTs area. This is specifically a problem for RGB+White LED systems. The system will have a large gamut defined by the RGB chromaticities, but for decreasing CCT the contribution from the white LEDs will decrease. This causes the CRI to decrease due to the narrow band contributions from green, orange, and red LEDs that are available along the gamut boundary.

## 6.4 Summary

In order to optimize and thereby characterize multicolor LED light sources consisting of individually controlled light sources, with respect to color quality, an algorithm has been developed using the a steepest decent hill climber. The optimization characteristics used, are the standardized characteristics recommended by the CIE for use in evaluation of light sources. In the preceding chapter the multi-objective optimization method has been described along with the concept of Pareto optimality. The implementation of the algorithm has been described along with possible ways to increase the efficiency of the algorithm. Results of optimizations have been presented. The

results show that the the optimization finds relatively smooth boundaries for the optimizations. If we assume that these boundaries are Pareto optimal, this method could be used to classify clustered light sources according to maximum light quality for instance as a function of CCT. For RGBW systems results are shown for three different white LEDs at three different correlated color temperatures. High values for CRI are found to extend outwards for CCTs surrounding the CCT of the white LED as well as for higher values of the chromaticity difference. The method is general enough that other characteristics can be optimized in a similar way, such as efficacy, addressed by Žukauskas et al. [158], individual $R_i$ indices, or competing lighting evaluation schemes such as the color quality scale (CQS) [35, 34]. It might be suggested that the chromaticity difference be worked in in a new light quality standard. Such that an increase in chromaticity distance would directly decrease a light quality index.

An LED cluster and the multitude of settings, from the optimization, corresponding to illumination with various quality characteristics, could be used to create tests for human subjects for various spectral power distribution with regard to preference or task performance. As an example human test subjects could be exposed to illumination with chromaticities along an isotherm and monitoring for instance visual comfort for varying values of $\Delta_{u,v}$. Similarly illumination with similar $T_C$ and $\Delta_{u,v}$ but with varying $R_a$ or another quality metric could be tested on human subjects being tested in color related tasks.

Other measures could be investigated by this method as well. For instance by incorporating luminous efficacy in the optimization, a Pareto optimal front could be drawn for CRI and efficacy, similar to the work done by Žukauskas et al. [158], or for CCT vs. efficacy with high overall CRI.

# Chapter 7

# Applications

LED lighting has diverse application in many fields: Lighting, signage, automotive lighting, aeronautic, architectural and industrial settings. To illustrate the uses of the techniques and tools developed and presented in this work, two cases will be described where different aspects of LED lighting is emphasized and utilized. The cases are projects wherein the Diode Lasers & LED Systems group at DTU Fotonik has taken part.

**Museum Lighting.** A project on illumination of valuable historical artifacts at the The Royal Danish Collections, is described in section 7.1.

**Plant illumination.** An ongoing project regarding LED lighting for green houses is described in terms of the characterization of the LED light sources in section 7.2.

## 7.1 Museum Lighting

In the *The Royal Danish Collections* at Rosenborg castle in Copenhagen, Denmark, a small treasury of unique and exceedingly valuable historical artifacts are exhibited, namely the Danish crown jewels. Among these are several crowns of Danish royalty. The artifacts are stored in secured display cases, and require special lighting. Illumination of rare and fragile objects in museums present unique opportunities and challenges for implementation of LED lighting, due to the requirement of low color temperature and high color rendering.

Due to the shifting nature of daylight, and the need for adequate lighting, artificial lighting in museums is often turned on all year round and for the duration of the opening hours. Therefore lighting takes up a significant part of the energy consumption in museums. In the exhibition vault at Rosenborg, no daylight is available and full artificial lighting is therefore necessary. Lighting solutions with higher energy efficiency than existing solutions can contribute significantly to reductions in energy consumption. In order to meet the general requirements for increased energy conservation, new lighting solutions must have higher energy efficiency than existing solutions. Most historic objects are highly sensible to changes in temperature and

humidity. Infrared and ultraviolet radiation also causes problems with de-coloration and material degrading. Use of LED lighting with high energy efficiency and no UV or IR radiation can minimize or eliminate these issues. The following is a description of a lighting project done at the treasury at Rosenborg castle. The project (PSO 339-025) was done in collaboration between DTU Fotonik, *Danish Technological Institute*, The Royal Danish Collections, *Lumodan*, *Osram*, *Thermex* and *DONG Energy*. A description of the traditional lighting method is given in section 7.1.1. The development of the LED solution is described in section 7.1.2 and the characterization of spectral light quality and spatial distribution performed on the system is described in section 7.1.3. A summary is given in section 7.1.4. For more information, see the concluding report (in Danish) [33].

### 7.1.1 Traditional Lighting Solution

In the case of illumination of objects with gold components it is generally required that the color temperature be lower than for normal lighting. If the CCT of the light source is too high, the yellow/reddish reflections that characterize gold (see figure 7.1 (b)) will be less visible and visitors will perceive the metal objects as "silver like", reducing the visitor's general impression of the objects. The objects on display are often delicate works of art, where effort has been put into color composition and material selection. Color rendering is therefore critical for this kind of application. Normally $R_a < 90$ will be unacceptable for this type of application [111]. The traditional method of illuminating these objects is to use incandescent light bulbs with a CCT around 2200 K. At Rosenborg castle the traditional light sources are Festoon bulbs[1] run at a lower than rated voltage to achieve the needed CCT. The unfiltered light from these source has $R_a$-index near the maximum of 100 (measured to 98.9) due to the definition of the CRI, described in section 3.6. The low filament temperature means that most radiation is emitted as IR radiation, giving a luminous efficiency around 5 lm/W. The lifetime of these incandescent bulbs is below 1000 hours. This causes the maintenance cost to increase dramatically, since strict security measures have to be deployed whenever replacements are performed, due to the high value of the artifacts. Colored objects are prone to de-coloration and general degrading when exposed to light for extended periods of time, deterioration is increased with decreasing wavelength and increasing intensity [95]. Therefore blue light and UV light must be minimized in the spectral emission of the light source. Radiant heat is also detrimental to fragile objects [32], which is why incandescent light sources must be fitted with IR-filters when used in this setting. Normally illuminance levels are kept relatively low, around 200 lx.

The dimensions of the display cases in question are 100 cm × 70 cm, with a depth of 25 cm with minor variations among the individual cases. An example is shown in

[1] "Pinol pære" in Danish.

figure 7.1 (a). To reach the required illumination level, using traditional light sources, 130 W - 150 W of electrical power is needed per case. The IR radiation from the traditional incandescent light sources cause considerably heating of the display cases during operating hours, causing fluctuations in temperature and humidity, with temperature variations in the 9 - 12 °C range. The radiant heat can introduce temperature differences in the artifacts. This can cause cracking and warping of the artifacts [149, p. 45] and temperature variations can cause drying from humidity variations and fatigue from mismatch coefficients of thermal expansion [149, p. 46]. A ventilation system for temperature and humidity stabilization inside the display cases was disabled due to problems with dust buildup.

The minimum light level for appreciation of color paintings was found by Loe et al. [84] to be 200 lux, and to minimize artifact deprecation the illuminance level in the display cases has traditionally been held around this level. Since the luminance function $V(\lambda)$ is not similar to the spectral light degradation sensitivity of artifacts, one should be careful to use the standard recommendations for maximum illuminance values of 50 - 200 lx [149, p. 23]. The traditional recommendation has been made for spectral power distributions of traditional light sources and the spectral power distributions of LED light sources have not been considered.

The reason for the low CCT is seen when looking at figure 7.1 (b), which shows the reflectance curve of gold at room temperature [9]. For visitors to be able to appreciate the golden objects, the spectral power distribution of the light source must overlap as much as possible with this reflectance spectrum. This will increase the perception of the yellow, orange and red colors that are particular to golden objects. In relation to this issue it could be of interests to calculate the color rendering of the actual materials on display, to evaluate the light source in a realistic setting.

### 7.1.2 LED Solution

The responsibility of the Diode Lasers & LED Systems Group at DTU Fotonik within the project was to design, fabricate and characterize a prototype with similar characteristics to the traditional solution using LED technology. The following is a description of this process and the outcome. To achieve the needed light quality the composite light source is required replicate the chromaticity and color rendering of the incandescent solution it replaces. From the preceding section we find the specifications needed from a new light source used in this application. The correlated color temperature must be $T_C \approx 2200$ K with a $\Delta_{uv}$ within the white light threshold and a color rendering in the range of $R_a > 90$. Further more the color rendering of red and orange colors are particularly important. There are two requirements for the spatial distribution of the illumination. The light field should be smooth, i.e. have small gradients and the CCT should be uniform in all directions.

(a)

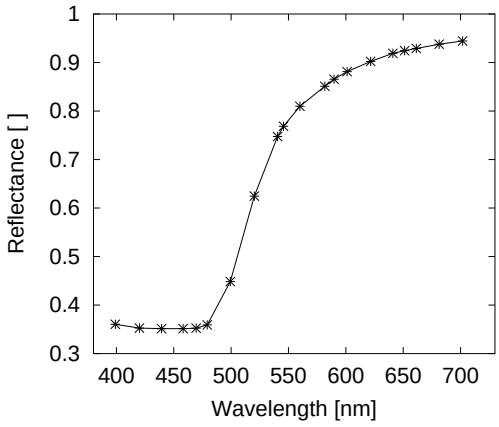


(b)

*Figure 7.1: Display case with golden artifacts at Rosenborg (a), the reflectance spectrum of gold at room temperature [9] (b).*

At the time of the project there were no standard components available with the needed specifications. The market for commercial solid-state lighting covers the range from 2700 K to 6500 K as described in the ANSI Standard for solid-state lighting [4]. Outside this range standard components are rarely available, and no devices were available with the light quality specification needed for in this application. White LEDs with a $R_a$-index above 90 were only available down to 2900 K at the time. It must be considered unlikely that white LEDs with the needed characteristic will be available in the near future, since theses specifications fall outside the needs in the general lighting industry. The fabrication of a specialized wavelength converting white LED was not a viable option within the financial scope of the project. Therefore, standard components were used to create the solution. To achieve the low correlated color temperature, the amount of red light must be increased compared to standard white LEDs. This can be done by mixing the light from a white LED with the light from a red LED. As the white LED will have a chromaticity with a small $\Delta_{uv}$ addition of another light source would only increase $\Delta_{uv}$. By applying a filter, the white LED can have its chromaticity moved towards higher values of $u$ and $v$ in the chromaticity diagram. The red LED can then be added so the chromaticity can be shifted to intersect with the Planckian locus at 2200 K.

With the choice of a bi-color system the possibilities in chromaticity are limited to a straight line in the chromaticity diagram. The line connects the two chromaticities of the light sources with the filter applied. The LED based solution that was selected among several different systems is based on a low CCT white LED white a CCT of 2960 K. The filter is used to attenuate the blue components and a red LED (630 nm)

used to decrease the color temperature. The two LEDs were SMD mounted as close as possible on a custom made metal PCB. This maximizes the color mixing due to the minimization of the distance between the light sources.

Current is provided by two separate constant current power supplies, which can be adjusted to facilitate the wanted chromaticity. The metal PCB is placed in a groove in an aluminum block such that the thermal contact area is maximized. Further more thermal contact is made with the aluminum casing. The casing is painted black to increase thermal radiation from the surface. The light source casing is thermally connected to the display casings metal frame. This means that the heat is conducted away from the fragile artifacts, outward in the exhibition room, thus minimizing heat buildup in the cases.

### 7.1.3 Characterization

During development the intermediate solutions were tested both by visual inspection and with a spatial and spectral characterization setup. The spectral characteristics were determined using the calibrated spectrometer and integrating sphere described in Chapter 4. Spatial variation in the spectral composition was measured using a goniometric setup.

To ensure good color rendering of the red and orange colors of the gold it must be made certain that the individual color rendering indices $R_9$ and $R_{10}$ are high. The indices $R_9$ and $R_{10}$ signify color rendering of red and yellow colors and are not part of the average $R_a$ specification. Figure 7.2 shows the spectral distribution measurement with corresponding Planckian reference radiator for comparison. From the distribution the chromaticity, $T_C$, $R_a$ and additional $R_i$ can be calculated. The CCT is 2220 K, with a chromatic distance of $\Delta_{uv} = 1.3 \cdot 10^{-3}$. The color rendering $R_a = 95.2$ and $R_9 = 92.9$ and $R_{10} = 99.2$.

To achieve maximum uniformity in the chromaticity of the light, from two distinct light sources, the light has to be diffused. If a high degree of diffusion is achieved any point on the diffusing structure will reflect a near equal ratio between different light sources. The diffusing structure used to create homogeneous chromaticity developed for the project is in the process of being patented and will not be discussed in any further detail. To test whether the diffusing structure perform the mixing of the light from the distinct light sources, two tests has been preformed. With regards to chromatic constancy the CCT was calculated for Spuds measured for varying angles.

To determine if the light source gives a smooth light field, corresponding to a Lambertian radiator, the angular intensity distribution was measured. To test to what degree the light source behaves like an ideal diffuse light source the luminous intensity is compared to a *Lambertian* radiator. For a Lambertian the radiance is constant across all measured angles $\theta$. From this follows that the luminous intensity is given by $I(\theta) = I_0 \cos(\theta)$, were $I_0$ is the intensity parallel to the surface normal [120]. The

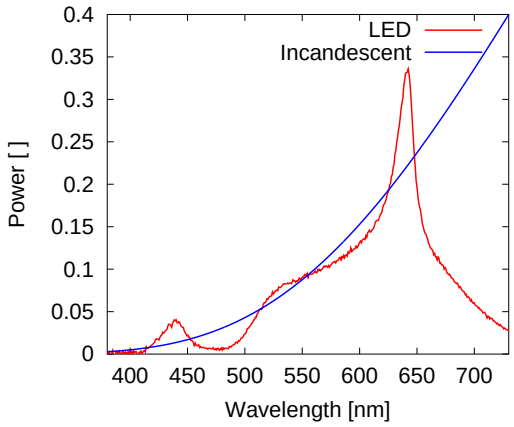


*Figure 7.2: Spectral power distribution of the LED system and the corresponding incandescent light source for 2200 K.*

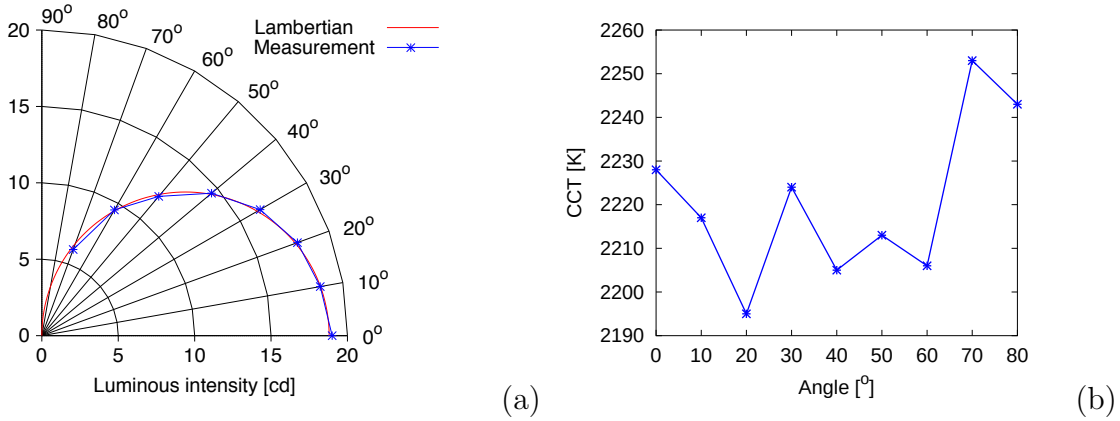


(a) (b)

*Figure 7.3: Luminous intensity of the lamp as a function of angle, compared to a Lambertian distribution (a). Correlated color temperature measured as a function of angle (b).*

lamp was tested in a goniometric setup. Figure 7.3 (a) shows the luminous intensity in candela as a function of the angle, measured in steps of 10 degrees from 0 to 70 ° with a Lambertian for comparison. It is seen that the distribution is very close to the fitted cosine function. The coefficient of determination between the measurement and Lambertian is $r^2 = 0.999$, signifying a highly diffuse light source. Spectral measurements has been performed for varying angles, where after the CCT has been calculated. The results are seen in figure 7.3 (b). The CCT has been calculated to be $T_C = 2220 \pm 37$ across the measured angles. The standard deviation corresponds to 7.5 mired, which is close to the just noticeable difference (see section 3.7). This indicates that the homogeneity of the light source is high enough to be satisfactory. The IR radiation from the LEDs system have been measured and compared to the IR radiation from the Festoon bulbs. The IR radiation is reduced with 98 %. The

resulting temperature variation in the cases was measured to be around 1 °K over 24 hours.

### 7.1.4 Summary

Illumination of exhibited rare gold objects, with high light quality has been realized using LED technology. This is done by combining a broad spectrum, high CRI white LED with a red LED, and a dichroic filter (1/2 CTO), creating the needed spectrum. The result is a lowering of the energy usage, high chromatic homogeneity, and a high color rendering index at the wanted low CCT. These characteristics are satisfactory compared to the traditional solution. Furthermore, improvements have been made in the environment around the artifacts with respect to harmful radiant energy and temperature changes. The diffusing structure is in the process of being patented, but has been characterized and found to produce satisfactory results with regards to creating a spatial homogeneous with respect to CCT and a smooth Lambertian illumination field. The power consumption is reduced from 130 W to 30 - 35 W, per cease, giving a 70 % reduction, while retaining the same light level. The heat from the LEDs is dissipated backwards in the light source casing, decreasing the IR radiation by 98 %. The combination of the two LEDs creates a SPD with a color rendering index $R_a \approx 95$ and high individual indices. The a slightly altered version of the system is in the process of being manufactured in larger quantities and installed in all the display cases in the treasury at Rosenborg Castle.

When regarding illuminating objects consisting of materials with well-known reflectance spectra it would be of interest to evaluate the color rendering of theses materials. In this example relevant materials could be gold, silver, ruby and emerald etc. This could be done by replacing the test color samples described in section 3.6 with the reflectance spectra of the specific materials and calculate the individual relevant indices such as $R_{Au}, R_{Ag}, R_{\text{Ruby}}$. Using real materials could increase the intuitiveness of the color rendering index and also the usefulness when illuminating objects composed of known materials.

## 7.2 Plant Illumination

LED illumination of plants, to enhance growth and optimize photosynthesis, has attracted much attention [145, 52, 14]. Plants are dependent on light for growth and development, they produce the various organic compounds used by the plant and $O_2$ from $CO_2$ and $H_2O$ by the process of *photosynthesis*. Photosynthesis requires light, irradiated on to the chloroplasts which resides predominately on the leaves of the plant. For effective growth and development the illumination level has to be sufficient to ensure the required level of photosynthesis. The yield from production of plants is highly dependent on the amount of available light. Artificial light sources is therefore used as supplementary lighting where the daylight levels are too low for efficient production, due to geographic location or other constrictions. This means that the energy requirement for supplementary lighting can be very high. By utilizing LED technology energy consumption can be reduced, furthermore plant growth can be manipulated by changing the spectral composition of the illumination.

The following section is a description of work done on a project aimed at showing energy saving in green houses by using LED illumination. Emphasis is given to the considerations on spectral design with regard to photosynthesis, and the characterization of LED for this purpose that was done as part of this work. The project was a collaboration between the Diode Lasers & LED Systems Group at DTU Fotonik, the *Faculty of Life Science* at Copenhagen University (LIFE), *AgroTech*, and DONG Energy. For more information see the concluding report (in Danish) [1] and Thestrup et al. [148]. The purpose of the project was to test LED light sources for the application of plant illumination, and investigate plant response to LED illumination compared to traditional methods.

Photosynthesis is spectrally dependent, with reaction peaks in the red and blue (see figure 7.4). LED lighting can be used to address specific wavelength regions with high quantum yield providing a higher plant yield per emitted photon. The idea to use LEDs in this application for was first proposed by Bula et al. [14]. The traditional method of supplementary plant illumination is to use high pressure sodium (HPS) lamps. These light sources has a fixed emission spectrum with low ratio of blue light, and are generally non-dimmable. LED illumination offers possibilities of loss-free dimming and spectral customization that is not offered by conventional plant lighting methods. By overlapping the spectral radiance of the light source with the peaks in the action spectrum for the photosynthesis process, a higher quantum yield can be obtained. With the rising prices of energy and lowering of prices of LED lighting the application of LED has become viable for specialized production. Energy efficiency is a key parameter in plant lighting especially at latitudes where daylight is scares for a large part of the year. To achieve efficient conversion from electrical energy to photosynthesis, it is important not only that the light source is efficient, but also that the photon energy to conversion in the plants is at a maximum. Section 7.2.1 deals

with optimization of plant illumination and section 7.2.2 describes the implementation of LEDs for plant illumination. A summary of the results is given in section 7.2.3.

### 7.2.1 Optimized Photosynthesis

Photosynthesis is the process of converting $CO_2$, $H_2O$ and light to $O_2$ and organic compounds, the process is by mediated chlorophyll. The active spectral region of chlorophyll is approximately within the range of 400 - 700 nm. Radiation in this wavelength interval is called photosynthetic active radiation (PAR). The standard way of quantifying this is by measuring the number of photons within this range incident on a given surface per unit area, by the photosynthetic photon flux density (PPFD).

$$F_{\mathrm{PAR}} = \int_{400nm}^{700nm} \frac{\Phi(\lambda)\lambda}{hc} d\lambda, \tag{7.1}$$

where $F_{\mathrm{PAR}}$ is measured in $\mu$mol/sm$^2$. The rate of photosynthesis is commonly measured by observing the absorption of $CO_2$ from the ambient atmosphere by the plant. Since plants generate $CO_2$ from cellular respiration, the rate of absorption from photosynthesis must be larger than the generation by respiration for the pant to increase it's dry matter mass. This happens when the PAR illumination level exceeds the *light compensation level*. When growing plants for production purposes, illumination will typically be required to be much larger than the light compensation level.

The rate of photosynthesis as a function of wavelength is not uniform across the PAR region. The active molecules in photosynthesis, chlorophyll a and chlorophyll b both have two distinctive absorption peaks at 425 nm and 660 nm and 625 nm for molecules a and b respectively. Figure 7.4 shows the absorption spectra of chlorophyll a and b responsible for photosynthesis in most plants [40, 116]. However there are other photo reactive molecules, contributing to growth, such as carotenoids, which broadens the action spectra. Measuring the yield for varying wavelength McCree [94] found the mean action spectra for various plants, which is also shown in figure 7.4. From the mean action spectrum it is seen that the yield has a local minimum around 475 nm where it is reduced to 50 - 70 % relative to the maximum at 625 nm. A smaller peak is located near 450 nm. Beoyond the PAR region the action spectrum is reduced.

It has been found that the amount of blue light has an influence on the type of growth. Absence of blue light has been seen to lead to stretch growth [39]. This is consistent with the notion that lack of blue light causes the plant to increase the length of branches and twigs to reach ideal illumination conditions. Ideal lighting conditions will generally be found where the sky is unobscured in all directions. When the sky is unobscured the ratio of Rayleigh scattered blue light from the sky dome will be at a maximum. Therefore, plants will tend towards stretch growth when the sky dome is obscured, while the full exposure to the blue component of sky light will cause the growth to tend towards other aspects than stretch.

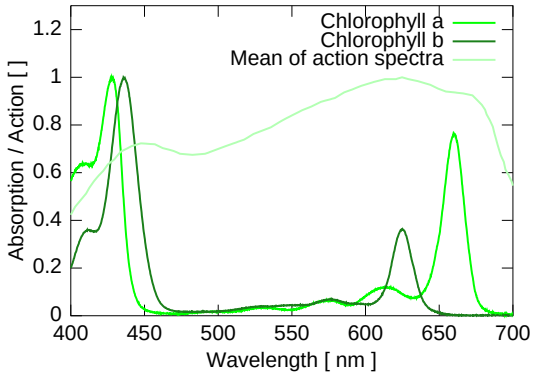


*Figure 7.4: Absorption spectra of chlorophyll a and b in solution [40, 116]. Mean action spectra of selected plants [94].*

Daylight can vary from 100 W/m$^2$ to over 1000 W/m$^2$. Artificial lighting must therefore supply illumination in a similar range to meet requirements for the supplementary illumination. It was shown by Albright et al. [3] that in lettuce production the total amount of PAR is the critical parameter. Here the dimming of LEDs can be used for precise daylight supplementation.

A similar lamp using Lumileds K2 LEDs has already been tested at LIFE on *chrysanthemum x morifolium*, a plant that has been extensively studied [74, 17, 119, 167]. Figure 7.5 shows the relative canopy photosynthesis as a function of the ratio between red and blue PAR. The figure shows results from two measurements with 300 $\mu$mol/m$^2$s, 100 $\mu$mol/m$^2$s. The predicted change calculated as a linear relation between the different response of the action spectra to a similar photon flux. There is a significant difference between the amount of photosynthesis as a function of red and blue PAR ratio. Photosynthesis is decreased for increasing ratio of blue light.

It is seen from the figure that the measured influence of the red/blue ratio on photosynthesis is much larger than the change predicted by use of the action spectra. From this it is seen that spectral considerations are of even larger consequence then indicated by the action spectra curves.

### 7.2.2 High Output LED Fixtures

In order to perform the tests of LED illumination for production of plants, high light output grow lights were built by the Diode Lasers & LED Systems Group. The illumination of plants and the measuring of effects on plant growth was doen at LIFE.

Four similar lamps were built, each in the following way: 112 LEDs in 16 series of 7 similar LEDs were SMD mounted on a PCB with low thermal resistance. The PCB was mounted on a copper block with inlaid water cooling pipes. The pipes were connected to an external water cooler, set to a temperature of 21 °C. A temperature

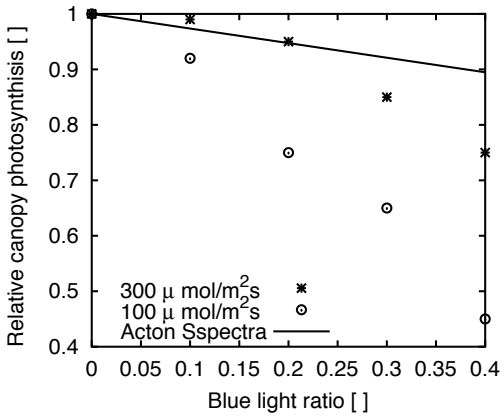


*Figure 7.5: Photosynthesis for Chrysanthemum canopy as a function of blue light ratio for two different lighting levels [148] and the prediction calculated from action spectra.*

sensor was soldered to the PCB to monitor the temperature of the cooling mechanism. The LED driving circuit consists of 4 *4016 QuadPuck DMX Driver* control circuit, each with four 1000 mA *LuxDrive* buckpucks. A LabVIEW computer program has been developed to control the lamps using the DMX signal. The normal operation of the lamps is maximal current but the buckpucks can also be controlled by a pulse width signal for dimming.

The lamps were designed to provide 100 $\mu$mol/s of PAR on a surface area of 1 m$^2$. To ensure that this was achieved, the LEDs had to be characterized in terms of the spectral response to forward current and thermal pad temperature. The evaluation of these LEDs, using the the newly developed automated setup, with results shown in section 5.1 was done in relation to this project. For this particular design the important LEDs were the red, and blue Luxeon Rebel LEDs. The spectral power distribution measured with the setup described in section 4.4.1 were used to calculate the photosynthetic flux using equation (7.1). Figure 7.6 shows the photosynthetic flux as a function of current and temperature from single LED components blue LED 7.6 (a) and 7.6 red LED (b). The results for the blue LED shown in figure 7.6 (a) can be used to find an appropriate temperature and current setting, to achieve a wanted photosynthetic flux. From figure 7.6 (b) it is clear that the optimal current level is around 600 mA bending slightly towards lower current levels for higher thermal pad temperatures. This is lower than the rated maximum current from the data sheet [88], which was also discussed in section 5.1. This light output was so much lower than expected that another LED had to be chosen for the final design of the lamps, the characterization of which falls out of the time scope of this work. These lamps will be tested in a new round of plant experiments in the spring of 2011 at the LIFE.

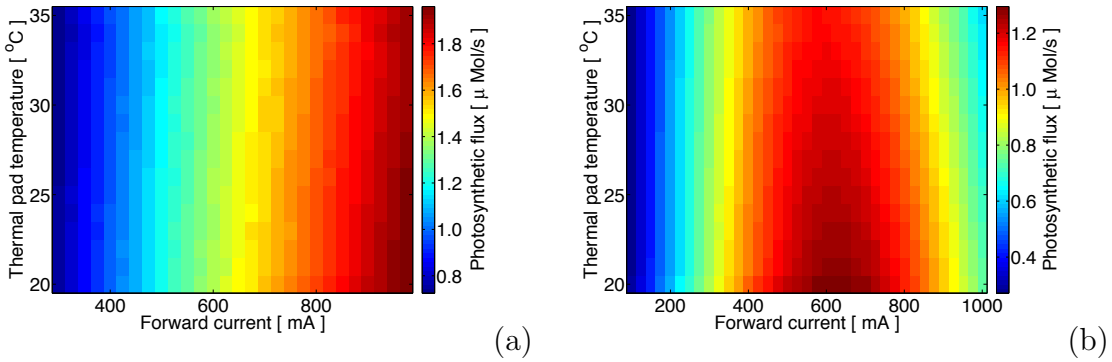


*Figure 7.6: Photosynthetic flux as a function of thermal pad temperature and forward current, for the blue LED (a) and red LED (b).*

### 7.2.3 Summary

The use of LED illumination for plant production is discussed in the preceding sections. It is shown the how non-uniformity of the spectral response is well suited for LED illumination. Using LED illumination allows for direct addressing of wavelengths with optimal photosynthetic yield. The photosynthetic response has an average difference of around 35 %, between minimum and maximum response. The plant tests performed in this project show an even greater disparity between illumination at different wavelengths with the same PAR illumination. However, this is not generally accounted for in calculations for plant illumination. The test of photosynthetic response to changes in the blue/red ratio shows an even bigger effect than estimated from the action spectra. Contrary to traditional light sources LEDs are inherently narrow spectrum emitters, where the spectrum can be designed with a high degree of freedom. To make more accurate prediction on plant yield from LED illumination the definition PAR should be substituted for one which takes the spectral dependence of photosynthetic process [94] into account.

It has further been shown how the newly developed characterization setup presented in section 4.4 can be used to investigate high power LED devices with regard to their photosynthetic photon flux, as a function of operational parameters forward current and operation temperature, for use in plant illumination. As a result of the characterization with this tool, the choice of LEDs for the test lamps was altered.

# Conclusion and Outlook

This thesis has investigated methods for characterization, modeling, and optimization of LED illumination systems. By developing and employing an automated setup it has been shown by extensive and precise spectral radiometric measurement how LED light sources can be characterized with regards to changes in the operational parameters: Forward current and ambient temperature.

Empirical and semi-empirical models for the spectral power distribution (SPD) from LEDs have been investigated by fitting the free model parameters to measured SPDs. The comparison is made with regard to the coefficient of determination and chromaticity. It was found that the double Gaussian model is the model that have the closest correlation to measurements. However, all models deviate chromatically from the measured LED illumination. This may hinder precision modeling of spectral characteristics using these models.

Future work could also include using the automated setup for larger current and temperature ranges of more types of LED, to test the conclusions in this work, and possibly developing or testing more reliable models for spectral dependence of current and temperature. The measurement apparatus could be refined by including an implementation of the tested method for determining the junction temperature from the electric properties of LEDd in the automated setup. Which would give more precise measurement with respect to temperature.

The automated setup has been used to show that the efficiency droop caused by increased forward current can be approximated by a parabolic function. The curvature found by this method could be used to classify commercial LEDs according to this droop parameter. This could result in a more transparent market, and expand the use of current lowering dimming schemes which could potentially save large amounts of energy.

A method has been developed to optimize and thereby characterize multicolored LED clusters with respect to standard light quality characteristics. The limitation of various LED clusters was found to be Pareto optimal boundaries of light output setting with high light quality. The optimization method could be implemented with other quality characteristics to find similar collections of configurations of high quality light. The found settings could be used to test human perception of gradual changes in light quality, or test for color related tasks under highly dynamic lighting conditions.

The tools developed in this work has been used for museum lighting for historical artifacts causing large energy savings with similar light quality. The automated setup has been used to characterize LED illumination of plants for optimization of photosynthesis. These project has shown that metrics for evaluation of illumination of both precious materials and greenhouse plants could be improved by taking spectral properties more into consideration.

# Bibliography


[1] J. M. Aaslyng, J. B. Lund, C. Dam-Hansen, B. Thestrup Nielsen, T. D. Nielsen, and E. Rosenqvist. *Slutrapport for PSO 338-022: Elbesparelser i væksthuse med LED vækstlys systemer : Electricity savings in green houses with LED grow light systems*. AgroTec, 2009.

[2] I. Akasaki, H. Amano, K. Itoh, N. Koide, and K. Manabe. GaN based UV/blue light-emitting devices, GaAs and Related Compounds conference. *Inst. Phys. Conf. Ser*, 127:851, 1992.

[3] L. Albright, I. Ioslovich, and I. Seginer. Improved Strategy for a Constant Daily Light Integral in Greenhouses. *Biosystems engineering*, 93(1):69–80, 2006.

[4] ANSI. ANSI NEMA ANSLG C78.377-2008: Specifications for the chromaticity of solid state lighting products, 2008.

[5] I. Ashdown, S. Robinson, and M. Salsbury. Binning and Filtering: The Six-Color Solution. *Proceedings of SPIE*, 6337:63371A–1, 2006.

[6] K. Astrom and B. Wittenmark. *Adaptive control*. Addison-Wesley Longman Publishing Co., Inc. Boston, MA, USA, 1994.

[7] Avian Technologies LLC. Avian-D White Reflectance Coating. `http://www.aviantechnologies.com/products/coatings/highreflectance.php`, 2010.

[8] R. E. Bedford and G. W. Wyszecki. Wavelength discrimination for point sources. *J. Opt. Soc. Am.*, 48(2):129–130, 1958.

[9] A. Beran. The reflectance behaviour of gold at temperatures up to 500° C. *Mineralogy and Petrology*, 34(3):211–215, 1985.

[10] D. Blackburn. Temperature measurements of semiconductor devices-a review. *Semiconductor Thermal Measurement and Management Symposium, 2004. Twentieth Annual IEEE*, 20:70–80, 2004. doi: 10.1109/STHERM.2004.1291304.

[11] P. Bodrogi, P. Csuti, F. Szabó, and J. Schanda. Why does the CIE Colour Rendering Index fail for white RGB LED light sources. *CIE Expert Symposium*

*on LED Light Sources: Physical Measurement and Visual and Photobiological Assessment, Tokyo, Japan*, 2004.

[12] J. Bower and C. Christensen. Disruptive technologies: catching the wave. *Harvard Business Review*, 73(1):43, 1995.

[13] E. Bretschneider. Efficacy limits for solid-state white light sources. *Photonics Spectra*, 41(3):72–81, March 2007.

[14] R. Bula, R. Morrow, T. Tibbitts, D. Barta, R. Ignatius, and T. Martin. Light-emitting diodes as a radiation source for plants. *HortScience: a publication of the American Society for Horticultural Science*, 26(2):203, 1991.

[15] Bureau International des Poids et Mesures. *The International System of Units (SI)*. BIPM, 8 edition, 2006.

[16] H. Casey. *Devices for integrated circuits: silicon and III-V compound semiconductors*. Wiley New York, 1999.

[17] D. Charles-Edwards and B. Acock. Growth response of a Chrysanthemum crop to the environment. II. A mathematical analysis relating photosynthesis and growth. *Annals of Botany*, 41(1):49, 1977. ISSN 0305-7364.

[18] S. Chhajed, Y. Xi, Y. Li, T. Gessmann, and E. Schubert. Influence of junction temperature on chromaticity and color-rendering properties of trichromatic white-light sources based on light-emitting diodes. *Journal of Applied Physics*, 97:054506, 2005.

[19] Y. Cho, J. J. Song, S. Keller, M. S. Minsky, E. Hu, U. K. Mishra, and S. P. DenBaars. Influence of Si doping on characteristics of InGaN/GaN multiple quantum wells. *Applied Physics Letters*, 73:1128, 1998.

[20] CIE. CIE free documents for download. `http://www.cie.co.at/main/freepubs.html`.

[21] CIE. CIE 1931. Cambridge University Press, Cambridge., 1932.

[22] *Proceedings of the CIE Session 1959 in Bruxelles*, number 004, Brussels, 1960. CIE.

[23] CIE. Colorimetry, official recommendations of the international commission on illumination, publication cie no. 15 (e-1. 3. 1). Bureau Central de la CIE, 4 Av. du Recteur Poincare, 75 Paris 16e, France, 1971.

[24] CIE. CIE 13.3 method of measuring and specifying colour rendering properties of light sources, 1995.

[25] CIE. *CIE S 014-5/E:2009 CIE 1976 L*u*v* Colour Space and u', v' Uniform Chromaticity Scale Diagram*. Commission Internationale de L'Eclairage, 2009.

[26] CIE Division 1. *CIE 177:2007 Colour Rendering of White LED Light Sources*. CIE, Vienna, Austria, 2007.

[27] D. Corell, H. Ou, C. Dam-Hansen, P. Petersen, and D. Friis. Light Emitting Diodes as an alternative ambient illumination source in photolithography environment. *Optics Express*, 17(20):17293–17302, 2009.

[28] Cree. Cree XLamp XR-E LED Data Sheet. `http://www.cree.com/products/pdf/xlamp7090xr-e.pdf`, 2009.

[29] Cree Inc. XLamp XR LED datasheet. `www.cree.com/products/pdf/XLamp7090XR.pdf`, 2006.

[30] Cree Inc. Cree announces revolutionary new led platform delivering 160 lumens per watt. `http://cree.com/press/`, April 2010.

[31] P. Csuti, S. Gy, and J. Schanda. Decreasing the uncertainty of photometric and colorimetric measurements of LED. 2006.

[32] C. Cuttle. Damage to museum objects due to light exposure. *Lighting Research & Technology*, 28(1):1, 1996. doi: 10.1177/14771535960280010301.

[33] C. Dam-Hansen. Slutrapport for implementering af energibesparelser ved benyttelse af højkvalitets led belysning pso 339-025, March 2010.

[34] W. Davis and Y. Ohno. Toward an improved color rendering metric. *Proceedings of SPIE*, 5941:59411G, 2005.

[35] W. Davis and Y. Ohno. Evaluation of color difference formulae for color rendering metrics. `http://physics.nist.gov/Divisions/Div844/facilities/photo/Publications/DavisOhnoCIE2006.pdf`, 2006.

[36] W. Davis and Y. Ohno. Color quality scale. *Optical Engineering*, 49(3):033602, 2010. doi: 10.1117/1.3360335.

[37] P. Deurenberg, C. Hoelen, J. van Meurs, and J. Ansems. Achieving color point stability in RGB multi-chip LED modules using various color control loops. *Proceedings of SPIE*, 5941:59410C, 2005. doi: 10.1117/12.623020.

[38] F. Dongradi. European lamps become more energy efficient, 2007.

[39] T. Dougher and B. Bugbee. Differences in the response of wheat, soybean and lettuce to reduced blue radiation. *Photochemistry and Photobiology*, 73(2):199–207, 2001.

[40] H. Du, R. Fuh, J. Li, L. Corkan, and J. Lindsey. PhotochemCAD: A Computer-Aided Design and Research Tool in Photochemistry. *Photochemistry and Photobiology*, 68(2):141–142, 2008.

[41] A. R. Duggal, J. J. Shiang, C. M. Heller, and D. F. Foust. Organic light-emitting devices for illumination quality white light. *Applied Physics Letters*, 80 (19):3470–3472, 2002. doi: 10.1063/1.1478786.

[42] J. Edmond, H. Kong, and C. Carter. Blue LEDs, UV photodiodes and high-temperature rectifiers in 6H-SiC. *Physica B Condensed Matter*, 185:453–460, 1993.

[43] N. Eklund. *Multiobjective Visible Spectrum Optimization: A Genetic Algorithm Approach*. PhD thesis, Rensselaer Polytechnic Institute, 2002.

[44] P. G. Eliseev, P. Perlin, J. Lee, and M. Osiński. "Blue" temperature-induced shift and band-tail emission in InGaN-based light sources. *Applied Physics Letters*, 71(5):569–571, 1997. doi: 10.1063/1.119797.

[45] D. Farnsworth. A temporal factor in colour discrimination. In *Nat. Phys. Lab. Symposiom No. 8*, volume II, chapter Visual Problems of Colour, page 429. Her Majesty's Stationary Office, 1958.

[46] M. Figueiro, J. Bullough, and M. Rea. Spectral sensitivity of the circadian system. *Proceedings of SPIE*, 5187:207–214, 2003.

[47] A. Fisher and A. Christie. A note on disability glare. *Vision Research*, 5(10-11): 565 – 571, 1965. ISSN 0042-6989. doi: 10.1016/0042-6989(65)90089-1.

[48] M. Fontoynont and L. Piqueras. Innovative lighting for monna lisa. *Annex 45 Energy Efficient Electric Lighting for Buildings*, 2:1–3, 2005.

[49] A. García-Botella, A. Alvarez Fernández-Balbuena, D. Vázquez-Moliní, and E. Bernabeu. Thermal influences on optical properties of light-emitting diodes: a semiempirical model. *Applied Optics*, 40(4):533–537, 2001.

[50] N. Gardner, G. Mueller, Y. Shen, G. Chen, S. Watanabe, W. Gotz, and M. Krames. Blue-emitting InGaN-GaN double-heterostructure light-emitting diodes reaching maximum quantum efficiency above 200 A/cm 2. *Applied Physics Letters*, 91(24), 2007.

[51] P. Godfrey, R. Shipley, and J. Gryz. Algorithms and analyses for maximal vector computation. *The VLDB Journal*, 16(1):5–28, 2007.

[52] G. Goins, N. Yorio, M. Sanwo, and C. Brown. Photomorphogenesis, photosynthesis, and seed yield of wheat plants grown under red light-emitting diodes (LEDs) with and without supplemental blue lighting. *Journal of Experimental Botany*, 48(7):1407, 1997.

[53] O. Graydon. Leds and their applications: Technology focus. *Nature Photonics*, 1(1), Jan 2007.

[54] D. Griffith. Report for Calibration for One Standard of Spectral Irradiance OL FEL-C, S/N: F-911, Sep 2007.

[55] Y. Gu and N. Narendran. A noncontact method for determining junction temperature of phosphor- converted white LEDs. *Proceedings of SPIE*, 5187:107–114, 2003.

[56] J. Guild. The colorimetric properties of the spectrum. *Philosophical Transactions of the Royal Society of London. Series A, Containing Papers of a Mathematical or Physical Character*, 230:149–187, 1932.

[57] X. Guo and K. Houser. A review of colour rendering indices and their application to commercial light sources. *Lighting Research and Technology*, 36(3):183–197, 2004. doi: 10.1191/1365782804li112oa.

[58] R. N. Hall, G. Fenner, J. Kingsley, T. Soltys, and R. Carlson. Coherent light emission from GaAs junctions. *Physical Review Letters*, 9(9):366–368, 1962.

[59] S. T. Henderson and D. Hodgkiss. The spectral energy distribution of daylight. *British Journal of Applied Physics*, 14(3):125, 1963.

[60] S. T. Henderson and D. Hodgkiss. The spectral energy distribution of daylight. *British Journal of Applied Physics*, 15(8):947, 1964.

[61] N. Holonyak Jr and S. Bevacqua. Coherent (visible) light emission from Ga (AsP) junctions. *Applied Physics Letters*, 1:82, 1962.

[62] E. Hong and N. Narendran. A method for projecting useful life of LED lighting systems. *Proceedings of SPIE*, 5187:93–99, 2003.

[63] IEC. IEC 61966-2-1:1999 Multimedia systems and equipment - Colour measurement and management - Part 2-1: Colour management - Default RGB colour space - sRGB, Octoper 1999.

[64] IES. Electrical and photometric measurements of solid-state lighting products, IES LM-79-08, 2007.

[65] Illuminating Engineering Society. Ies lm-80-08 measuring lumen maintenance of led light sources, Sep 2008.

[66] W. James, T. Berger, D. Elston, and R. Odom. *Andrews' diseases of the skin: clinical dermatology*. Saunders Elsevier, 2006.

[67] D. Judd, D. MacAdam, G. Wyszecki, H. W. Budde, H. R. Condit, S. T. Henderson, and J. L. Simonds. Spectral distribution of typical daylight as a function of correlated color temperature. *Journal of the Optical Society of America*, 54(8): 1031–1036, 1964. doi: 10.1364/JOSA.54.001031.

[68] D. B. Judd. Sensibility to color-temperature change as a function of temperature. *J. Opt. Soc. Am.*, 23(1):7–14, 1933.

[69] D. B. Judd. A maxwell triangle yielding uniform chromaticity scales. *J. Opt. Soc. Am.*, 25(1):24–35, 1935.

[70] D. B. Judd, D. L. Macadam, G. Wyszecki, H. W. Budde, H. R. Condit, S. T. Henderson, and J. L. Simonds. Spectral distribution of typical daylight as a function of correlated color temperature. *J. Opt. Soc. Am.*, 54(8):1031–1036, 1964.

[71] Keithley Inc. Models 2700, 2701, 2750 multimeter/data acquisition/switch systems, November 2010.

[72] H. A. E. Keitz. *Light calculations and Measurements*. MacMillan and Co. Ltd., 2nd ed. edition, 1971.

[73] M.-H. Kim, M. F. Schubert, Q. Dai, J. K. Kim, E. F. Schubert, J. Piprek, and Y. Park. Origin of efficiency droop in gan-based light-emitting diodes. *Applied Physics Letters*, 91(18):183507, 2007. doi: 10.1063/1.2800290.

[74] S. Kim, E. Hahn, J. Heo, and K. Paek. Effects of LEDs on net photosynthetic rate, growth and leaf stomata of chrysanthemum plantlets in vitro. *Scientia Horticulturae*, 101(1-2):143–151, 2004.

[75] C. Kittel and P. McEuen. *Introduction to solid state physics*. Wiley New York, 1996.

[76] A. Knulst, L. Stassen, C. Grimbergen, and J. Dankelman. Choosing Surgical Lighting in the LED Era. *Surgical Innovation*, 2009.

[77] M. Krames, H. Amano, J. Brown, and P. Heremans. Introduction to the issue on high-efficiency light-emitting diodes. *Selected Topics in Quantum Electronics, IEEE Journal of*, 8(2):185–188, 2002.

[78] M. Krames, O. Shchekin, R. Mueller-Mach, G. Mueller, L. Zhou, G. Harbers, and M. Craford. Status and future of high-power light-emitting diodes for solid-state lighting. *Journal of Display Technology*, 3(2):160–175, 2007.

[79] J. Kries. Die gesichtsempfindungen. *Handbuch d. Physiol d. Menchen*, 3:211, 1904.

[80] H. T. Kung, F. Luccio, and F. P. Preparata. On finding the maxima of a set of vectors. *J. ACM*, 22(4):469–476, 1975. ISSN 0004-5411. doi: 10.1145/321906.321910.

[81] W. Kurdthongmee. Design and implementation of an fpga-based multiple-colour led display board. *Microprocessors and Microsystems*, 29(7):327 – 336, 2005. ISSN 0141-9331. doi: 10.1016/j.micpro.2004.12.002.

[82] Labsphere Inc. Spectraflect reflectance coating. `http://www.labsphere.com/data/userFiles/Spectraflect%20Datasheet_1.pdf`.

[83] Labsphere Inc. A guide to integrating sphere theory and applications, 1994.

[84] D. Loe, E. Rowlands, and N. Watson. Preferred lighting conditions for the display of oil and watercolour paintings. *Lighting Research and Technology*, 14 (4):173, 1982. ISSN 1477-1535.

[85] R. Longini and R. Greene. Ionization Interaction between Impurities in Semiconductors and Insulators. *Physical Review*, 102(4):992–999, 1956.

[86] O. V. Losev. Luminous carborundum detector and detection effect oscillation with crystals. *Phil. Mag*, 6:1024–1044, 1928.

[87] Lumileds. Understanding power led lifetime analysis. Technical report, Philips Lumileds Lighting Company, 2007.

[88] Lumileds. Luxeon rebel datasheet DS56. Technical report, Philips Lumileds Lighting Company, 2009.

[89] Lumileds. Luxeon rebel direct color portfolio. `http://www.philipslumileds.com/uploads/36/DS68-pdf`, Philips Lumileds Lighting Company, 2010.

[90] D. MacAdam. Visual sensitivities to color differences in daylight. *J. Opt. Soc. Am*, 32(5):247–274, 1942.

[91] D. L. MacAdam. Projective Transformations of I. C. I. Color Specifications. *J. Opt. Soc. Am.*, 27(8):294–297, 1937.

[92] K. Man and I. Ashdown. Accurate Colorimetric Feedback for RGB LED Clusters. *Proceedings of SPIE*, 6337:633702–1, 2006.

[93] M. Marder. *Condensed matter physics*. Wiley-Interscience, 2000.

[94] K. McCree. The action spectrum, absorptance and quantum yield of photosynthesis in crop plants. *Agricultural Meteorology*, 9:191–216, 1972. doi: 10.1016/0002-1571(71)90022-7.

[95] S. Michalski. Damage to museum objects by visible radiation (light) and ultraviolet radiation (UV). In *Lighting in Museums, Galleries and Historic Houses Seminar*, pages 3–16. The Museums Association, 1987.

[96] E. Mills. The $230-billion global lighting energy bill. In *Proceedings of the 5th International Conference on Energy-Efficient Lighting*, Nice, France, May 2002.

[97] J. P. Miras, L. G. Novakosky, and M. Fontoynont. Illumination of monna lisa - new lighting solutions. *Light and Engineering*, 5:28–33, 2005.

[98] E. Muller, R. Diab, M. Binedell, and R. Hounsome. Health risk assessment of kerosene usage in an informal settlement in Durban, South Africa. *Atmospheric Environment*, 37(15):2015–2022, 2003.

[99] S. Muthu, F. Schuurmans, and M. Pashley. Red, green, and blue leds for white light illumination. *Selected Topics in Quantum Electronics, IEEE Journal of*, 8 (2):333–338, March-April 2002. doi: 10.1109/2944.999188.

[100] S. Muthu, F. Schuurmans, and M. Pashley. Red, green, and blue LED based white light generation: Issues and control. *37th IAS Annual Meeting. Record of the Industry Applications Conference*, pages 327–333, 2002.

[101] R. Muzic and A. Jutan. Levenberg-marquardt nonlinear regression of f(x,p) to y(x). `http://octave.sourceforge.net/optim/function/leasqr.html`.

[102] S. Nakamura and G. Fasol. *The blue green diode*. Springer, Berlin, 1997.

[103] S. Nakamura, T. Mukai, and M. Senoh. Candela-class high-brightness InGaN/AIGaN double-heterostructure blue-light-emitting. *Appl. Phys. Lett*, 64: 1687–1215, 1994.

[104] S. Nakamura, M. Senoh, N. Iwasa, and S. Nagahama. High-brightness InGaN blue, green and yellow light-emitting diodes with quantum well structures. *Japanese Journal of Applied Physics part 2 letters*, 34:797–797, 1995.

[105] N. Narendran and Y. Gu. Life of led-based white light sources. *J. Display Technol.*, 1(1):167, 2005.

[106] N. Narendran, Y. Gu, and R. Hosseinzadeh. Estimating junction temperature of high-flux white LEDs. *Proceedings of SPIE*, 5366:158–160, 2004.

[107] M. Nathan, W. Dumke, G. Burns, F. Dill Jr, and G. Lasher. Stimulated Emission of Radiation from GaAs pn Junctions. *Applied Physics Letters*, 1:62–64, 1962.

[108] Next Generation Lighting Industry Alliance with the U. S. Department of Energy. Led luminaire lifetime: recommendations for testing and reporting. `http://apps1.eere.energy.gov/buildings/publications/pdfs/ssl/led_luminaire-lifetime-guide.pdf`, May 2010.

[109] W. Ng, M. Lourenco, R. Gwilliam, S. Ledain, G. Shao, and K. Homewood. An efficient room-temperature silicon-based light-emitting diode. *Nature*, 410(6825): 192–194, 2001.

[110] I. Nimeroff. Propagation of errors in spectrophotometric colorimetry. *JOSA*, 43 (6):531–533, 1953.

[111] H. Nyström. Private communication. The Royal Danish Collections, 2007.

[112] K. O'Donnell and X. Chen. Temperature dependence of semiconductor band gaps. *Applied Physics Letters*, 58(25):2924, 1991.

[113] A. O'Dwyer. *Handbook of PI and PID Controller Tuning Rules*. Imperial College Press, 2009.

[114] Y. Ohno. Spectral design considerations for white LED color rendering. *Optical Engineering*, 44:111302, 2005. doi: 10.1117/12.677417.

[115] Y. Ohno and B. Kranicz. Spectroradiometer characterization for colorimetry of LEDs. In *Proceedings of the 2nd CIE Expert Symposium on LED Measurement, May*, pages 11–12, 2001.

[116] Oregon Medical Laser Center. PhotochemCAD Spectra by Category. `http://omlc.ogi.edu/spectra/PhotochemCAD/html/index.html`.

[117] OSRAM Opto Semiconductors GmbH. OSTAR - SMT LE ATB S2W. Regensburg, March 2009.

[118] J. I. Pankove and B. J. E. Injection luminescence from GaAs. *Bull. Am. Phys. Soc.*, 7:88, 1962.

[119] M. Parrella, V. Jones, R. Youngman, and L. Lebeck. Effect of leaf mining and leaf stippling of Liriomyza spp. on photosynthetic rates of chrysanthemum. *Annals of the Entomological Society of America*, 78(1):90–93, 1985. ISSN 0013-8746.

[120] F. Pedrotti and L. Pedrotti. *Introduction to Optics*. Prentice Hall, 1993.

[121] R. Peon, G. Doluweera, I. Platonova, D. Irvine-Halliday, and G. Irvine-Halliday. Solid State Lighting for the Developing World-The Only Solution. In *Fifth International Conference on Solid State Lighting*, pages 109–123, 2005.

[122] A. Perduijn, S. de Krijger, J. Claessens, N. Kaito, T. Yagi, S. Hsu, M. Sakakibara, T. Ito, and S. Okada. Light Output Feedback Solution for RGB LED Backlight Applications. *SID Intl. Symp. Digest Tech. Papers*, 2003.

[123] N. Pousset, B. Rougié, and A. Razet. Uncertainty evaluation for measurement of LED colour by Monte Carlo simulations. *Metrologia*, 46:704–718, 2009. doi: 10.1088/0026-1394/46/6/013.

[124] I. G. Priest. The colorimetry and photometry of daylight and incandescent illuminants by the method of rotatory dispersion. *J. Opt. Soc. Am.*, 7(12):1175–1209, 1923.

[125] I. G. Priest. A proposed scale for use in specifying the chromaticity of incandescent illuminants and various phases of daylight. *J. Opt. Soc. Am.*, 23(2):41–45, 1933.

[126] O. Pursiainen, N. Linder, A. Jaeger, R. Oberschmid, and K. Streubel. Identification of aging mechanisms in the optical and electrical characteristics of light-emitting diodes. *Applied Physics Letters*, 79(18):2895–2897, 2001. doi: 10.1063/1.1413721.

[127] Y. Ralchenko, A. Kramida, J. Reader, and NIST ASD Team. Nist atomic spectra database (version 3.1.5). `http://physics.nist.gov/asd3`, September 2009.

[128] M. S. Rea. A practical and predictive two-metric system for characterizing the color rendering properties of light sources for architectural applications. In *International Optical Design Conference*, page IMB1. Optical Society of America, 2010.

[129] S. Robinson and I. Ashdown. Polychromatic Optical Feedback Control, Stability, and Dimming. *Proceedings of SPIE*, 6337:633714–1, 2006.

[130] H. J. Round. A note on carborundum. *Electrical World*, 47:309, 1907.

[131] N. Sándor and J. Schanda. Direct visual assessment of colour rendering. *Publications-Commission Internationale d'Eclairage CIE*, 152:1–42, 2003.

[132] J. Schanda. *Colorimetry: Understanding the CIE system.* Wiley-Interscience, 2007.

[133] E. Schubert. *Light-Emitting Diodes.* Cambridge University Press, 2006.

[134] E. F. Schubert. *Doping in III-V Semiconductors.* Cambridge University Press, 2005.

[135] C. Schultz, I. Platonova, G. Doluweera, and D. Irvine-Halliday. Why the developing world is the perfect market place for solid state lighting. In *Proceedings of SPIE*, volume 7058, page 705802, 2008.

[136] Y. C. Shen, G. O. Mueller, S. Watanabe, N. F. Gardner, A. Munkholm, and M. R. Krames. Auger recombination in InGaN measured by photoluminescence. *Applied Physics Letters*, 91(14):141101, 2007. doi: 10.1063/1.2785135.

[137] J. Shimada, Y. Kawakami, and S. Fujita. Medical lighting composed of LED arrays for surgical operation. *Proceedings of SPIE*, 4278:165, 2001.

[138] A. Smith and K. F. Brennan. Comparison of non-parabolic hydrodynamic simulations for semiconductor devices. *Solid State Electronics*, 39(7):1055–1063, 1996.

[139] A. W. Smith and K. F. Brennan. Non-parabolic hydrodynamic formulations for the simulation of inhomogeneous semiconductor devices. *Solid State Electronics*, 39(11):1659–1668, 1996.

[140] R. V. Steel. The story of a new light source. *Nature photonics*, 1:26, 2007.

[141] Strategies Unlimited. High-brightness led market review and forecast 2009. `http://www.optoiq.com/index/market-research.html`, Mountain View, California, August 2009.

[142] Strategies Unlimited. The market for high-brightness leds in lighting applications 2010. `http://www.optoiq.com/index/market-research.html`, Mountain View, California, March 2010.

[143] L. Sugiura. Dislocation motion in GaN light-emitting devices and its effect on device lifetime. *Journal of Applied Physics*, 81:1633, 1997.

[144] T. Tarczali, P. Bodrogi, and J. Schanda. Colour rendering properties of LED sources. In *Proc. 2nd CIE Expert Symposium on LED Measurement,*, pages 65–68, Gaithersburg, Maryland, USA, 2001. CIE.

[145] D. Tennessen, E. Singsaas, and T. Sharkey. Light-emitting diodes as a light source for photosynthesis research. *Photosynthesis research*, 39(1):85–92, 1994. ISSN 0166-8595.

[146] The Australian Greenhouse Office. Phase-out of inefficient incandescent lamps and standards for compact fluorescent lamps. Technical report, Equipment Energy Efficiency Committee, Ministerial Council on Energy, 2007.

[147] The Commission of The European Communities. implementing directive 2005/32/ec of the european parliament and of the council with regard to ecodesign requirements for non-directional household lamps. Official Journal of the European Union, March 2009.

[148] B. Thestrup, C. Dam-Hansen, J. Lund, and E. Rosenqvist. High-power LED illumination system for photosynthetic research on potted plant canopies. In *Proceedings of SPIE*, volume 6910, page 17, 2008.

[149] G. Thomson. *The museum environment*. Butterworth-Heinemann, 1986.

[150] D. Tibbitts. Status and trends in solid state lighting. `http://lednet.dk/`, Dec 2009.

[151] J. Y. Tsao, P. Waide, and H. D. Saunder. The world's appetite for light: A simple empirical expression spanning three centuries and six continents. `http://www.sandia.gov/~jytsao/appetite_for_light_2008_05_18_the_energy_journal.pdf`, 2008.

[152] U. S. Department of Energy. ENERGY STAR CFL Market Profile, March 2009.

[153] R. Ulbricht. *Das Kugelphotometer*. Oldenbourg, 1920.

[154] Y. P. Varshni. Temperature dependence of the energy gap in semiconductors. *Physica*, 34(1):149–154, 1967.

[155] J. Veitch and S. McColl. Modulation of fluorescent light: Flicker rate and light source effects on visual performance and visual comfort. *Lighting Research & Technology*, 27(4):243, 1995.

[156] L. d. Vinci. *The Notebooks of Leonardo Da Vinci, Compiled and Edited from the Original Manuscripts*. Dover Publications Inc., New York, 1970.

[157] I. Vurgaftman, J. R. Meyer, and L. R. Ram-Mohan. Band parameters for III–V compound semiconductors and their alloys. *Journal of Applied Physics*, 89(11): 5815–5875, 2001. doi: 10.1063/1.1368156.

[158] A. Žukauskas, R. Vaicekauskas, F. Ivanauskas, R. Gaska, and M. Shur. Optimization of white polychromatic semiconductor lamps. *Applied Physics Letters*, 80:234, 2002.

[159] A. Žukauskas, R. Vaicekauskas, F. Ivanauskas, G. Kurilcik, Z. Bliznikas, K. Breive, J. Krupic, A. Rupsys, A. Novickovas, P. Vitta, et al. Quadrichromatic white solid state lamp with digital feedback. *Proceedings of SPIE*, 5187: 185, 2004.

[160] J. W. T. Walsh. *Photometry.* Constable & Co. Ltd., 3 edition, 1958.

[161] Wavelength Electronics, Inc. *TEC 2000 Instruction manual*, 1997.

[162] B. Widrow and S. Stearns. *Adaptive signal processing.* 1985.

[163] W. D. Wright. A re-determination of the trichromatic coefficients of the spectral colours. *Transactions of the Optical Society*, 30(4):141, 1929.

[164] W. D. Wright and F. H. G. Pitt. Hue discrimination in normal colour vision. *Proc. Phys. Soc. (London)*, 46:459, 1934.

[165] G. Wyszecki. Proposal for a new colour-difference formula. *J. Opt. Soc Am.*, 53: 1318–1319, 1963.

[166] G. Wyszecki and W. Stiles. *Color Science:: Concepts and Methods, Quantitative Data and Formulae.* Wiley New York, 1982.

[167] S. Xian-zhi, Z. Cheng-shu, and W. Xiu-feng. Effects of high temperature stress on photosynthesis and chlorophyll fluorescence of cut flower chrysanthemum (Dendranthema grandiflora'Jinba').[J]. *Chinese Journal of Applied Ecology*, 10, 2008.

[168] J. Zhao, J. Bardecker, A. Munro, M. Liu, Y. Niu, I. Ding, J. Luo, B. Chen, A. Jen, and D. Ginger. Efficient CdSe/CdS quantum dot light-emitting diodes using a thermally polymerized hole transport layer. *Nano letters*, 6(3):463, 2006.

[169] N. Zheludev. The life and times of the LED - a 100-year history. *Nature Photonics*, 1(4):189–192, 2007.